Universitá degli Studi di Pavia

Facoltá di Ingegneria

Dipartimento di Ingegneria Civile e Architettura

Corso di Laurea Magistrale in Ingegneria Civile

Derivation of non-prismatic beam models by a mixed variational method

Derivazione di modelli di travi rastremate con l'utilizzo di un metodo variazionale misto

Supervisor: Professor

Ferdinando Auricchio

Co - supervisors:

Giuseppe Balduzzi

Giulio Alfano

Author:

Angela Beltempo

UIN: **405613**

Academic year 2012/2013

alla mia famiglia

Ringraziamenti

Alla conclusione del mio percorso di studi ed al conseguimento della laurea magistrale, sento dal profondo del cuore il forte desiderio di ringraziare tutte le persone care che mi sono state vicine e mi hanno sempre incoraggiata, sostenuta, ascoltata e aiutata, durante l'intero percorso.

In particolare, nella redazione del presente elaborato finale, vorrei ringraziare il Professor Ferdinando Auricchio per avermi dato l'opportunitá di approfondire interessanti aspetti della Meccanica Computazionale ed il Dottor Giuseppe Balduzzi per la notevole disponibilitá e per lo sprono a migliorare ed approfondire le tematiche trattate.

Ringrazio il Professor Giulio Alfano della Brunel University per l'accoglienza, la disponibilitá e l'assistenza continua che mi ha offerto durante il periodo di studio a Londra.

Un grazie speciale a tutte le persone fantastiche che ho incontrato a Pavia. In particolare ringrazio Junlei, Camilla, Evis e Sanaz che ho conosciuto e apprezzato per le notevoli doti umane e professionali, i quali hanno colmato il vuoto di affetto per la lontananza dalla famiglia. Grazie Mohammad per i momenti divertenti trascorsi all'universitá. Il soggiorno a Pavia ha rappresentato un periodo significativo e profondo della mia esperienza di vita, che ricorderó sempre con grande affetto. Grazie di cuore!

Inoltre, esprimo tutta la mia riconoscenza alla famiglia, il mio piú grande punto di riferimento nelle scelte di vita. Grazie di cuore a tutti, mamma, papá, Giusy, Pasqualino e Maria Sara, per avermi sempre sostenuta sotto ogni punto di vista, affettivo e morale, con preziosi consigli, suggerimenti e con tanta pazienza. Grazie ai miei genitori per aver creduto in me, per avermi incoraggiata e dato l'opportunitá di conseguire la laurea magistrale a Pavia. Nel vostro affetto e nella fiducia che riponete in me ho trovato la forza per superare i momenti difficili e la motivazione a fare sempre di piú. Grazie Pasqualino, per la calma e

la collaborazione che hai dimostrato nella rilettura del presente elaborato finale, perché a qualsiasi ora sei stato disponibile ad ascoltarmi, nonostante i tuoi innumerevoli impegni. É stato il piú bel regalo che potessi farmi e certo queste parole non potrebbero colmare la mia riconoscenza. Grazie anche alle mie sorelle Giusy e Maria Sara per avermi sempre ascoltata e incoraggiata. Entrambe hanno saputo sostenermi anche a distanza, dimostratomi tanto affetto. Grazie perché ognuno di voi ha dato un contributo unico e indispensabile per farmi diventare la persona che sono oggi.

Grazie zii, cugini, famiglia di Pasquale e amici per l'attenzione e la sensibilitá che avete mostrato nel seguire da lontano il mio percorso di studi finale.

Un grazie speciale a Pasquale, mio compagno di vita, che ha avuto sempre la pazienza di ascoltarmi nei miei mutevoli spunti di riflessione e di avermi sempre consigliata per "il verso giusto"; grazie a lui per l'affetto ed il calore che mi ha offerto con la massima disponibilitá, sensibilitá e con tanto amore.

Voi tutti siete stati la carica fondamentale nella riuscita di questa importante tappa della mia vita e il vostro amore incondizionato ha rappresentato la mia casa in questi ultimi due anni. Grazie!

Abstract

The aim of this thesis is the derivation of planar non-prismatic beam models by means of a mixed variational principle. The beam under investigation is initially modelled as a 2D body in the hypotheses of an isotropic material with a linear elastic behaviour and small displacements.

First, referring to models already existing in literature, two formulations of the elastic problem (Total Potential Energy and Hellinger-Reissner principles) and the classical beam theories (Euler-Bernoulli and Timoshenko) are illustrated.

Then, starting from the Hellinger-Reissner functional and through the dimensional reduction method, six differential equations, governing the mechanical behaviour of a generic tapered beam, are analytically achieved by means of the software Mathematica.

In order to find the solution of the aforementioned six differential equations, thus testing the developed model, five kinds of cantilever beam, undergoing a concentrated load on the free end, are considered and respectively characterized by a linear and a curvilinear taper, not necessarily symmetric with respect to the longitudinal axis.

The comparison between the results obtained with this model and the ones provided by the finite element analysis are almost perfectly coincident, showing a highly accurate stress distribution along the cross-section.

Sommario

Oggetto del lavoro di tesi é la derivazione di modelli di travi non prismatiche piane, partendo dalla scrittura di un principio variazionale misto. La trave in esame viene modellata come un corpo bidimensionale nelle ipotesi di: materiale isotropo, comportamento elastico lineare e piccoli spostamenti.

In primo luogo, riferendosi ai modelli di trave esistenti, sono illustrate alcune possibili formulazioni del problema elastico. L'attenzione é posta sui modelli classici (teorie di Eulero-Bernoulli e di Timoshenko) e sui modelli relativi, rispettivamente, al principio dell'Energia Potenziale Totale e al principio di Hellinger-Reissner.

Successivamente, partendo dal funzionale di Hellinger-Reissner e mediante l'utilizzo del Dimensional Reduction Method, si giunge analiticamente, con l'ausilio del software Mathematica, alla scrittura delle equazioni differenziali, che governano il comportamento meccanico della trave genericamente rastremata.

Al fine di trovare la soluzione del sistema di equazioni differenziali e quindi di testare il modello sviluppato, sono considerate travi a mensola, sottoposte ad un carico concentrato nell'estremo libero e caratterizzate da una rastremazione lineare o curvilinea, non necessariamente simmetriche rispetto all'asse longitudinale. Il confronto dei risultati ottenuti dal modello proposto e da un'analisi agli elementi finiti mostra una corrispondenza tra le due soluzioni e un'elevata accuratezza della distribuzione delle tensioni lungo la sezione trasversale.

Contents

List of Tables

List of Figures

Chapter 1

Introduction

1.1 Tapered beams

The study of the beam is one of the fundamental topics in the Theory of the Structures. The most common definition of the beam considers it as a three-dimensional (3D) body with two dimensions negligible in relation to its third dimension. This definition is too extensive because, apart from its dimensions, there are many more characteristics that identify a beam, such as the material, the shape and the structural behaviour. For the purposes of this thesis, the geometrical classification plays a key role. It includes such features as the beam being straight or curved or also prismatic or tapered. A prismatic beam is a structural element with a constant cross-section along its predominant axis; whereas a tapered beam is characterized by a variable cross-section. This work focuses on tapered beams with a straight longitudinal axis, considering that there are different types of taper, such as linear and curvilinear.

One of the ways of testing the efficiency of the beam is to develop a model. The research conducted towards beam modelling is nowadays very much fertile, considering the huge variability of properties describing a beam. The simplest models referring to a beam with one dimension predominant in relation to the other two are the Euler-Bernoulli and Timoshenko theories. The former is adopted for slender beams whose cross-section is forced to be orthogonal and rigid with respect to the deformed axis. The latter is used for less slender beams and its cross-section does not necessarily stay orthogonal in relation to its deformed axis. Both of them, though, incur in some limitations, such as a loss of accuracy for beams with a low ratio between the length and cross-section dimensions and the difficulty to accurately describe the stress profiles because displacements only are assumed as variables of the problem. It is evident that the more complex the shape of the beam, the more sophisticated its modelling must be. Hence the Euler-Bernoulli and Timoshenko theories are not sufficiently suitable for the modelling of a tapered beam. Therefore, a mixed model, more refined and advanced, is adopted in order to keep a high degree of accuracy despite the larger number of variables.

Tapered beams represent an useful and reliable tool in civil engineering being able to provide the maximum resistance with the least amount of materials. Furthermore, they could improve the strength of a structure and lessen its weight characteristics with architectural and aesthetic benefits. These outstanding properties make tapered beams fundamental in optimizing the structural performance of major engineering works, such as steel roofs and bridges. The latter can achieve large spans thanks to the presence of a reduced cross-section in the areas where a minor resistance is requested. As a result, the weight of the whole structure decreases, with a consequential reduction of the loads.

An example of tapered beam is shown in Figure 1.1(a). The London Bridge comprises three spans of prestressed-concrete box girders, a total of 283 m long. The site of the present London Bridge is the same place where the Romans built the first bridge in London.

This bridge is a continuous curvilinear tapered beams supported in correspondence of each column. The maximum height of the cross-section is where the bending moment and the shear stress are higher. On the other hand, since the stresses are not too high in the middle of each span, a reduced cross-section is adopted in that region.

It is evident how the taper leads to a variability of the cross-section, implying a change of weight along the beam axis. Despite the structural convenience of the taper, it must be considered that additional costs are involved in the production of a tapered beam as opposed to the manufacture of a prismatic one. It is therefore necessary to compare the savings coming from the purchase of a lesser amount of material with the increase in cost due to the taper. The economic impact of this topic is palpable and thus object of further investigation, nevertheless it is clearly not inherent to this thesis.

Going back to tapered beams, it is important to remind their uses in many other fields apart from structural engineering, such as in aviation. The taper of the wings of a plane allows the aerodynamic force to induce minor bending moments on them, resulting in a reduction of the weight of the whole body (see Figure 1.1(b)).

In mechanical engineering, the leaf spring can be considered an example of taper. Leaf springs are widely used in suspension systems of railway carriages and automobiles. They are normally seen as laminated leaf springs (see Figure 1.1(c)) and their main characteristic is a uniform strength. It is possible to model a leaf spring as a cantilever beam (beam only anchored at one end) with a specific geometry and a variable cross-section along the axis in order to guarantee the property of uniform strength.

(a) London Bridge

(b) Plane

(c) Leaf spring

(d) Spruce

Figure 1.1: Some applications of taper

Another example of taper could be found in nature. During their evolution, the trees avail themselves of some anatomical and structural tricks in order to achieve an appropriate height, such as a reduction of the cross-section. Spruces provide a great example of taper, considering that their cross-section can vary from five metres to the size of a finger reaching an average height of sixty metres (see Figure 1.1(d)).

1.2 Literature review

This section presents a summary of some previously conducted studies concerning different modelling approaches of beams.

Focusing on linearly tapered beams, symmetric with respect to their longitudinal axis, their modelling takes advantage of their simple geometry. Even though the cross-section area depends on the beam-axis coordinate, the position of the cross-section barycentre (the point where a resulting axial force can be applied without inducing any bending moment) and of the shear-centre (the point where a shear force can be applied without inducing any torsion) does not depend on their beam-axis coordinate. A further important advantage of the symmetry is that there is a decoupling between the axial and bending behaviours and between the shear and torsional behaviours. This kind of beam has a more complex geometry than a prismatic beam, nevertheless, being symmetric with respect to its longitudinal axis, and thus easier to model, it is object of many studies.

The simplest approach for a tapered beam modelling consists in modifying the coefficients of the Euler-Bernoulli and Timoshenko beam model equations in order to take the variation of the cross-section geometrical properties into account. Unfortunately, it is well-known, since the sixties, that this approach is only satisfactory for beams with negligible variations of cross-section size (see Boley (1963)). The procedure on how the equations derived for prismatic beams can be used with sufficient accuracy for bars of variable cross-sections, provided that the variation is not too extreme, is also shown in Timoshenko (1976). The authors analyse two interesting examples about a cantilever beam with uniform strength by considering that the section modulus varies along the beam in the same proportion as the bending moment. These results are intriguing because they may be used to compute the approximate stresses and deflections in a leaf spring. Banerjee and Williams (1986) illustrate another application of this simple approach. The authors derive the exact static stiffness matrix for a range of tapered beam-columns, by means the Euler-Bernoulli theory. The authors consider the cross-section area, the second moment of area and the torsional rigidity as functions of the beam-axis coordinate. Then they assume that the cross-sections are such that warping and coupling between bending and torsion are non-existent and negligible. Therefore the paper presents three subsections: axial, torsional and flexural behaviours and each subsection gives a contribution to the stiffness matrix. They show, for several standard end conditions, that the buckling load increases by using a tapered column instead of a prismatic column of the same mass. Unfortunately, this approach is satisfactory for beams with negligible variations of cross-section size only. A previous study (Banerjee and Williams, 1985) derives the exact dynamic stiffness matrix but without including the axial force. Another paper about tapered beams based on the traditional Euler-Bernoulli beam theory is (Arturo Tena Colunga, 1996). This paper presents a method to define two-dimensional and three-dimensional elastic-stiffness matrices for non-prismatic elements, including shear deformations and the shape of the cross-section.

(Hodges, Ho, and Yu, 2008) and (Hodges, Rajagopal, Ho, and Yu, 2011) greatly influenced the study on tapered beams. They consider a more complex approach than the classical beam theory with the aim of obtaining accurate results on stress, strain and displacement fields. The object of the study is a linearly tapered beam with a symmetric cross-section in relation to its longitudinal axis. The hypotheses are an isotropic, homogeneous and linearly elastic material and small displacements. The method used to solve this problem is the Variational Asymptotic Method (VAM), which was developed by Berdichevsky (Berdichevskii, 1979). Hodges, Ho, and Yu (2008) use VAM to perform cross sectional beam analysis using the principle of minimum total potential energy. The model is based on considering the parameter $\delta = a/l$ and the slope of the lateral surface τ, where a is the maximum height of the cross-section and l is the wavelength of deformation along the beam axis. The VAM gives an approximate solution of the strain energy without considering the terms with an order higher than δ^2. The relations obtained from the VAM are compared to the exact elasticity solutions increasing the values of τ and δ till the point at which the VAM solution deviates from the exact elasticity solutions, thus determining the range of applicability of the VAM solution. The limitation is that the authors do not provide information about the generalization of their model, for example to non-symmetric beams. The importance of this work is that the authors investigate the effect of lateral-surface slope associated to the taper. They notice that, imposing the equilibrium on the upper and lower boundary of the beam, the unique parameter necessary to define the boundary equilibrium is the slope τ. The main reason is that the outward unit vector, of the upper and lower boundary, has a non-zero component along the beam longitudinal axis. Therefore it is not correct to consider a variation of cross-section area and a variation of the second moment of area only but it is vital to consider the slope too. There are a lot of recent works based on this non accurate methodology, for example (Abdel-Jaber et al., 2008) (Rosa et al., 2010).

Extending the discussion to beams without any symmetry, it is important to highlight that the barycentre and shear centre vary along the beam axis. In other words, an axial load produces a bending moment and a shear load produces a torque moment. To overcome this problem many authors introduce coupling terms in the formulation (Li and Li, 2002) in order to describe, as accurately as possible, the response of a tapered beam subject to an external load. In (Li and Li, 2002) an equilibrium differential equation is established for tapered beams. This equation simultaneously considers the effects of a constant axial force and shear deformation because a Timoshenko-Euler beam element is been used with appropriate additional terms.

An important contribution for this thesis can be found in the paper Auricchio et al.

(2010), because it shows an application of the dimensional reduction method (Kantorovich and Krylov,1964) and of a mixed formulation to beam models (for more details see Paragraph 2.3). Auricchio et al. (2010) study two-dimensional multi-layered beams, with a constant cross-section along the predominant axis and their goal is to obtain an accurate stress distribution along the cross-section. The hypotheses are limited to small displacements and an isotropic and linearly elastic material.

1.3 Aim of this thesis

The aim of this thesis is to derive models of both symmetric and non-symmetric tapered beams, highly accurate in stress description and free of the limitations encountered by previous studies. In fact, the model will consider the variation of the cross-section by introducing its area and second moment of area as functions of its position along the beam axis. Furthermore, the equilibrium on the upper and lower boundaries of the body will be imposed, emphasising the dependence on their slope. Another important aspect is that the model will also work for non negligible variations of the cross-section and that the coupling between the bending and the axial behaviour will naturally appear.

In Chapter 2 the elasticity theory is shortly illustrated in order to present the adopted notations and variables. After that the concept of variational principle is introduced, focusing on the Total Potential Energy (TPE) functional and the Hellinger-Reissner (HR) functional. By means of this discussion, an appropriate variational principle is chosen as a starting point for the model derivation. In Chapter 3 the attention is focused on the two classical beam theories: Euler-Bernoulli and Timoshenko, and on their integral forms. Chapter 4 describes the derivation of the analytical model under investigation and its application on a prismatic beam, two linearly tapered beams and two curvilinearly tapered beams. For each case a system of six ordinary differential equations in displacement and stress variables is analytically derived, then a system of three ordinary differential equations, in displacement variables only, is recovered from the former. Finally, in Chapter 5 the mentioned systems are solved, referring to appropriate boundary conditions. At this point, an important question should be answered: "How good are the results?". This answer requires the estimation of the solution accuracy, which is possible through the comparison with the Finite Element Method (FEM) and the well-known theories by Euler-Bernoulli and Timoshenko.

Chapter 2

Variational methods in elasticity

The object of the study is the planar body Ω made of a linear elastic material:

$$\Omega \subset \mathbb{R}^2 \text{ closed and bounded} \tag{2.1}$$

Ω is defined as a two-dimensional (2D) body. In engineering, this is equivalent to imposing the plane stress state hypotheses to a three-dimensional (3D) body or stating that the body width is negligible.

The boundary of the domain $\partial\Omega$ is divided in $\partial\Omega_t$ and $\partial\Omega_s$. They are the externally loaded and displacement constrained boundaries, respectively. The vector used to indicate the external load is $\boldsymbol{t}$, also the vector used to indicate the body load is $\boldsymbol{f}$.

The elastic body (Figure 2.1) is assumed homogeneous and continuously distributed over its volume. To simplify the discussion it will also be assumed that the body is isotropic, it means that the elastic properties are the same in all directions.

2.1 Elasticity theory

An elastic body, in a predetermined natural state and in absence of applied forces, can deform under the action of external forces, returning to its initial state once the forces are removed, without being affected by the process of loading and unloading. This phenomenon is therefore reversible, meaning that the strain energy is completely released by the unloading.

When the body Ω is subject to external forces, each point changes its initial position. Therefore, in view of describing the problem, it is necessary to introduce the coordinate

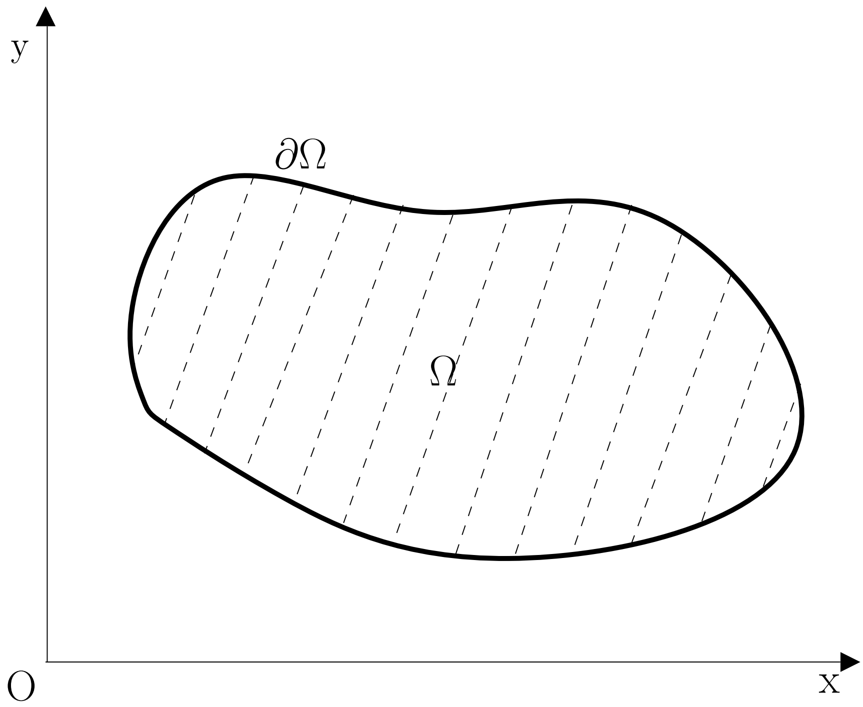

Figure 2.1: 2D elastic body

system xOy (where x and y are the two orthogonal reference axes) (Figure 2.1). A measure of deformation, representing the displacement between two points in the body relative to a reference length, is the strain. In this dissertation, only such small deformations as occur in engineering structures are considered. The small displacements of points of the body Ω can be resolved into components of the displacement field $\boldsymbol{s}$, $u(x, y)$ and $v(x, y)$, respectively parallel to the coordinate axes x and y.

$$\boldsymbol{s} = \begin{pmatrix} u(x, y) \\ v(x, y) \end{pmatrix} \tag{2.2}$$

A given small element of the body Ω, undergoing a deformation, shows a consequent increase in length in the x and y directions. The unit elongation in the x direction is represented by ε_{xx}, the unit elongation in the y direction by ε_{yy} and lastly the distortion of the angle between x and y by ε_{xy}. Therefore, the strain components (ε_{xx}, ε_{yy} and ε_{xy}) completely define the entire state of deformation in the neighborhood of a certain point of the domain and they can be arranged in the well-known strain symmetric tensor $\boldsymbol{\varepsilon}$:

$$\boldsymbol{\varepsilon} = \begin{pmatrix} \varepsilon_{xx} & \varepsilon_{xy} \\ \varepsilon_{xy} & \varepsilon_{yy} \end{pmatrix} \tag{2.3}$$

From the above discussion, it is easy to spell out the relations between the displacement field and the strain components.

$$\varepsilon_{xx} = \frac{\partial u(x,y)}{\partial x} \tag{2.4a}$$

$$\varepsilon_{yy} = \frac{\partial v(x,y)}{\partial y} \tag{2.4b}$$

$$\varepsilon_{xy} = \frac{1}{2}\left(\frac{\partial u(x,y)}{\partial y} + \frac{\partial v(x,y)}{\partial x}\right) \tag{2.4c}$$

Equation (2.4) presents the compatibility equations for the 2D given problem and it can also be written as:

$$\boldsymbol{\varepsilon} = \nabla^s \boldsymbol{s} \tag{2.5}$$

Where ∇^s represents the symmetric gradient operator.

Under the action of external forces, even internal forces are produced between the parts of the body. The magnitudes of such forces are usually defined by their intensity, i.e., by the amount of force per unit area of the surface on which they act. In discussing internal forces, the aforementioned intensity is called stress (Timoshenko and Goodier, 1951). Considering a square neighborhood of a certain point P in a 2D body, three stress components (σ_{xx}, σ_{yy} and σ_{xy}) are sufficient in order to describe the stresses acting on its sides. In fact, by a simple consideration of the equilibrium of the element, the number of components for shear stress can be reduced to one.

$$\sigma_{xy} = \sigma_{yx} \tag{2.6}$$

In continuum mechanics, the Cauchy stress tensor $\boldsymbol{\sigma}$, or simply called the stress tensor, is used to completely define the state of stress at a point inside a material in the deformed configuration.

$$\boldsymbol{\sigma} = \begin{pmatrix} \sigma_{xx} & \sigma_{xy} \\ \sigma_{xy} & \sigma_{yy} \end{pmatrix} \tag{2.7}$$

Once the tensors $\boldsymbol{\sigma}$ and $\boldsymbol{\varepsilon}$ have been defined, it is possible to introduce the relation between the stress components and the strain components. As commonly known, considering two bodies with the same geometry but made of different materials, the strains, generated by an applied force, are not the same. As a consequence, it is important to introduce the constitutive equations and, in the hypothesis of an isotropic linear elastic material, they result as follows:

$$\sigma_{xx} = \frac{E}{1-\nu^2}(\varepsilon_{xx} + \nu\varepsilon_{yy}) \tag{2.8a}$$

$$\sigma_{yy} = \frac{E}{1-\nu^2}(\nu\varepsilon_{xx} + \varepsilon_{yy}) \tag{2.8b}$$

$$\sigma_{xy} = \frac{E}{2(1+\nu)}\varepsilon_{xy} \tag{2.8c}$$

Where E and ν are the two well-known elastic constants: Young's modulus and Poisson's ratio. Equation (2.8) can also be written in a matrix form:

$$\boldsymbol{\sigma} = \boldsymbol{C} : \boldsymbol{\varepsilon} \tag{2.9}$$

Where $\boldsymbol{C}$ represents the fourth order linear elastic tensor, whose full verbalization follows below:

$$\frac{E}{1-\nu^2}\begin{pmatrix} 1 & \nu & 0 \\ \nu & 1 & 0 \\ 0 & 0 & \dfrac{1-\nu}{2} \end{pmatrix} \tag{2.10}$$

Since the tensor $\boldsymbol{C}$ is invertible, it is possible to calculate the inverse tensor $\boldsymbol{D}$:

$$\boldsymbol{D} = \frac{1}{E}\begin{pmatrix} 1 & -\nu & 0 \\ -\nu & 1 & 0 \\ 0 & 0 & 2(1+\nu) \end{pmatrix} \tag{2.11}$$

By doing this, another way of writing the constitutive equations can be obtained:

$$\boldsymbol{\varepsilon} = \boldsymbol{D} : \boldsymbol{\sigma} \tag{2.12}$$

Lastly, in the matter of introducing the equilibrium of the body Ω, a square neighborhood of a certain point P is considered. Therefore, its translational equilibrium for the horizontal components and its translational equilibrium for the vertical components can be written as follows:

$$\frac{\partial \sigma_{xx}}{\partial x} + \frac{\partial \sigma_{yx}}{\partial y} + f_x = 0 \tag{2.13a}$$

$$\frac{\partial \sigma_{xy}}{\partial x} + \frac{\partial \sigma_{yy}}{\partial y} + f_y = 0 \tag{2.13b}$$

The equilibrium equations, illustrated in (2.13), can also be expressed in matrix form:

$$\nabla \cdot \boldsymbol{\sigma} + \boldsymbol{f} = \mathbf{0} \tag{2.14}$$

Where the symbol ∇ represents the gradient operator.

Once the elastic problem is formulated, the solution of a given problem must satisfy the compatibility equations (2.4), the constitutive equations (2.8) and the equilibrium equations (2.13). The solving process of a 2D linear elastic body, subject to external forces, then, consists of deriving the three components of the stress tensor $\boldsymbol{\sigma}$, the three components of the strain tensor $\boldsymbol{\varepsilon}$ and the two components of the displacement vector $\boldsymbol{s}$ for each point of its domain.

2.2 Variational principles

The equations related to an elastic problem, subject to given conditions, may be frequently intractable. In such event, the variational principles can provide a means of obtaining an approximation to the desired solution. This section will cover the description of the main variational principles in elasticity, considering the hypotheses and the 2D body illustrated in the previous paragraph.

It is possible to classify the variational principles in "one-field" principles and mixed principles. The basic variational principle in structural mechanics is the principle of Total Potential Energy (TPE). It can be called "one-field" principle (Kardestuncer et al., 1987) because the displacements are the only solution variables. Sometimes, the mixed principles could also be used in mechanics problems, since they present some advantages with respect to the "one-field" principle. An example of a mixed principle is the Hellinger-Reissner (HR) principle and it can be called "two-field" principle because the displacements and the stresses are the solution variables. The HR principle is very useful because it solves directly for the stresses, which are the primary variables of interest.

The main steps to be followed in order to describe the classical variational procedure, for finding the desired solution, are listed below (Reddy, 2006):

- To cast a given differential equation in variational form
- To determine the approximate solution using a variational method, such as the Ritz

method, the Galerkin method, or other methods

There are two possible ways related to the first step. The first one provides that the variational form is achieved from the differential form, the second one that the variational form is recovered from a variational principle suitable to describe the given problem. The variational form thus obtained represents the weak form or the integral form used for the study of the problem. For example, considering the TPE principle, its weak formulation is equivalent to the minimization of its functional. The term "functional" is used to describe a function, defined by integral, whose arguments are functions themselves. Loosely speaking, a functional is a "function of functions" (Reddy, 2006).

Once the variational form is derived, the solution can be calculated by using different analysis methods, according to the previously listed second step.

The adopted methods are easily classified into analytical methods and numerical ones. An analytical procedure allows to obtain an exact solution by using exact methods, or to determine an approximate solution by referring, for example, to the Ritz method and the Galerkin method. On the other hand, the numerical methods are divided into numerical solution of the differential equations (numerical integration and finite differences) and FEM (RAO, 2011).

In the next paragraphs the following variational principles are presented: the TPE functional (par. 2.2.1) and the HR functional (par. 2.2.2), considering for each of them different possible stationarity conditions.

2.2.1 Total Potential Energy functional

The TPE functional is referred to the TPE principle and it is one of the most common principles in solid mechanics.

The integral form of the TPE can be expressed as follows:

$$J_{TPE}(\boldsymbol{s}) = \frac{1}{2}\int_{\Omega} \left(\nabla^s \boldsymbol{s} : \boldsymbol{C} : \nabla^s \boldsymbol{s}\right) d\Omega - \int_{\Omega} \left(\boldsymbol{s} \cdot \boldsymbol{f}\right) d\Omega - \int_{\partial\Omega_t} \left(\boldsymbol{s} \cdot \boldsymbol{t}\right) dS \tag{2.15}$$

Minimizing the functional in (2.15), the correspondent weak form or, in other words, the variational form is achieved:

$$\delta J^s_{TPE} = \int_{\Omega} \left(\nabla^s (\delta \boldsymbol{s}) : \boldsymbol{C} : \nabla^s \boldsymbol{s}\right) d\Omega - \int_{\Omega} \left(\delta \boldsymbol{s} \cdot \boldsymbol{f}\right) d\Omega - \int_{\partial\Omega_t} \left(\delta \boldsymbol{s} \cdot \boldsymbol{t}\right) dS = 0 \tag{2.16}$$

The procedure followed to find the minimum of a functional is also called stationarity.

The weak problem consists of finding $\boldsymbol{s}$ such that, for all admissible variations of $\boldsymbol{s}$ ($\delta\boldsymbol{s}$), Equation (2.16) is satisfied. The operator "δ" is called variational symbol (Reddy, 2006). If δ is applied to a variable, in this case to $\boldsymbol{s}$, it means that the variation $\delta\boldsymbol{s}$ of the variable $\boldsymbol{s}$ is an admissible change in the variable $\boldsymbol{s}$ at a fixed value of x and y. According to Equation (2.16), the vector $\boldsymbol{s}$ must belong to $H^1(\Omega)$. More precisely, both $\boldsymbol{s}$ and $\nabla^s\boldsymbol{s}$ are square integrable on Ω. Its variation $\delta\boldsymbol{s}$ must belong to $H^1(\Omega)$ too.

When the TPE principle is applied to an elastic body, it gives the equilibrium equations in terms of the displacements because the constitutive and compatibility relations are assumed to replace the stresses in terms of the displacements (Reddy, 2002). Moreover, it has been found that the displacements are the only solution variables and they must satisfy suitable displacement boundary conditions. Once the displacements are calculated, the other variables of interest such as strains and stresses can be directly obtained.

2.2.2 Hellinger-Reissner functional

The HR functional is associated to a saddle point problem and it represents an example of mixed formulation.

Generally, the objective in mixed formulations is to relax the conditions to be satisfied by the solution variables, and enlarge the solution variables which may simultaneously include displacements, strains and stresses (Bathe, 1982).

In the case of HR functional, the displacement field and the stress field are unknown, meaning that an accurate selection of displacement functions, but mainly of stress functions, are required. This aspect sometimes causes difficulties, but other times can give great advantages to the formulation. The HR functional can be expressed as follows:

$$J_{HR}(\boldsymbol{s},\boldsymbol{\sigma}) = \int_{\Omega}(\boldsymbol{\sigma}:\nabla^s\boldsymbol{s})\,d\Omega - \frac{1}{2}\int_{\Omega}(\boldsymbol{\sigma}:\boldsymbol{D}:\boldsymbol{\sigma})\,d\Omega - \int_{\Omega}(\boldsymbol{s}\cdot\boldsymbol{f})\,d\Omega - \int_{\partial\Omega_t}(\boldsymbol{s}\cdot\boldsymbol{t})\,dS \tag{2.17}$$

Invoking the stationarity of the HR functional (2.17), that corresponds to a saddle point problem, the following expression is obtained:

$$\begin{aligned}\delta J_{HR}^{gg} = \int_{\Omega}(\nabla^s\delta\boldsymbol{s}:\boldsymbol{\sigma})\,d\Omega + \int_{\Omega}(\delta\boldsymbol{\sigma}:\nabla^s\boldsymbol{s})\,d\Omega - \int_{\Omega}(\delta\boldsymbol{s}:\boldsymbol{D}:\boldsymbol{\sigma})\,d\Omega \\ - \int_{\Omega}(\delta\boldsymbol{s}\cdot\boldsymbol{f})\,d\Omega - \int_{\partial\Omega_t}(\delta\boldsymbol{s}\cdot\boldsymbol{t})\,dS = 0\end{aligned} \tag{2.18}$$

The related weak problem consists of finding $\boldsymbol{s}$ and $\boldsymbol{\sigma}$ such that for all $\delta\boldsymbol{s}$ and for all $\delta\boldsymbol{\sigma}$ the weak form (2.18) is satisfied. The vector $\boldsymbol{s}$ belongs to $H^1(\Omega)$ and the symmetric stress tensor $\boldsymbol{\sigma}$ belongs to $L^2(\Omega)$. The variation $\delta\boldsymbol{s}$ must belong to $H^1(\Omega)$ too. It is important to remark that the kinematic boundary condition represents an essential condition, while the equilibrium turns out to be a natural boundary condition of the problem. Equation (2.18) is called HR grad-grad stationarity by Auricchio et al. (2010) because two gradient operators appear in the formulation.

Integrating by parts the first and the second terms of (2.18), it results as follows:

$$\int_\Omega (\nabla^s \delta\boldsymbol{s} : \boldsymbol{\sigma})\, d\Omega = \int_{\partial\Omega} (\delta\boldsymbol{s} \cdot \boldsymbol{\sigma} \cdot \boldsymbol{n})\, dS - \int_\Omega (\delta\boldsymbol{s} \cdot \nabla \cdot \boldsymbol{\sigma})\, d\Omega \tag{2.19a}$$

$$\int_\Omega (\delta\boldsymbol{\sigma} : \nabla^s \boldsymbol{s})\, d\Omega = \int_{\partial\Omega} (\delta\boldsymbol{\sigma} \cdot \boldsymbol{n} \cdot \boldsymbol{s})\, dS - \int_\Omega (\nabla \cdot \delta\boldsymbol{\sigma} \cdot \boldsymbol{s})\, d\Omega \tag{2.19b}$$

Where $\boldsymbol{n}$ indicates the outward unit vector on the border $\partial\Omega$ (Figure 2.1). By substituting (2.19) in (2.18) the weak problem becomes: find the vector $\boldsymbol{s}$ and the symmetric stress tensor $\boldsymbol{\sigma}$ such that for all $\delta\boldsymbol{s}$ and for all $\delta\boldsymbol{\sigma}$:

$$\begin{aligned} \delta J^{dd}_{HR} = -\int_\Omega (\delta\boldsymbol{s} \cdot \nabla \cdot \boldsymbol{\sigma})\, d\Omega - \int_\Omega (\nabla \cdot \delta\boldsymbol{\sigma} \cdot \boldsymbol{s})\, d\Omega - \int_\Omega (\delta\boldsymbol{s} : \boldsymbol{D} : \boldsymbol{\sigma})\, d\Omega \\ - \int_\Omega (\delta\boldsymbol{s} \cdot \boldsymbol{f})\, d\Omega - \int_{\partial\Omega_s} (\delta\boldsymbol{\sigma} \cdot \boldsymbol{n} \cdot \bar{\boldsymbol{s}})\, dS = 0 \end{aligned} \tag{2.20}$$

From Equation (2.20), it can be noticed that less conditions on the displacement field are required; therefore the vector $\boldsymbol{s}$ must belong at least to the space $L^2(\Omega)$ and it is no longer necessary that $\nabla^s \delta\boldsymbol{s}$ be square integrable on Ω. On the other hand, σ must belong to $H(div, \Omega)$ so a heavier condition on the stress field must be imposed, where $H(div, \Omega)$ is the space of square integrable symmetric matrix fields with square integrable divergence (Arnold and Falk, 1988). In this case, the kinematic boundary condition is a natural boundary condition, on the other hand the equilibrium becomes an essential condition of the problem. Equation (2.20) is here called div-div stationarity according to (Auricchio et al., 2010) because two divergence operators appear in it.

The difference between the HR grad-grad formulation and the HR div-div formulation is that in the first one the derivatives are applied to the displacement field, whereas in the second one they are applied to the stress field.

2.3 Dimensional reduction method

The dimensional reduction method occupies an intermediate position between the exact solution of the problem and the methods of Ritz and Galerkin. In the Ritz method the problem of the minimum of a double integral is reduced to the problem of the minimum of a function of several variables. This is accomplished by choosing the form of the solution a priori and only afterwards selecting the best values of the constants figuring in it (Kantorovich and Krylov, 1964).

The dimensional reduction method is a general mathematical procedure proposed by Kantorovich and Krylov (1958), therefore it is sometimes associated with the name of L.V. Kantorovich. This method uses the geometry of the domain to reduce the problem dimension. For example, considering a 2D body, a problem characterized by a double integral is reduced to a problem with a single integral. This method is capable of giving a solution with a greater accuracy and only part of the expression giving the solution is chosen a priori.

There are different approaches for solving a problem by means of the dimensional reduction method. Here follows the procedure illustrated in (Auricchio et al., 2010), but many other ways can be used to reduce the dimension of the problem, for example the ones proposed by Vogelius and Babuska (1981a,b,c).

A generic variable of the problem is indicated with $\gamma(x, y)$. The aim of the dimensional reduction method is to approximate, as well as possible, the variable $\gamma(x, y)$ in a linear combination of other two variables: the first one is function of y only and the second one is function of x only. By doing this, the dimension of the problem is reduced. Therefore $\gamma(x, y)$ is expressed as:

$$\gamma(x, y) = \boldsymbol{p}_\gamma(y)\bar{\boldsymbol{\gamma}}^T(x) \tag{2.21}$$

Where $\boldsymbol{p}_\gamma(y)$ is a set of arbitrary functions of y and $\bar{\boldsymbol{\gamma}}^T(x)$ (superscript T denotes transposition) is a set of arbitrary functions of x.

For instance, the variable $\gamma(x, y)$ can be assumed to be a linear function with respect to the variable y. Therefore $\boldsymbol{p}_\gamma(y)$ is considered as a set of linearly functions of y and $\bar{\boldsymbol{\gamma}}^T(x)$ as a set of arbitrary functions of x.

$$\gamma(x, y) = \boldsymbol{p}_\gamma(y)\bar{\boldsymbol{\gamma}}^T(x) \qquad \boldsymbol{p}_\gamma(y) = \{1 \quad y\} \qquad \bar{\boldsymbol{\gamma}}^T(x) = \{\gamma_0(x) \quad \gamma_1(x)\} \tag{2.22}$$

From Equation (2.22), the decoupling between x and variable y is evident.

2.4 Finite element method

The FEM consists of converting a problem with an infinite number of degrees of freedom to one with a finite number, in order to simplify the solution process (Weaver and Johnston, 1986). Referring to the variational formulations, previously discussed in Paragraph (2.2), the FEM can be seen as a piecewise application of a variational method. Therefore it makes use of the variational principles to formulate the discrete equations for a sub domain, called element.

A standard FEM is organized into the following steps, according to Kardestuncer et al. (1987). The first step consists of defining the problem and its domain, in which the first source of approximation appears. The second source of approximation concerns the discretization of the domain, which represents one of the basic concepts of the FEM.

The discretization consists of choosing a certain number of discrete points of a body and focusing on them only. This is equivalent to describe a structure by a finite number of points. One way to discretize a structure is to divide it into an equivalent system of structures or small units, such that their assembly corresponds to the real structure. By doing this, a mesh for a large number of subdivisions is generated. Since it is not possible to manually analyse a lot of data, the electronic processor is used, also because the method can be programmed in a relatively straightforward way. Most commercial softwares are based on the FEM and it is one of the most used methods in engineering. The development of the method essentially coincided with the development of computers, although its mathematical foundations can be traced back to years ago (Courant et al., 1943).

The third step of the standard FEM is the formulation of the problem. Very often a physical problem is formulated either by a system of differential equations or by an integral equation (a functional) subject to stationarity requirement (minimum or saddle), as previously discussed (Paragraph 2.2). The first formulation is referred to as the operational form of the problem, the second formulation is referred to as the variational form of the same problem.

After the local coordinate system has been chosen, it is necessary to construct approximate functions for each element. At this stage, the modelling of the problem has been completed. After that, by substituting the approximate functions in the problem formulation, the element matrices and the equations are obtained.

The assembly of element equations is another important step. It is done according to the local coordinate system of the elements and, after this, the transformation into the global system follows. The assembly is made through the nodes at the interfaces, which are common to the adjacent elements.

The last step of the FEM is the introduction of boundary conditions and the solution of the final system of equations.

2.5 Conclusions on variational methods

In this section a general overview of the problem to be analysed has been described.

The considered 2D body is made of a linear elastic isotropic material and its study is based on the hypothesis of small displacements. Then two different possible variational formulations have been described, noticing that the TPE principle is a "one-field" principle and the HR principle is a "two-field" principle because the stress field is also considered as a independent variable of the problem.

The main advantage in using a mixed formulation, in particular the HR formulation, is that it gives the possibility to accurately describe the stress profiles, even if simple assumptions on the displacement and stress fields are considered(as it will be clearly noticed in the next chapters). Another reason to prefer a mixed method is that the variable of most interest and one of the fundamental unknown to be computed is the stress. For a "one-field" formulation, instead, this variable is not a fundamental unknown and it is obtained a posteriori, which means a loss in accuracy.

The variational formulation is the starting equation of a variational method, it is then important to choose the principle in such way that ensures a correct study of the problem.

Chapter 3

Classical beam theories

3.1 Geometry definition

The term "beam" is referred to a 3D body with two dimensions negligible with respect to the third dimension. Considering the cross-section in the plane yz and applying a translation along the direction of x, the beam will be generated. This way, it is possible to define its longitudinal axis as the locus of the cross-section barycentres. The axes x, y and z (see Figure 3.1) are the local axes of the beam and, in the case under investigation, they are coincident with the global axes. In Figure 3.1, it can clearly be noticed that x is the coordinate of the beam longitudinal axis and, obviously, it is the predominant dimension of the body.

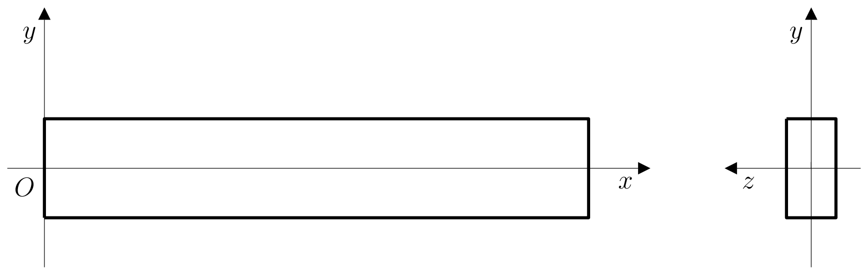

Figure 3.1: 3D beam and adopted coordinate system

In the next sections the main assumptions of the two classical beam theories, Euler-Bernoulli and Timoshenko, will be illustrated. Then, for each of them, the differential forms and the integral forms, used as an alternative starting point to solve the same problem, will be derived.

3.2 Euler-Bernoulli beam theory

3.2.1 Assumptions

Several beam theories have been developed, each characterized by a different level of accuracy. The classical and simplest beam theory is the Euler-Bernoulli beam theory. One of its fundamental assumptions is that the cross-section of the beam is rigid in its own plane; in other words, no deformations occur in the plane of the cross-section (Bauchau and Craig, 2009). An additional assumption is that the cross-section remains plane and normal to the deformed axis of the beam, it means that there are no shear flows.

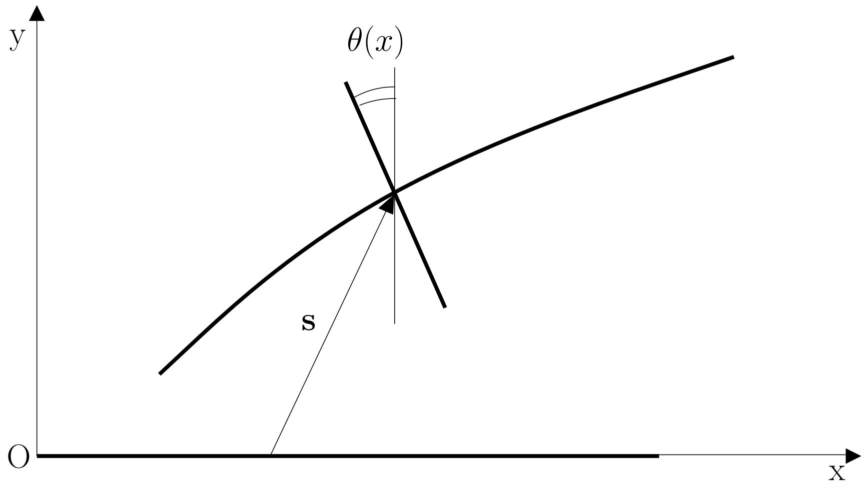

Figure 3.2: Kinematics of Euler-Bernoulli beam theory

As a consequence of these three assumptions, the two functions that govern the kinematics of the beam are the axial displacement $u(x)$ and the deflection $v(x)$. The rotation $\theta(x)$ depends on $v(x)$ and it is given by the following expression (Figure 3.2):

$$\theta(x) = -tan^{-1}v'(x) \tag{3.1}$$

Equation (3.1) can also be written as follows because the hypothesis of small displacement is considered:

$$\theta(x) = -v'(x) \tag{3.2}$$

Where $\theta(x)$ represent the rotation of the cross-section in the plane xy and it is positive if clockwise with respect to the undeformed configuration. Moreover, Equation (3.2) dictates that the shear flows in the beam are equal to zero.

At this point, suitable hypotheses on the displacement field are assumed, according to the mentioned assumptions:

$$u(x, y) = u(x) + y\theta(x) \tag{3.3a}$$

$$v(x, y) = v(x) \tag{3.3b}$$

Where $u(x, y)$ and $v(x, y)$ are the two components of the displacement vector $\boldsymbol{s}$, defined in Equation (2.2).

Two ways to formulate the Euler-Bernoulli beam are illustrated. The first one is the Euler-Bernoulli equation (differential form) and the second one is the principle of virtual work (integral form). The Euler-Bernoulli equation describes the relationship between the beam deflection and the applied load, the principle of virtual work, instead, is an alternative writing of the beam equilibrium.

3.2.2 Differential form

The Euler-Bernoulli equation is widely used in engineering practice and it arises from a combination of these equations: force resultant, equilibrium, compatibility and constitutive equations. The procedure used to derive the Euler-Bernoulli equation is here illustrated.

When the beam is subject to a generic external force, characterized by a component in the direction of x and a component in the direction of y, the following stresses are generated:

- axial force N
- bending moment M, acting in the plane xy
- shear force V, acting in the direction of y

Referring to the symmetric stress tensor, defined in Equation (2.7), and assuming the component σ_{yy} equal to zero, the three stresses, N, M and V, can easily be calculated for a chosen cross-section. Their expressions are hereby written as force resultants of σ_{xx} and σ_{xy}, where A is the area of the cross-section:

$$N = \int_A \sigma_{xx} dA \qquad M = -\int_A y\sigma_{xx} dA \qquad V = \int_A \sigma_{xy} dA \tag{3.4}$$

The translational equilibrium in the direction of x, in the direction of y and the rotational equilibrium follow below, noticing that p indicates the distributed load in the direction of

x and q is the distributed load in the direction of y:

$$\frac{dN}{dx} + p = 0 \qquad \frac{dV}{dx} - q = 0 \qquad \frac{dM}{dx} - V = 0 \tag{3.5}$$

After that, according to the assumptions of the Euler-Bernoulli beam theory, the compatibility equations and the constitutive equations can be written as follows (see the compatibility equations and the constitutive equations in (2.4) and (2.8):

$$\varepsilon_{xx} = u'(x) + y\theta'(x) \qquad \varepsilon_{yy} = 0 \qquad \varepsilon_{xy} = 0 \tag{3.6}$$

$$\sigma_{xx} = E\varepsilon_{xx} \qquad \sigma_{yy} = 0 \qquad \sigma_{xy} = 0 \tag{3.7}$$

Where ε_{xx}, ε_{yy} and ε_{xy} are the components of the strain symmetric tensor $\boldsymbol{\varepsilon}$, defined in (2.3).

Once all equations have been derived, by suitably collecting them, it is possible to achieve the well-known Euler-Bernoulli equation and the equation that governs the extensional behaviour of the beam.

$$EIv^{IV}(x) + q = 0 \tag{3.8}$$

$$EAu''(x) + p = 0 \tag{3.9}$$

Where E represents Young's modulus, I the second moment of area, $v(x)$ the deflection and $v^{IV}(x)$ the fourth derivative of $v(x)$ with respect to x.

As an example, a 2D cantilever beam with a point load P at its free end is considered. The distributed loads q and p are equal to zero and the following boundary conditions are imposed:

$$\begin{aligned} v(0) &= 0 \qquad & v''(L) &= 0 \\ v'(0) &= 0 \qquad & v'''(L) &= -P/(EI) \\ u(0) &= 0 \qquad & u(L) &= 0 \end{aligned} \tag{3.10}$$

Solving Equation (3.8) and Equation (3.9) in the conditions (3.10), the following results are obtained:

$$v(x) \to \frac{3LPx^2 - Px^3}{6EI} \tag{3.11}$$

$$u(x) \to 0 \tag{3.12}$$

From this result it is possible to recover the stresses N, M and V, in each cross-section of the beam.

As it is possible to notice, there is a basic inconsistency in the Euler-Bernoulli beam theory. In particular, it is impossible to define the shear force V as resultant of the shear stress component σ_{xy}, because this component is zero by assumption. Furthermore, since one of the Euler-Bernoulli assumptions is that, during the deformation, the shear flows are zero, this theory is used to study thin beams in which bending behaviour is predominant compared to shear behaviour and the latter can be considered negligible.

3.2.3 Integral form

The principle of virtual work can be chosen as an integral form to solve a beam in Euler-Bernoulli assumptions, as shown in Chapter 5.

Considering a force system that must satisfy the equilibrium equations and a displacement-deformation system that must verify the compatibility equations, the principle of virtual work states that the virtual work of the applied forces is zero for all virtual displacements of the system from the static equilibrium. Then, in order to guarantee the static equilibrium, it is necessary that the applied forces and the constraint forces on the beam equilibrium be such that the body does not move.

The main steps, followed in order to pass from the differential form (3.8) to the integral form (the principle of virtual work), are here illustrated. Assuming p equal to zero, only the bending contribution will be considered to derive the integral form. First of all it is necessary to multiply the differential form (3.8) by any function w (weight function) and integrate over the longitudinal axis ℓ.

$$\int_\ell \left[w\left(EIv^{IV}(x) - q\right)\right] dx = 0 \tag{3.13}$$

After that, integrating twice by parts, the principle of virtual work arises:

$$\int_\ell \left[w'' EIv''(x)\right] dx = \int_\ell \left[wq\right] dx - \left[wEIv'''(x)\right]_{\partial\ell} + \left[w' EIv''(x)\right]_{\partial\ell} \tag{3.14}$$

It can be noticed that the first member of Equation (3.14) represents the internal work, the second member, instead, represents the external work.

Equation (3.14) represents the principle of virtual work for a beam in the hypotheses of Euler-Bernoulli. It will be used in Chapter 5 to evaluate the deflection of some cantilever beams in their free end, in particular prismatic and non-prismatic beams.

3.3 Timoshenko beam theory

3.3.1 Assumptions

When considering the Timoshenko theory, the main hypothesis is that the cross-sections remain plane but not necessarily normal to the centreline of the beam. Then the cross-section of the beam is rigid in its own plane; in other words, no deformations occur in the plane of the cross-section. The variation of the angle between the cross-section and the normal to the deformed axis represents the shear flow γ (Figure 3.3) and it is assumed positive if the cross-section rotates clockwise with respect to the normal of the deformed axis. In the hypothesis of small displacements it results as follows:

$$\gamma = \theta(x) + v'(x) \tag{3.15}$$

It can be noticed that the Euler-Bernoulli model is obtained from the Timoshenko model by imposing the shear flow equal to zero.

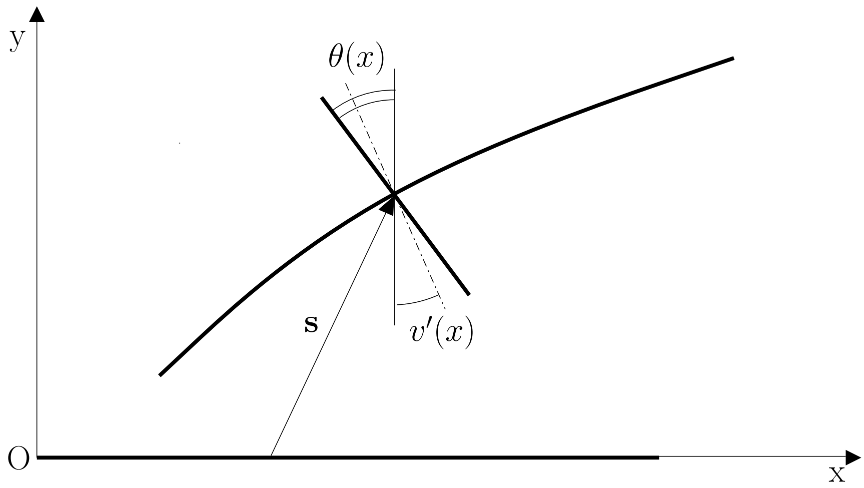

Figure 3.3: Kinematics of Timoshenko beam theory

Two ways to formulate the Timoshenko beam can be adopted, as shown for the Euler-Bernoulli beam. The first one is the differential form, in which both the shear contribution and the bending contribution to the deflection are considered, the second one, instead, is the integral form, such as the principle of virtual work, as shown in Chapter 5.

At this point, in order to introduce the differential form, suitable hypotheses on the displacement field are assumed:

$$u(x, y) = u(x) + y\theta(x) \tag{3.16a}$$

$$v(x, y) = v(x) \tag{3.16b}$$

Where $u(x, y)$ and $v(x, y)$ are the two components of the displacement vector $\boldsymbol{s}$, defined in Equation (2.2), $u(x)$ and $v(x)$ are the axial displacement and the deflection of the beam, lastly $\theta(x)$ represents the rotation of the cross-section in the plane xy and it is assumed positive, if clockwise with respect to its undeformed configuration.

The Timoshenko theory is widely used in engineering practice, in particular for cases with a non-negligible shear contribution to the deflection.

3.3.2 Differential form

The differential form of the Timoshenko theory arises from a combination of the following equations: force resultant, equilibrium, compatibility and constitutive equations.

According to the assumptions of the Timoshenko theory, the compatibility and the constitutive equations can be written as follows (see the compatibility equations and the constitutive equations in (2.4) and (2.8)):

$$\varepsilon_{xx} = u'(x) + y\theta'(x) \qquad \varepsilon_{yy} = 0 \qquad \varepsilon_{xy} = \frac{1}{2}(\theta(x) + v'(x)) \tag{3.17}$$

$$\sigma_{xx} = E\varepsilon_{xx} \qquad \sigma_{yy} = 0 \qquad \sigma_{xy} = \frac{E}{2(1+\nu)}\varepsilon_{xy} \tag{3.18}$$

Considering the force resultant equations (3.4) and the equilibrium equations (3.5), suitably collected with (3.17) and (3.18), it is possible to achieve the differential form of the Timoshenko beam theory.

$$\frac{EA_s}{2(1+\nu)}(\theta(x) + v'(x)) - EI\theta''(x) = 0 \tag{3.19a}$$

$$\frac{EA_s}{2(1+\nu)}(\theta'(x) + v''(x)) = -q \tag{3.19b}$$

$$EAu''(x) = -p \tag{3.19c}$$

Where A_s is equal to kA, the constant k is the shear factor and A is the area of the cross-section. Focusing on the system (3.19), the third equation governs the extensional behaviour of the beam and it is perfectly analogous to Equation (3.9) obtained for the Euler-Bernoulli beam theory.

The assumptions of the Timoshenko beam theory imply that the distribution of the shear stress must be constant along the cross-section. In order to overcome this limitation, the shear factor k must be introduced and, since the cross-section is rectangular, it can be assumed equal to 5/6 according to Jourawsky theory.

The Jourawsky theory is an approximate theory valid for relatively thin and prismatic beams and it is used to evaluate the distribution of the shear stress along the beam cross-section. Its main hypotheses are that the distribution of the shear stress is considered parabolic and the values on the upper and lower borders of the cross-section are equal to zero.

3.3.3 Integral form

The main steps, followed in order to pass from the differential form (3.19) to the integral form (the principle of virtual work) are here illustrated. Assuming p equal to zero, the bending and the shear will be the only contributions to be considered in order to derive the principle of virtual work. First of all it is necessary to multiply Equation (3.19a) by any function r (weight function) and integrate over the longitudinal axis ℓ.

$$\int_\ell r \left[\frac{EA_s}{2(1+\nu)} (\theta(x) + v'(x)) \right] dx - \int_\ell rEI\theta''(x)dx = 0 \tag{3.20}$$

After that, integrating once by parts the second integral, the following expression is derived:

$$\int_\ell r \left[\frac{EA_s}{2(1+\nu)} (\theta(x) + v'(x)) \right] dx + \int_\ell r'EI\theta'(x)dx - [rEI\theta'(x)]_{\partial\ell} = 0 \tag{3.21}$$

By following the same procedure and considering the function t as weight function, Equation (3.19b) becomes:

$$\int_\ell t \left[\frac{EA_s}{2(1+\nu)} (\theta'(x) + v''(x)) \right] dx + \int_\ell tqdx = 0 \tag{3.22}$$

Then, integrating once by parts the first integral, the following expression is obtained:

$$-\int_\ell t' \left[\frac{EA_s}{2(1+\nu)} (\theta(x) + v'(x)) \right] dx + \int_\ell tqdx + \left[\frac{EA_s}{2(1+\nu)} t\,(\theta(x) + v'(x)) \right]_{\partial\ell} = 0 \tag{3.23}$$

The principle of virtual work for a beam in the hypotheses of Timoshenko arises from summing (3.21) with (3.23):

$$\int_\ell (r - t') \left[\frac{EA_s}{2(1+\nu)} (\theta(x) + v'(x)) \right] dx + \int_\ell r' EI\theta'(x) dx = - \int_\ell tq dx + \\ + [rEI\theta'(x)]_{\partial\ell} - \left[\frac{EA_s}{2(1+\nu)} t \left(\theta(x) + v'(x)\right) \right]_{\partial\ell} \tag{3.24}$$

It can be noticed that the first member of Equation (3.24) represents the internal work, the second term, instead, represents the external work.

The principle of virtual work, written in the Timoshenko hypotheses, will be used in Chapter 5 to evaluate the deflection of some cantilever beams in their free end.

3.4 Conclusion on classical beam theories

The Euler-Bernoulli and Timoshenko beam theories are two simplifications of the linear theory of elasticity and they provide a means of calculating the deflection characteristics of beams. The difference between these two theories is that the Timoshenko beam theory considers the shear flow and it is applicable for thick beams too. The Euler-Bernoulli beam theory, instead, takes account of the bending behaviour only, therefore it is applicable for thin beams where the shear behaviour is negligible.

These well-known theories were mentioned because they will be used in Chapter 5 to evaluate the deflection in the right end of some non-prismatic cantilever beams. The results, obtained with the Euler-Bernoulli and Timoshenko beam theories, will be compared to the results obtained by using the analytical variational method (Chapter 4) and the FEM (by means the software Abaqus).

Chapter 4

Non-prismatic beams: new analytical analysis

In this chapter, prismatic and non-prismatic beam models are analytically derived by the dimensional reduction method based on the HR principle. The five cases analysed are: a prismatic beam, two linearly tapered beams, symmetric and non symmetric with respect to the longitudinal axis, and lastly two curvilinearly tapered beams, in symmetric and non-symmetric configurations. The HR principle is preferred to the TPE principle, both of them illustrated in Chapter 2, because HR principle also introduces stresses as variables of the problem. The stresses are the variables of much interest and, by using a mixed approach, they can be directly evaluated and considered separately.

Starting from the HR principle, a system of six ordinary differential equations (ODEs) is derived because six unknown variables are considered in the formulation: three displacement and three stress variables. After that, by means of the static condensation procedure, the system of three ODEs is obtained, in which the only variables are the displacements. The method used in order to solve the double integral of the HR principle is the dimensional reduction method, illustrated in Chapter 2. This method is here adopted for the great advantage in reducing the dimension of the problem.

The adopted programming software is Wolfram Mathematica version 7. Mathematica is a very large system and it contains thousands of functions for performing various tasks in science, mathematics, engineering, and many other disciplines. The following manuals have been consulted for the implementation: Wellin (2013), Abell and Braselton (2008) and Hazrat (2010).

4.1 Geometry definition

The object of the study is a planar beam Ω with a generic non-prismatic shape and described as a 2D body as shown in Figure 4.1. This is equivalent to imposing the plane stress state hypotheses to a 3D body or to stating that the body width is negligible. Moreover, the following hypotheses are considered: small displacements and a linear elastic isotropic material.

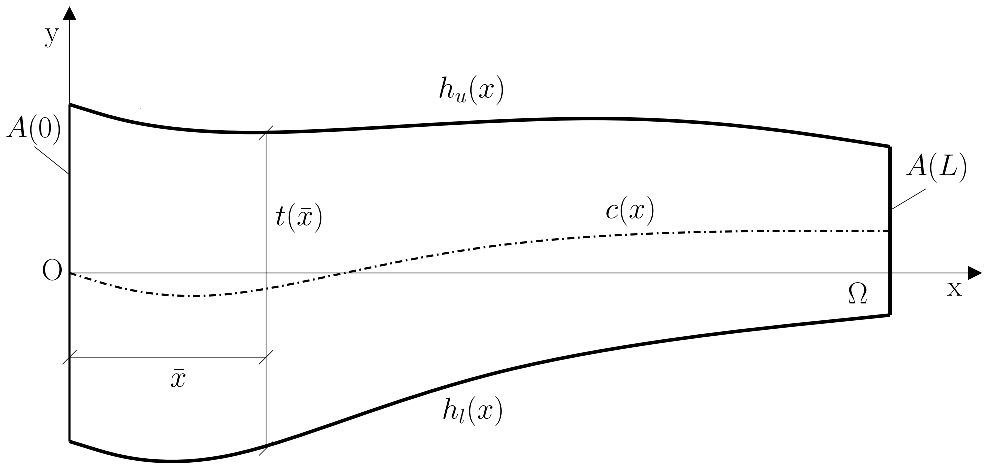

Figure 4.1: Generic non-prismatic beam

The domain of the problem is here defined:

$$\Omega \subset \mathbb{R}^2 : (x, y) \mid x \in \ell \text{ and } y \in A(x) \tag{4.1}$$

Where ℓ is the beam longitudinal axis and $A(x)$ is the area of the cross-section. In particular they are expressed as follows, indicating with L the beam length and with $h_u(x)$ and $h_l(x)$ the upper and lower limits of the domain:

$$\ell = \{x \in \mathbb{R} | x \in [0, L]\}\,,\ A(x) = \{y \in \mathbb{R} | y \in [h_l(x), h_u(x)]\} \tag{4.2}$$

Obviously, the longitudinal axis ℓ is the predominant dimension of the body, as usually assumed by the beam definition . The right and the left limits of the domain Ω are indicated with $A(0)$ and $A(L)$ as shown in Figure 4.1, therefore the border $\partial\Omega$ can be expressed as $A(0) \cup A(L) \cup h_u(x) \cup h_l(x)$. Furthermore $\partial\Omega$ is divided into the following parts: $\partial\Omega_t$ and $\partial\Omega_s$ according to whether the loaded and displacement constrained boundaries are considered.

With regards to the definition of the two limits, $h_u(x)$ and $h_l(x)$, two magnitudes are introduced. The first one is the centreline equation $c(x)$ and the second one is the thickness equation $t(x)$ of the beam (Figure 4.1). Therefore the functions $h_u(x)$ and $h_l(x)$ can be written as:

$$h_u(x) = c(x) + \frac{t(x)}{2} \tag{4.3a}$$

$$h_l(x) = c(x) - \frac{t(x)}{2} \tag{4.3b}$$

The centreline $c(x)$ represents the locus of the cross-section barycentres; the thickness $t(x)$, instead, is the beam height that is assumed as a positive definite function. In the case of prismatic beams and beams that are symmetric with respect to the longitudinal axis, $c(x)$ is a constant function and it is coincident with the x axis. In the other cases, instead, $c(x)$ is function of x and it results not coincident with x axis. Afterwards a specific expression of $c(x)$ and $t(x)$ is given to study each case.

4.2 Hypotheses on displacement and stress fields

In order to use the dimensional reduction method (see Paragraph 2.3), the beam model is studied according to specific hypotheses on displacement and stress fields. The following independent variable fields are considered: $\boldsymbol{\sigma}$ and $\boldsymbol{s}$, where $\boldsymbol{\sigma}$ is the symmetric stress tensor, defined in Equation (2.7), and $\boldsymbol{s}$ is the displacement vector, defined in Equation (2.2).

To get started, a linear function (with respect to y) to describe the horizontal displacements $u(x, y)$ and a constant function to describe the vertical displacement $v(x, y)$ are assumed:

$$u(x, y) = u(x) + \tilde{y}\,\frac{t(x)}{2}\,\theta(x) \tag{4.4a}$$

$$v(x, y) = v(x) \tag{4.4b}$$

in which $u(x)$, $\theta(x)$ and $v(x)$ are the displacement independent variables and $\tilde{y}$ is a function of y and it varies as follows: $\tilde{y} = 1$ on the upper boundary, $\tilde{y} = 0$ on the centreline and $\tilde{y} = -1$ on the lower boundary. Therefore it is possible to assume $\tilde{y}$ equal to:

$$\tilde{y} = (-c(x) + y)\frac{2}{t(x)} \tag{4.5}$$

Substituting Equation (4.5) in (4.4a), it can be noticed that the variable $\theta(x)$ is a rotation.

In the matter of the stress field, in order to guarantee the boundary equilibrium, considering zero traction on both boundary regions, it results as follows:

$$\boldsymbol{\sigma} \cdot \boldsymbol{n}|_{h_u \cup h_l} = \mathbf{0} \tag{4.6}$$

Where the vector $\boldsymbol{n}$ represents the outward unit vector respectively evaluated on the upper and lower limits:

$$\mathbf{n}|_{h_u} = \frac{1}{\sqrt{1 + h_u'(x)^2}} \begin{pmatrix} -h_u'(x) \\ 1 \end{pmatrix} \qquad \mathbf{n}|_{h_l} = \frac{1}{\sqrt{1 + h_l'(x)^2}} \begin{pmatrix} h_l'(x) \\ -1 \end{pmatrix} \tag{4.7}$$

The array $\boldsymbol{\sigma}|_{h_u \cup h_l}$, instead, is the stress tensor, separately evaluated on the two borders $h_u(x)$ and $h_l(x)$. Considering the equilibrium (4.6), the horizontal stress, σ_{xx}, manages to describe all stresses on the considered boundaries by itself, as shown hereunder:

$$\begin{pmatrix} \sigma_{xx} & \sigma_{xy} \\ \sigma_{xy} & \sigma_{yy} \end{pmatrix} \cdot \begin{pmatrix} n_x \\ n_y \end{pmatrix} \Bigg|_{h_u \cup h_l} = \begin{pmatrix} 0 \\ 0 \end{pmatrix} \rightarrow \begin{cases} \sigma_{xy}\big|_{h_u \cup h_l} = -\left(n_x/n_y\right)\, \sigma_{xx}\big|_{h_u \cup h_l} \\ \sigma_{yy}\big|_{h_u \cup h_l} = \left(n_x/n_y\right)^2\, \sigma_{xx}\big|_{h_u \cup h_l} \end{cases} \tag{4.8}$$

More precisely, $\sigma_{xy}\big|_{h_u}$ and $\sigma_{yy}\big|_{h_u}$ are expressed as follows for the upper boundary:

$$\sigma_{xy}\big|_{h_u} = h_u'(x)\, \sigma_{xx}\big|_{h_u} \tag{4.9a}$$

$$\sigma_{yy}\big|_{h_u} = h_u'(x)^2\, \sigma_{xx}\big|_{h_u} \tag{4.9b}$$

and for the lower boundary:

$$\sigma_{xy}\big|_{h_l} = h_l'(x)\, \sigma_{xx}\big|_{h_l} \tag{4.10a}$$

$$\sigma_{yy}\big|_{h_l} = h_l'(x)^2\, \sigma_{xx}\big|_{h_l} \tag{4.10b}$$

Where $h_u'(x)$ and $h_l'(x)$ represent the derivative of $h_u(x)$ and $h_l(x)$ with respect to x. It is now possible to assume the following hypotheses on the stress field: a linear function to describe the horizontal stress σ_{xx} along the beam cross-section; a linear easing function which interpolates the previously evaluated values of the vertical stress σ_{yy} (4.9b)(4.10b); and a quadratic function to describe the shear stress σ_{xy} as a linear easing function of the two boundary values (4.9a)(4.10a) added to a quadratic function. Therefore, the components of the stress tensor are expressed as follows:

$$\sigma_{xx} = \sigma_{x0}(x) + \tilde{y}\sigma_{x1}(x) \tag{4.11a}$$

$$\sigma_{yy} = (\sigma_{yy}\big|_{h_u} - \sigma_{yy}\big|_{h_l})\frac{y - h_l(x)}{h_u(x) - h_l(x)} + \sigma_{yy}\big|_{h_l} \tag{4.11b}$$

$$\sigma_{xy} = (\sigma_{xy}\big|_{h_u} - \sigma_{xy}\big|_{h_l})\frac{y - h_l(x)}{h_u(x) - h_l(x)} + \sigma_{xy}\big|_{h_l} + \tilde{b}\,\tau(x) \tag{4.11c}$$

By substituting Equation (4.9) and Equation (4.10) in (4.11), the components of the stress tensor can be written as:

$$\sigma_{xx} = \sigma_{x0}(x) + \tilde{y}\sigma_{x1}(x) \tag{4.12a}$$

$$\begin{aligned}\sigma_{yy} = {} & \left[h_u'(x)^2\left(\sigma_{x0}(x) + \sigma_{x1}(x)\right) - h_l'(x)^2\left(\sigma_{x0}(x) - \sigma_{x1}(x)\right)\right]\frac{y - h_l(x)}{h_u(x) - h_l(x)} + \\ & + h_l'(x)^2\left(\sigma_{x0}(x) - \sigma_{x1}(x)\right)\end{aligned} \tag{4.12b}$$

$$\begin{aligned}\sigma_{xy} = {} & \left[h_u'(x)\left(\sigma_{x0}(x) + \sigma_{x1}(x)\right) - h_l'(x)\left(\sigma_{x0}(x) - \sigma_{x1}(x)\right)\right]\frac{y - h_l(x)}{h_u(x) - h_l(x)} + \\ & + h_l'(x)\left(\sigma_{x0}(x) - \sigma_{x1}(x)\right) + \tilde{b}\,\tau(x)\end{aligned} \tag{4.12c}$$

in which $\sigma_{x0}(x)$, $\sigma_{x1}(x)$ and $\tau(x)$ are the stress independent variables; $\tilde{y}$ and $\tilde{b}$, instead, are function of y and they vary as follows: $\tilde{y} = 1$ on the upper boundary, $\tilde{y} = 0$ on the centreline and $\tilde{y} = -1$ on the lower boundary, according to Equation (4.5); $\tilde{b} = -1$ on the centreline of the beam and $\tilde{b} = 0$ on the upper and lower limits. Here is the expression of $\tilde{b}$:

$$\tilde{b} = (-c(x) + y)^2\,\frac{4}{t(x)^2} - 1 \tag{4.13}$$

Also the variations of $\boldsymbol{\sigma}$ and $\boldsymbol{s}$ ($\delta\boldsymbol{\sigma}$ and $\delta\boldsymbol{s}$ respectively) must be introduced in order to solve the HR functional. Therefore the following variational variables are defined $\delta u(x)$, $\delta\theta(x)$, $\delta v(x)$, $\delta\sigma_{x0}(x)$, $\delta\sigma_{x1}(x)$, $\delta\tau(x)$ and the components of $\delta\boldsymbol{s}$ follow below:

$$\delta u(x, y) = \delta u(x) + \tilde{y}\,\frac{t(x)}{2}\,\delta\theta(x) \tag{4.14a}$$

$$\delta v(x, y) = \delta v(x) \tag{4.14b}$$

The components of $\delta\boldsymbol{\sigma}$, instead, are expressed as:

$$\delta\sigma_{xx} = \delta\sigma_{x0}(x) + \tilde{y}\delta\sigma_{x1}(x) \tag{4.15a}$$

$$\delta\sigma_{yy} = \left[h_u'(x)^2\left(\delta\sigma_{x0}(x) + \delta\sigma_{x1}(x)\right) - h_l'(x)^2\left(\delta\sigma_{x0}(x) - \delta\sigma_{x1}(x)\right)\right]\frac{y - h_l(x)}{h_u(x) - h_l(x)} + \\ + h_l'(x)^2\left(\delta\sigma_{x0}(x) - \delta\sigma_{x1}(x)\right) \tag{4.15b}$$

$$\delta\sigma_{xy} = \left[h_u'(x)\left(\delta\sigma_{x0}(x) + \delta\sigma_{x1}(x)\right) - h_l'(x)\left(\delta\sigma_{x0}(x) - \delta\sigma_{x1}(x)\right)\right]\frac{y - h_l(x)}{h_u(x) - h_l(x)} + \\ + h_l'(x)\left(\delta\sigma_{x0}(x) - \delta\sigma_{x1}(x)\right) + \tilde{b}\,\delta\tau(x) \tag{4.15c}$$

The above equations are achieved by substituting into Equations (4.4) and Equation (4.12) the variables $u(x)$, $\theta(x)$, $v(x)$, $\sigma_{x0}(x)$, $\sigma_{x1}(x)$, $\tau(x)$ with their variations $\delta u(x)$, $\delta\theta(x)$, $\delta v(x)$, $\delta\sigma_{x0}(x)$, $\delta\sigma_{x1}(x)$, $\delta\tau(x)$.

This way, simple assumptions on the displacement and stress fields are introduced in order to study a homogeneous planar beam with a generic shape in the hypotheses of small displacements and a linear elastic isotropic material. Moreover, they meet the requirements imposed by the dimensional reduction method; the components of the displacement vector, $u(x, y)$ and $v(x, y)$, and the component of the symmetric stress tensor, σ_{xx}, σ_{yy} and σ_{xy}, in fact, are function of x and y but they are expressed as a product and sum of variables ($u(x)$, $v(x)$, $\theta(x)$, $\sigma_{x0}(x)$, $\sigma_{x1}(x)$ and $\tau(x)$) function of x only and functions ($\tilde{y}$ and $\tilde{b}$) depending on y only. In other words there is a clear decoupling of x and y.

4.3 Formulation of the problem

The aim of this study is to determine unknown functions, displacement and stress independent variables, which satisfy a system of differential equations in the given domain (4.1) and some boundary conditions on the border.

In this work, the starting equation to be considered in order to obtain the system of differential equations is a variational principle (see Paragraph 2.2). In Chapter 2, two variational principles are introduced, the TPE principle and the HR principle. In order to achieve accurate stress distribution along the cross-section by assuming simple hypotheses on the displacement and stress fields, the use of a mixed variational method (such as the HR) is preferred to a "one-field" variational method (such as the TPE). The rightness of this choice is emphasised in Paragraph 4.6 by means of the comparison between the two systems of differential equations, obtained for a prismatic beam by using the TPE formulation (see Equation 2.16) and by using the HR div-div formulation (see Equation 2.20).

As a consequence, the problem under investigation (Figure 4.1) can be expressed in terms of the HR div-div formulation, which represents the saddle point of the HR functional.

$$\begin{aligned} \delta J_{HR}^{dd} = -\int_{\Omega} (\delta \boldsymbol{s} \cdot \nabla \cdot \boldsymbol{\sigma})\, d\Omega - \int_{\Omega} (\nabla \cdot \delta \boldsymbol{\sigma} \cdot \boldsymbol{s})\, d\Omega - \int_{\Omega} (\delta \boldsymbol{s} : \boldsymbol{D} : \boldsymbol{\sigma})\, d\Omega \\ - \int_{\Omega} (\delta \boldsymbol{s} \cdot \boldsymbol{f})\, d\Omega - \int_{\partial\Omega_s} (\delta \boldsymbol{\sigma} \cdot \boldsymbol{n} \cdot \bar{\boldsymbol{s}})\, dS = 0 \end{aligned} \tag{4.16}$$

In any variational formulation, but specifically in this one, the classification of boundary conditions into natural and essential ones is naturally facilitated. In fact it results that $\boldsymbol{s}|_{\partial\Omega_s} = \bar{\boldsymbol{s}}$ is the natural condition and the boundary equilibrium $\boldsymbol{\sigma} \cdot \boldsymbol{n}|_{\partial\Omega_t} = \boldsymbol{t}$ is the essential condition, where $\boldsymbol{t}$ represents an external load distribution. Moreover, in this work, the distributed load $\boldsymbol{f}$ is assumed equal to zero.

It is important to highlight that the adopted formulation considers both displacements and stresses as the solution variables, therefore it is possible to proceed in two different ways: either by achieving a system of six differential equations and solving them with six displacement and stress boundary conditions, or by obtaining, through the static condensation method, a system of three differential equations in displacement variables only and recovering, after solving the reduced ODEs, other variables of interest, such as stresses.

4.4 Mixed equations

In this section, by using the HR variational formulation (4.16), a system of six ODEs is derived for the beam shown in Figure 4.1 .

Once suitable hypotheses on the displacement and stress fields are assumed (see Paragraph 4.2), it is possible to write, in Mathematica, the full expressions of the stress tensor components (4.12), of the displacement vector components (4.4) and of their respective variations (4.14) and (4.15).

Since the hypotheses on the displacement and stress fields meet the requirements imposed by the dimensional reduction method, the integral over Ω (4.16), properly written in Mathematica, is reduced into an integral over ℓ. Its expression is reported in Appendix A, Equation (A.1), in which it is possible to notice that the first derivatives of $\delta\sigma_{x0}(x)$, $\delta\sigma_{x1}(x)$, $\delta\tau(x)$ appear. Therefore, by means of the software mathematica, it is necessary to create a function able to integrate once by parts Integrating by parts all terms with $\delta\sigma'_{x0}(x)$, all terms with $\delta\sigma'_{x1}(x)$ and all terms with $\delta\tau'(x)$, the resulting expressions are inserted into the integral (A.1) in the place of all terms containing the first derivative.

Now, considering the resulting integral, by separately collecting the variational variables, it is possible to obtain six first-order differential equations function of six independent variables $u(x)$, $\theta(x)$, $v(x)$, $\sigma_{x0}(x)$, $\sigma_{x1}(x)$, $\tau(x)$ (in order to easily read the equations, (x) is omitted after each variable):

$$t\ \{5E\theta + 8(1+\nu)\tau - 5[2(1+\nu)c'\sigma_{x0} + (1+\nu)t'\sigma_{x1} - Ev']\} = 0 \tag{4.17a}$$

$$\begin{aligned} &t\ \{\sigma_{x0}[48 + 48(c')^4 + (8-16\nu)(t')^2 + 3(t')^4 + 8(c')^2(12 + 5(t')^2)] + \\ &- 16[4(1+\nu)c'\tau - c't'(4 + 4(c')^2 + (t')^2)\sigma_{x1} + 3E(u' + c'v')]\} = 0 \end{aligned} \tag{4.17b}$$

$$\begin{aligned} &t\ \{-\sigma_{x1}[16 + 16(c')^4 + 8(3+2\nu)(t')^2 + (t')^4 + 8(c')^2(4 + 7(t')^2)] + \\ &+ 8[3Et'\theta + 4(1+\nu)t'\tau - 8c't'\sigma_{x0} - 8(c')^3t'\sigma_{x0} - 2c'(t')^3\sigma_{x0} + \\ &+ 3Et'v' + Et\theta']\} = 0 \end{aligned} \tag{4.17c}$$

$$t'\sigma_{x0} + t\sigma'_{x0} = 0 \tag{4.17d}$$

$$t(4\tau - t'\sigma_{x1} + t\sigma'_{x1}) = 0 \tag{4.17e}$$

$$4(t'\tau + t\tau') = 3\ [t(2\ c'\sigma'_{x0} + t'\sigma'_{x1}) + 2\sigma_{x0}(c't' + tc'') + \sigma_{x1}((t')^2 + t\ t'')] \tag{4.17f}$$

It can be noticed that the first three equations (4.17a, 4.17b and 4.17c) are the compatibility equations for the studied beam model. It is proven by the presence of the first derivatives of each displacement independent variable and by the coupling between the strain tensor components $\boldsymbol{\varepsilon}$, which are here expressed in terms of stress tensor components $\boldsymbol{\sigma}$, and the displacement vector components $\boldsymbol{s}$. The last three equations, instead, represent the equilibrium of a 2D beam and more precisely Equation (4.17d) is the translational equilibrium for the horizontal components, Equation (4.17e) is the rotational equilibrium and Equation (4.17f) is the translational equilibrium for the vertical components.

It is important to obtain the system of six mixed equations (4.17) because, by choosing a suitable geometry and appropriate boundary conditions, the six unknown variables $u(x)$, $\theta(x)$, $v(x)$, $\sigma_{x0}(x)$, $\sigma_{x1}(x)$, $\tau(x)$ can be calculated.

4.5 Displacement equations

The HR formulation (4.16) considers both displacements and stresses as the solution variables. Despite this, it is possible to achieve, through the static condensation method, a system of three differential equations in displacement variables only.

The static condensation method is a practical procedure of accomplishing the reduction of the dimension of the problem. It is necessary to identify the variables to be condensed and express them in terms of the remaining variables. The relationship between these two sets of variables is found by establishing the static relation between them, hence the name static condensation method (Paz and Leigh, 2004). This relationship provides the means to reduce the dimension of the problem. For example, in the Finite Element Method, the static condensation method is used to reduce the dimension of the stiffness matrix, or, in this study, to obtain three ODEs in displacement variables.

In the case under investigation, a system of three differential equations can be processed by expressing, through Equation (4.17a), (4.17b) and (4.17c), the stress variables, $\sigma_{x0}(x)$, $\sigma_{x1}(x)$ and $\tau(x)$, in function of the displacement variables, $u(x)$, $v(x)$ and $\theta(x)$, and then by substituting the resulting expressions in Equation (4.17d) (4.17e) (4.17f). The second-order differential equations are not obtained for a generically tapered beam, but are computed for each case to be analysed.

4.6 Prismatic beam

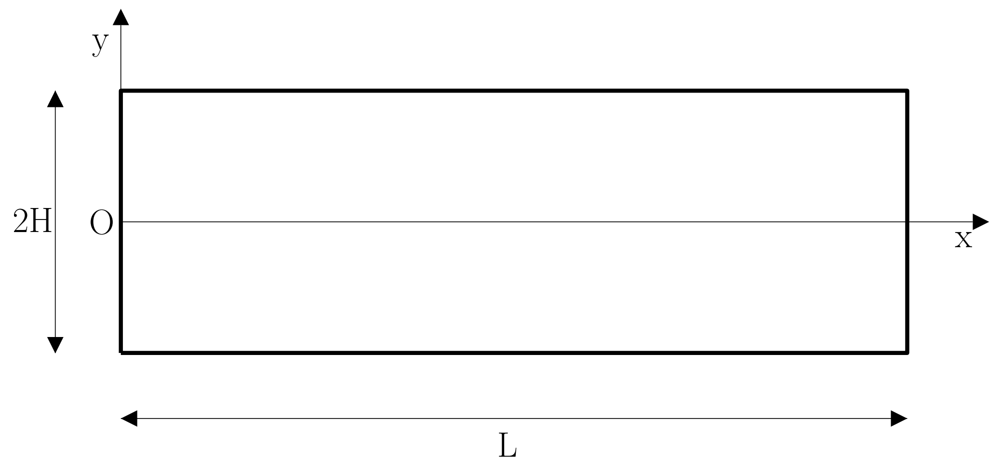

Figure 4.2: Prismatic beam

The object of the study is a planar beam which presents no taper; therefore the lower and upper boundaries of the domain result parallel to the beam longitudinal axis (Figure 4.2). In this case, the centreline $c(x)$ and the thickness $t(x)$ of the beam are expressed as follows:

$$c(x) = 0 \tag{4.18a}$$

$$t(x) = 2H \tag{4.18b}$$

Whereas the outward unit vectors on the upper $h_u(x)$ and lower $h_l(x)$ limits can be expressed as follows:

$$\mathbf{n}|_{h_u} = \begin{pmatrix} 0 \\ 1 \end{pmatrix} \qquad \mathbf{n}|_{h_l} = \begin{pmatrix} 0 \\ -1 \end{pmatrix} \tag{4.19}$$

Also, it is important to restate that $L \gg\ 2H$, so the beam longitudinal axis ℓ is the predominant dimension of the body.

This case represents the simplest one and, as a consequence, it is studied using two formulations: first of all TPE formulation and lastly the HR formulation.

4.6.1 Total Potential Energy

Starting from the TPE formulation and considering its functional, expressed with Equation (2.15), it is possible to notice that the problem is distinguished by three independent variables $u(x)$, $\theta(x)$ and $v(x)$.

Substituting the hypotheses on the displacement field (4.4) in (2.15) and using the well-known stationary procedure the weak form is obtained:

$$\begin{aligned} \delta J_{TPE} = \frac{1}{6(\nu^2-1)} \int_0^L 3EH \left[-2u'(x)\delta u'(x) + (1+\nu)\left(\theta(x)+v'(x)\right)\left(\delta\theta(x)+\delta v'(x)\right)\right] dx \\ -\frac{1}{6(\nu^2-1)} \int_0^L 2EH^3 \delta\theta'(x)\theta'(x) dx \end{aligned} \tag{4.20}$$

Where the variables $\delta u(x)$, $\delta v(x)$ and $\delta\theta(x)$ represent the variations of $u(x)$, $v(x)$ and $\theta(x)$, and $\delta u'(x)$, $\delta v'(x)$ and $\delta\theta'(x)$ are their respective first derivatives. From Equation (4.20) it can clearly be noticed that the double integral over Ω is reduced to a single integral over ℓ. Therefore it represents an application of the dimensional reduction method, made possible by the geometry of the problem and suitable assumptions on the displacement field.

Considering the weak form (4.20), it is now necessary to opportunely collect the first derivatives of the variational terms and integrate them once by parts. then, after substituting the resulting terms in (4.20), the following differential equations are obtained for each variational variable:

$$\frac{3EH}{\nu+1}(\theta(x)+v'(x))+\frac{2EH^3}{(\nu^2-1)}\theta''(x)=0 \tag{4.21a}$$

$$\frac{EHu''(x)}{(\nu^2-1)}=0 \tag{4.21b}$$

$$\frac{EH(\theta'(x)+v''(x))}{\nu+1}=0 \tag{4.21c}$$

Where the first equation is obtained collecting the variation $\delta\theta(x)$, the second equation collecting the variation $\delta u(x)$ and the third one collecting the variation $\delta v(x)$. From these equations, by imposing the boundary conditions, the kinematic solution of the problem can be obtain.

It is important to notice that Equation (4.21) presents the same structure of the Timoshenko equations (see Paragraph 3.3.2, Equation (3.19)) due to the fact that the Timoshenko kinematics is taken into consideration in the model under investigation. The only difference is that in (4.21) the shear factor, which is equal to 5/6 for a prismatic beam with a rectangular section, does not appear. This issue arises from the use of a "one-field" formulation with a too simple hypotheses on the displacements. Hence, considering beams with a more complex geometry, such as tapered beams, and the simple kinematics of Timoshenko, the TPE functional is not able to provide a high accuracy on the stress profiles.

4.6.2 Hellinger-Reissner

In this section it proceeds in a similar way, but using the HR formulation. The displacement field and the stress field are considered, for a total number of six independent variables $u(x)$, $\theta(x)$, $v(x)$, $\sigma_{x0}(x)$, $\sigma_{x1}(x)$, $\tau(x)$.

Since the system of six ODEs is calculated for the generic case (see Figure 4.1), in order to achieve the differential equations for the prismatic beam (see Figure 4.2) it is sufficient to replace the expressions of $c(x)$ and $t(x)$, reported in Equation (4.18), in the system of six ODEs, calculated for the generic case (4.17). By doing this, the following differential equations can be obtained:

$$
\begin{aligned}
&\frac{H}{E}\left[5E\theta(x) + 8\left(1+\nu\right)\tau(x) + 5Ev'(x)\right] = 0 \qquad && H\sigma'_{x0}(x) = 0 \\
&H\left(-\frac{\sigma_{x0}(x)}{E} + u'(x)\right) = 0 && H\left[2\tau(x) + H\sigma'_{x1}(x)\right] = 0 \\
&H\left(-\frac{\sigma_{x1}(x)}{E} + H\theta'(x)\right) = 0 && H\tau'(x) = 0
\end{aligned}
\tag{4.22}
$$

They are first-order differential equations; where $u(x)$, $\theta(x)$, $v(x)$, $\sigma_{x0}(x)$, $\sigma_{x1}(x)$, $\tau(x)$ are the unknown functions to be found. Then, extracting from the first three equations the three stress variables $\sigma_{x0}(x)$, $\sigma_{x1}(x)$ and $\tau(x)$ in function of the three displacement variables $u(x)$, $\theta(x)$ and $v(x)$, the following expressions are obtained:

$$
\sigma_{x0}(x) = Eu'(x) \qquad \sigma_{x1}(x) = EH\theta'(x) \qquad \tau(x) = -\frac{5E(\theta(x) + v'(x))}{8(1+\nu)} \tag{4.23}
$$

and substituting them in the last three equations of (4.22), it is possible to recover the differential equations in displacement variables only:

$$
\frac{5}{6}EH\frac{\theta(x) + v'(x)}{1+\nu} - \frac{2}{3}EH^3\theta''(x) = 0 \tag{4.24a}
$$

$$
\frac{5}{6}EH\frac{\theta'(x) + v''(x)}{1+\nu} = 0 \tag{4.24b}
$$

$$
2EHu''(x) = 0 \tag{4.24c}
$$

The equations written above (4.24) are the Timoshenko equations related to the prismatic beam shown in Figure 4.1. Contrary to Equation (4.21), the shear factor 5/6 (see Paragraph 3.3.2) naturally appears. Therefore, by using the HR functional (which is a mixed formulation) it is possible to achieve a great accuracy on the stress profiles even if a simple kinematics is assumed. This aspect is very important for the study of tapered beams because the calculation of the shear factor is naturally taken into account by the formulation.

4.7 Linearly tapered symmetric beam

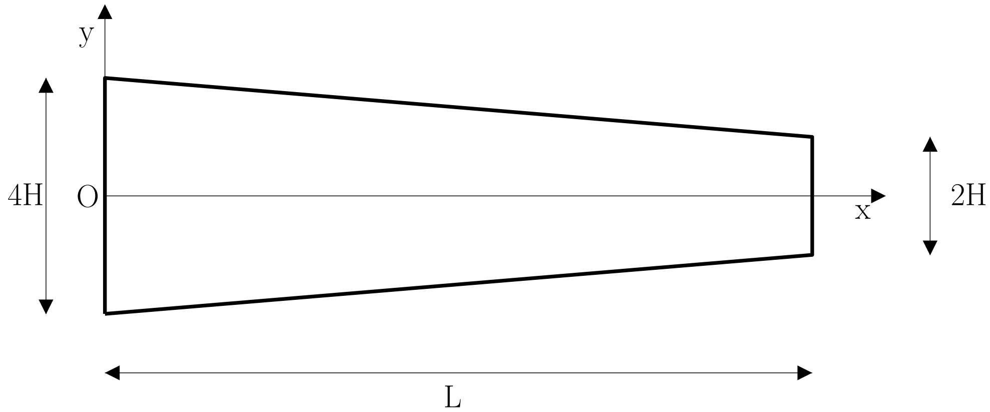

Figure 4.3: Linearly tapered symmetric beam

In the case of a beam with a linear taper and symmetric with respect to its longitudinal axis (Figure4.3), the following expressions of the centreline $c(x)$ and of the thickness $t(x)$ are assumed:

$$c(x) = 0 \tag{4.25a}$$

$$t(x) = -\frac{2H}{L}x + 4H \tag{4.25b}$$

It is also important to define the outward unit vectors on the upper and lower limits:

$$\mathbf{n}|_{h_u} = \frac{1}{\sqrt{1+(H/L)^2}}\begin{pmatrix} H/L \\ 1 \end{pmatrix} \qquad \mathbf{n}|_{h_l} = \frac{1}{\sqrt{1+(H/L)^2}}\begin{pmatrix} H/L \\ -1 \end{pmatrix} \tag{4.26}$$

As previously done for the study of a prismatic beam by means of the HR formulation, considering the system of differential equations calculated for the generic beam model (4.17), it is possible to obtain six first-order equations (in order to easily read the equations, (x) is omitted after each variable):

$$\frac{H(2L-x)[5EL\theta + 8L(1+\nu)\tau + 5(2H(1+\nu)\sigma_{x1} + Lv')]}{EL} = 0 \tag{4.27a}$$

$$\frac{H(4L-2x)}{EL}\left[\left(48 + \frac{48H^4}{L^4} + \frac{4H^2(8-16\nu)}{L^2}\right)\sigma_{x0} - 48Eu'\right] = 0 \tag{4.27b}$$

$$\frac{H(4L-2x)}{EL}\Big\{-\frac{16[H^4+L^4+2H^2L^2(3+2\nu)]\sigma_{x1}}{L^4}-\frac{16H}{L}\Big[3E\theta+$$
$$4(1+\nu)\tau+E(3v'+(-2L+x)\theta')\Big]\Big\}=0 \tag{4.27c}$$

$$\frac{H[\sigma_{x0}+(-2L+x)\sigma'_{x0}]}{L}=0 \tag{4.27d}$$

$$\frac{H(2L-x)}{L}\Big[2L\tau+H(\sigma_{x1}+(2L-x)\sigma'_{x1})\Big]=0 \tag{4.27e}$$

$$\frac{H}{L}\Big[-2L\tau-3H\sigma_{x1}+(2L-x)(2L\tau'+3H\sigma'_{x1})\Big]=0 \tag{4.27f}$$

from which the displacement and stress unknown variables $u(x)$, $\theta(x)$, $v(x)$, $\sigma_{x0}(x)$, $\sigma_{x1}(x)$, $\tau(x)$ can be evaluated for a given problem.

In order to obtain a system of three differential equations in displacement variables only, it is necessary to extract from the first three equations of (4.27) the three stress variables, $\sigma_{x0}(x)$, $\sigma_{x1}(x)$ and $\tau(x)$, in function of the three displacement variables, $u(x)$, $\theta(x)$ and $v(x)$:

$$\sigma_{x0}(x)=\frac{3EL^4u'(x)}{3H^4+3L^4+2H^2L^2(1-2\nu)} \tag{4.28a}$$

$$\sigma_{x1}(x)=\frac{EHL^3(-\theta(x)-v'(x)+4L\theta'(x)-2x\theta'(x))}{2(H^4+L^4-H^2L^2(-1+\nu))} \tag{4.28b}$$

$$\tau(x)=-\frac{5E[(H^4+L^4-2H^2L^2\nu)\theta(x)+(H^4+L^4-2H^2L^2\nu)v'(x)}{8[H^4(1+\nu)+L^4(1+\nu)-H^2L^2(-1+\nu^2)]}+$$
$$+\frac{2H^2L^2(2L-x)(1+\nu)\theta'(x)]}{8[H^4(1+\nu)+L^4(1+\nu)-H^2L^2(-1+\nu^2)]} \tag{4.28c}$$

Then they are substituted in the last three equations of (4.27) and, this way, the following second-order differential equations are calculated:

$$\frac{EH(2L-x)[(5H^45L^4+2H^2L^2(1-4\nu))(\theta-v')-2H^2L^2(2L-x)(1+\nu)}{L(H^4+L^4-H^2L^2(-1+\nu))(1+\nu)}+$$
$$+\frac{(-6\theta'-v''-2(-2L+x)\theta'')]}{L(H^4+L^4-H^2L^2(-1+\nu))(1+\nu)}=0 \tag{4.29a}$$

$$\frac{EH\{[5H^4 5L^4 + 2H^2L^2(3-2\nu)](\theta + v') - (2L-x)[5(H^2+L^2)\theta' + (5H^4}{L[(H^4+L^4)(1+\nu) - H^2L^2(-1+\nu^2)]} +$$
$$+ \frac{5L^4 + 2H^2L^2(3-2\nu))v'' - 2H^2L^2(2L-x)(1+\nu)\theta'']\}}{L[(H^4+L^4)(1+\nu) - H^2L^2(-1+\nu^2)]} = 0 \tag{4.29b}$$

$$\frac{EHL(-u' + (2L-x)u'')}{3H^4 + 3L^4 + 2H^2L^2(1-2\nu)} = 0 \tag{4.29c}$$

Since the linearly tapered symmetric beam is characterized by a more complex geometry than the prismatic one, comparing Equation (4.24) to Equation (4.29), it is possible to notice the presence of additional terms. In Equation (4.29a), $v''(x)$ and $\theta(x)$ appear; Equation (4.29b) is enhanced by the presence of $\theta(x)$, $v'(x)$ and $\theta''(x)$; lastly Equation (4.29c) presents the additional term $u'(x)$. Moreover, the complexity of the coefficients emphasises that the shear factor of a tapered beam has a different and more complicated expression compared to a prismatic one, as expected.

The numerical solution for the six ODEs (4.27) and for the three ODEs (4.29) follow in Chapter 5, considering a cantilever beam with a concentrated load in the free edge.

4.8 Linearly tapered non-symmetric beam

In this section, the beam to be examined is no more symmetric with respects to its longitudinal axis, therefore the upper limit of the domain is not assumed to be tapered, whereas the lower limit, is distinguished by a linear taper (Figure 4.4).

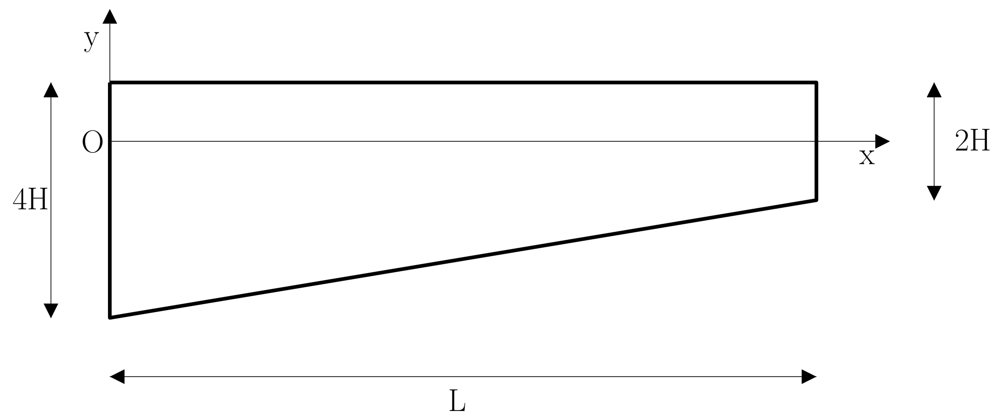

Figure 4.4: Linearly tapered non-symmetric beam

The following expressions of $c(x)$ and of $t(x)$ are assumed:

$$c(x) = \frac{H}{L}x - H \tag{4.30a}$$

$$t(x) = -\frac{2H}{L}x + 4H \tag{4.30b}$$

Furthermore The outward unit vectors on the upper and lower limits can be expressed as follows:

$$\mathbf{n}|_{h_u} = \begin{pmatrix} 0 \\ 1 \end{pmatrix} \qquad \mathbf{n}|_{h_l} = \frac{1}{\sqrt{1+(2H/L)^2}} \begin{pmatrix} 2H/L \\ -1 \end{pmatrix} \tag{4.31}$$

Once the geometry of the problem is defined, the following six differential equations are found, substituting $c(x)$ and $t(x)$ in the system 4.17 (in order to easily read the equations, (x) is omitted after each variable):

$$\begin{aligned}&\frac{H(2L-x)}{EL}\Big[5EL\theta + 8L(1+\nu)\tau + 5(-2H(1+\nu)\sigma_{x0} + 2H(1+\nu)\sigma_{x1} + \\ &+ ELv')\Big] = 0\end{aligned} \tag{4.32a}$$

$$\begin{aligned}&\frac{H(2L-x)}{EL}\Big\{4HL^3(1+\nu)\tau - [16H^4 + 3L^4 - 4H^2L^2(-2+\nu)]\sigma_{x0} + \\ &+ 16H^4\sigma_{x1} + 8H^2L^2\sigma_{x1} + 3EL^4u' + 3EHL^3v'\Big\} = 0\end{aligned} \tag{4.32b}$$

$$\begin{aligned}&\frac{H(2L-x)}{EL}\Big[-3EHL^3\theta - 4HL^3(1+\nu)\tau + 16H^4\sigma_{x0} + 8H^2L^2\sigma_{x1} + \\ &- 16H^4\sigma_{x1} - 8H^2L^2\sigma_{x1} - L^4\sigma_{x1} - 4H^2L^2\nu\sigma_{x1} - 3EHL^3v' + 2EHL^4\theta' + \\ &- EHL^3x\theta'\Big] = 0\end{aligned} \tag{4.32c}$$

$$\frac{H[\sigma_{x0} + (-2L+x)\sigma'_{x0}]}{L} = 0 \tag{4.32d}$$

$$\frac{H(2L-x)[2L\tau + H(\sigma_{x1} + (2L-x)\sigma'_{x1})]}{L} = 0 \tag{4.32e}$$

$$\frac{8H[\tau + (-2L+x)\tau']}{L} = -\frac{12H^2[-\sigma_{x0} + \sigma_{x1} + (2L-x)(\sigma'_{x0} - \sigma'_{x1})]}{L^2} \tag{4.32f}$$

Equation (4.32) presents more terms and coefficients than Equation (4.27) and (4.22).

It is evident that the more complex the geometry of the beam, the more sophisticated the equations to study its behaviour need to be. Moreover, in Equation (4.32f) the presence of the terms $\sigma_{x0}(x)$ and $\sigma'_{x0}(x)$ demonstrates that the model naturally takes the coupling between the axial and bending behaviours into account. As a result, additional terms for coupling must not be inserted in the formulation. On the other hand, the terms $\sigma_{x0}(x)$ and $\sigma'_{x0}(x)$ are not required in the case of a symmetric beam, as in Equation (4.29c), because of the decoupling between the axial and bending behaviours.

As done for the other two cases, in order to obtain a system of three differential equations in displacement variables only, it is necessary to extract from the first three equations of (4.32) the three stress variables, $\sigma_{x0}(x)$, $\sigma_{x1}(x)$ and $\tau(x)$, in function of the three displacement variables, $u(x)$, $\theta(x)$ and $v(x)$. Since the expressions of $\sigma_{x0}(x)$, $\sigma_{x1}(x)$ and $\tau(x)$ thus obtained are too long, their verbalization is omitted. The system of the three second-order differential equations is also omitted for the same reason.

The numerical solution for the six ODEs (mixed ODEs) (4.32) and for the three ODEs (displacement ODEs) follow in Chapter 5, considering a cantilever beam with a concentrated load in the free edge.

4.9 Curvilinearly tapered symmetric beam

In this section, the beam to be examined is symmetric with respect to its longitudinal axis but no more linearly tapered. An example of a beam with a variable cross-section and curvilinearly tapered is the cantilever beam with uniform strength, as known in literature. The geometry of this beam is such that the section modulus varies along the beam in the same proportion as the bending moment (Timoshenko, 1976) and it is favourable as regards the amount of material used, because each cross-section has only the area necessary to satisfy the conditions of strength.

The geometry to be chosen in order to consider a beam with uniform strength is taken from Timoshenko (1976) and, more precisely, the height of the beam varies following a parabolic law (Figure 4.5). The only change with respect to the geometry presented by Timoshenko (1976), is that the cross-section area, at $x = L$, is not equal to zero but sufficiently small to be considered negligible. The proposed method does not work in the case of vanishing sections for two reasons. The first one is that the cross-section area must be sufficient to transmit the shear force, the second one that an area equal to zero implies a non definition of the stresses. Equation (4.8) clearly shows that the values of $\sigma_{xy}\big|_{h_u \cup h_l}$ and $\sigma_{yy}\big|_{h_u \cup h_l}$ depend on the slope of the upper and lower limits. Hence, if the outward

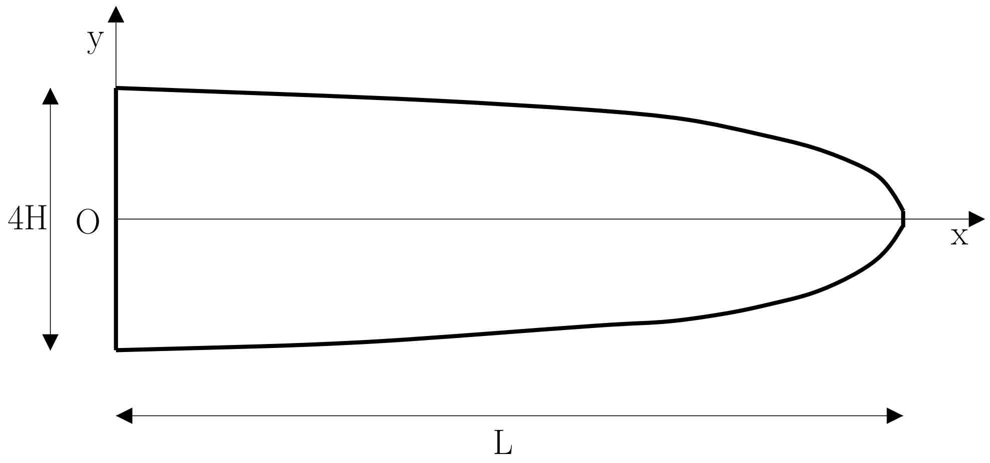

Figure 4.5: Curvilinearly tapered symmetric beam: beam with uniform strength

unit vector, at $x = L$, has only the component along the x axis, the ratio n_x/n_y approaches infinity.

In the case shown in Figure 4.9, the centreline $c(x)$ and this thickness $t(x)$ are expressed as follows:

$$c(x) = 0 \tag{4.33a}$$

$$t(x) = 4\sqrt{H^2\left(1 - \frac{100x}{101L}\right)} \tag{4.33b}$$

Furthermore, as previously done, after substituting $c(x)$ and $t(x)$ in the system of differential equations calculated for the generic beam model (4.17), six first-order differential equations are obtained for this specific case, whose full verbalization is reported in Appendix A, Equation (A.2). Due to the complexity of the six differential equations, the verbalization of the system of the three differential equations, recovered through the static condensation method, is omitted.

Different from Equation (4.32f), there is no $\sigma_{x0}(x)$ and $\sigma'_{x0}(x)$ in the last equation of (A.2), as expected due to the symmetry with respect to the longitudinal axis. Moreover, Equation (A.2) presents more sophisticated coefficients and terms in relation to the previous cases due to the very complex geometry of the beam shown in Figure 4.9.

The displacement and stress unknown variables $u(x)$, $\theta(x)$, $v(x)$, $\sigma_{x0}(x)$, $\sigma_{x1}(x)$, $\tau(x)$ can be evaluated for a given problem of the beam shown in Figure 4.6, by using the system of six ODEs (A.2) and the numerical solution follows in Chapter 5.

4.10 Curvilinearly tapered non-symmetric beam

The beam to be examined is no more symmetric with respect to the longitudinal axis. Precisely, the upper limit of the domain is assumed to be constant, whereas the lower limit, is distinguished by a quadratic function (Figure 4.6).

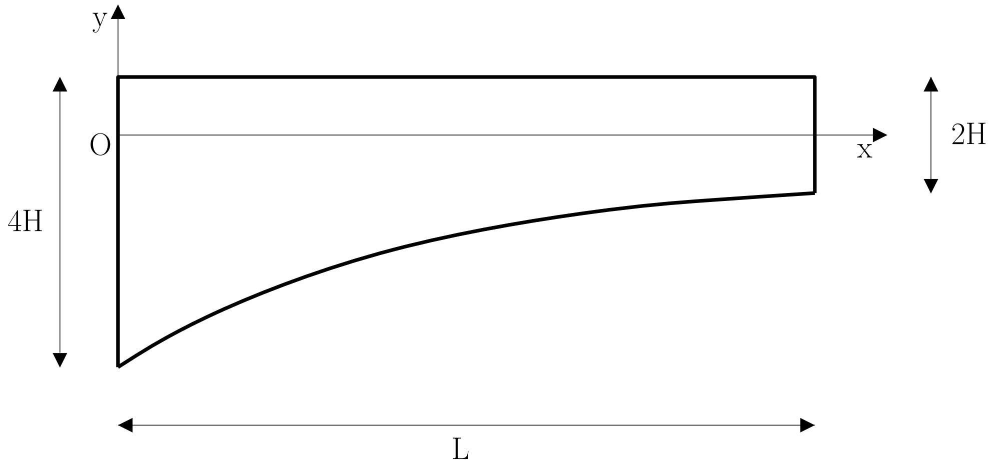

Figure 4.6: Curvilinearly tapered non-symmetric beam

The following expressions of $c(x)$ and of $t(x)$ are assumed:

$$c(x) = -\frac{H(L-x)^2}{L^2} \tag{4.34a}$$

$$t(x) = \frac{2H(2L^2 - 2Lx + x^2)}{L^2} \tag{4.34b}$$

The outward unit vectors on the upper and lower limits can be expressed as follows:

$$\mathbf{n}|_{h_u} = \begin{pmatrix} 0 \\ 1 \end{pmatrix} \qquad \mathbf{n}|_{h_l} = \frac{1}{\sqrt{1 + (-4Hx/L^2 + 4H/L)^2}} \begin{pmatrix} (4H/L^2)(L-x) \\ -1 \end{pmatrix} \tag{4.35}$$

Furthermore, as previously done, after substituting $c(x)$ and $t(x)$ in the system of differential equations calculated for the generic beam model (4.17), six first-order differential equations are obtained for this specific case, whose full verbalization is reported in Appendix A, Equation (A.3). Focusing on the last equation of (A.3), it is important to notice the presence of $\sigma_{x0}(x)$ and $\sigma'_{x0}(x)$. Hence, the coupling between the axial and bending behaviours is rightly considered in the proposed model. Moreover, the excessive length of the terms and coefficients in Equation (A.3) depends on the adopted complex geometry.

Despite the complexity of the six differential equations, the system of three differential equations is also found. Therefore the three stress variables $\sigma_{x0}(x)$, $\sigma_{x1}(x)$ and $\tau(x)$, in function of the three displacement variables $u(x)$, $\theta(x)$ and $v(x)$, are extracted from the first three compatibility equations of the system (A.3); then, these expressions, omitted due to their excessive length, are substituted in the last three equilibrium equations and the system of the three displacement ODEs is obtained, whose verbalization is here omitted because is too complex.

The numerical solution for the six ODEs (mixed ODEs) and for the three ODEs (displacement ODEs) follow in Chapter 5.

4.11 Conclusions on non-prismatic beam models

In this chapter, an analytical model of tapered beams is proposed. Starting from the formulation of HR, considering simple assumptions on the displacement and stress fields in the criteria of the dimensional reduction method, it is possible to calculate a system of six mixed differential equations. After that, a system of three differential equations, in the displacement variables only, is recovered through the static condensation method.

Considering the case of a prismatic beam, the three differential equations obtained from the TPE functional do not contain the shear factor. On the other hand, by using the HR functional, the shear factor naturally appears and the three differential equations are the same as the Timoshenko equations. This aspect is very important for the study of tapered beams because it means that the calculation of the shear factor is taken into account by the model even if a more complex geometry than the prismatic one is considered.

Comparing the systems of differential equations obtained for each case, it is evident that the more complex the geometry of the beam, the more sophisticated the equations to study its behaviour need to be. Moreover, the presence of the terms $\sigma_{x0}(x)$ and $\sigma'_{x0}(x)$, in the last equation of the mixed differential equations obtained for the two non-symmetric beams, demonstrates that the model naturally takes the coupling between the axial and bending behaviour into account. The same terms, $\sigma_{x0}(x)$ and $\sigma'_{x0}(x)$, are not present in the cases of tapered symmetric beams, due to the decoupling between these two behaviours.

It may be concluded that despite the length and the complexity of the differential equations, especially referring to the cases of non-symmetric beams, these equations are achieved with a reasonable computational time and by means of computers usually available in engineering practice. The validity of this model is made more explicit in the next chapter, through the comparison between the results obtained in Mathematica and the results achieved with the finite element analysis and with the classical beam theories of Euler-Bernoulli and Timoshenko.

Chapter 5

Numerical results

In order to test the developed analytical model (see Chapter 4), several examples about a cantilever beam with a concentrated load in the free edge are carried out in the following. More precisely, five cases are considered: one prismatic beam, two linearly tapered beams and two curvilinearly tapered beams according to the geometry introduced in Chapter 4.

The results, arising from the analytical model, are compared to the results achieved by means of the Euler-Bernoulli and Timoshenko beam theories and the results obtained by the finite element analysis using the software Abaqus

First of all, starting from the developed analytical model, the solution of the differential equations is found with the Mathematica commands DSolve or NDSolve. The command DSolve finds symbolic solutions to differential equations and it can particularly handle the following types of equations: ordinary differential equations, as in the studied case, partial differential equations and differential-algebraic equations. The Mathematica function NDSolve, on the other hand, is a general numerical differential equation solver and it is used, in this section, to solve tapered cantilever beams. Tapered beams, in fact, are characterized by a more complex geometry with respect to the prismatic beams, therefore Mathematica is not able to give an analytical solution with the command DSolve.

For each cantilever beam the deflection at the free edge and the maximum value of the shear stress at half length of the beam is calculated. Then, in order to test the results obtained with the developed model, the deflection is also evaluated by using the principle of virtual work (see Paragraph 3.2.3 and Paragraph 3.3.3) and the shear stress is also found with the Jourawsky theory (see Paragraph 3.3.2). Lastly a finite element analysis is conducted by means of the software Abaqus. Abaqus is particularly used to model prismatic and non-prismatic 2D beams and make a comparison with the results obtained in Mathematica.

5.1 Problem definition

The object of this chapter is a cantilever beam. More precisely, a cantilever is a beam which is only anchored at one end and carries the load to the fixed support. The beam under investigation is subject to a concentrated load $P = -100$[kN] on the free end, where the minus sign indicates that the force is directing downwards with respect to the y axis. Moreover the following two values of Young's modulus E and Poisson's ratio ν are assumed:

$$\begin{aligned} E &= 10 \cdot 10^7 \text{ kN/m}^2 \\ \nu &= 0.3 \end{aligned} \tag{5.1}$$

In order to solve the system of six ODEs, obtained for each case in Chapter 4, it is necessary to impose the following boundary conditions, where h represents the height of the beam at $x = L$:

$$\begin{aligned} \theta(0) &= 0 \qquad \sigma_{x0}(L) = 0 \\ v(0) &= 0 \qquad \sigma_{x1}(L) = 0 \\ u(0) &= 0 \qquad \tau(L) = -(3P)/(2h) \end{aligned} \tag{5.2}$$

Since the six mixed ODEs are first-order differential equations (see Equation (4.17)), six boundary conditions are sufficient to find the solution of the problem and, more precisely, three conditions on the displacement field and three conditions on the stress field. In the left edge of the beam there is a fixed support, therefore the components of the displacement vector, $u(x, y)$ and $v(x, y)$, must be equal to zero. This condition is guaranteed when the three displacement variables, $\theta(x)$ $u(x)$ and $v(x)$, are equal to zero at $x = 0$. The unknown variables are both displacement and stresses, thus the other three conditions are referred to the stress variables at the free end of the beam. The concentrated load P at $x = L$ imposes that the bending moment is zero at the free end. As a consequence the two variables, $\sigma_{x0}(x)$ and $\sigma_{x1}(x)$, are equal to zero at $x = L$. The variable $\tau(x)$, instead, must be different from zero at the free end because the shear force is constant and equal to P along the whole beam longitudinal axis. Its expression, reported in Equation (5.2), is referred to the shear distribution along the cross-section proposed by the Jourawsky theory (see Paragraph 3.3.2).

Considering now the set of three ODEs evaluated for each analysed beam in Chapter

4, the following boundary conditions are used in order to find the solution of the problem:

$$\begin{aligned} &\theta(0) = 0 \qquad && u(L) = 0 \\ &v(0) = 0 \qquad && \theta'(L) = 0 \\ &u(0) = 0 \qquad && (\theta(L) + v'(L)) = (6\,P)\,/\,(5\,GA(L)) \end{aligned} \tag{5.3}$$

In this case, the three displacements ODEs are second-order differential equations in displacement variables only, therefore six boundary conditions are necessary to solve the problem. The fixed support imposes that the displacements are zero at $x = 0$, as shown before; the concentrated load P at the free end imposes that the bending moment linearly varies along the beam axis and it is zero at the free end, also the shear force is constant.

In the next sections the solutions of the problem are illustrated for each analysed beam. First the system of six ODEs (mixed equations), then the system of three ODEs (displacement equations) are respectively solved considering the boundary conditions reported in Equation (5.2) and in Equation (5.3).

5.2 Prismatic beam

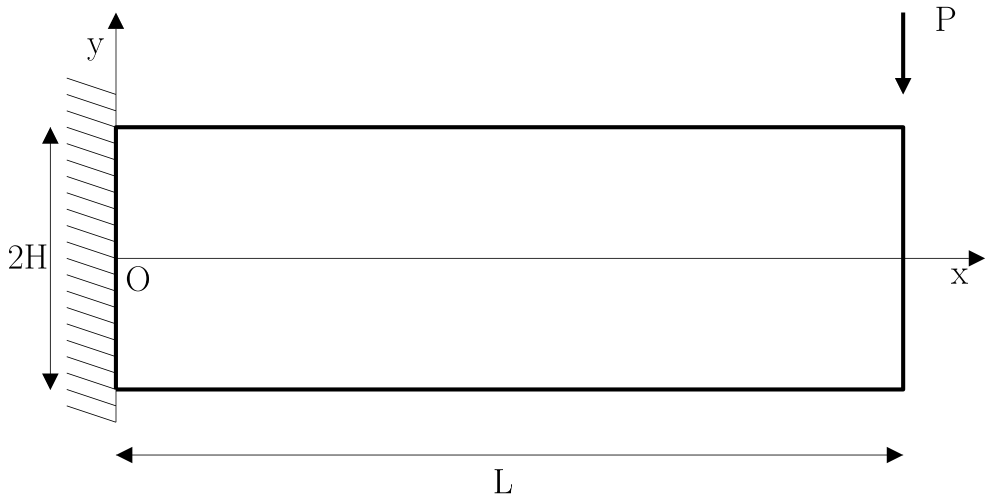

Figure 5.1: Cantilever prismatic beam

The following geometry dimensions are assumed in order to evaluate the numerical result for the beam shown in Figure 5.1:

$$\begin{aligned} H &= 0.5 \text{ m} \\ L &= 10 \text{ m} \\ A(L) &= 1 \text{ m}^2 \end{aligned} \tag{5.4}$$

Where the beam cross-section is supposed rectangular with a base equal to 1 m.

5.2.1 Mathematica results

The prismatic beam, shown in Figure 5.1, is characterized by a simple geometry. Therefore the system of ODEs, both mixed and displacement ones, can be solved either with the command DSolve or with the command NDSolve . It is preferred to illustrate the analytical solution rather than the numerical one, even if both of them have been calculated, because the analytical solution does not consider any approximation.

Analytical solution for the mixed ODEs

Considering the system of six ODEs (see Equation (4.22)) and the boundary conditions previously introduced (5.2), it is possible to solve the problem about the cantilever prismatic beam that is fixed on the left edge and subject to the concentrated load P on the right edge (Figure 5.1) by using the command DSolve:

$$\begin{aligned} v(x) &= \frac{24H^2Px + 15LPx^2 - 5Px^3 + 24H^2Px\nu}{20EH^3} & \sigma_{x0}(x) &= 0 \\ \theta(x) &= -\frac{3\left(2LPx - Px^2\right)}{4EH^3} & \sigma_{x1}(x) &= -\frac{3(LP - Px)}{2H^2} \\ u(x) &= 0 & \tau(x) &= -\frac{3P}{4H} \end{aligned} \tag{5.5}$$

Where $24H^2x(\nu + 1)$ is the shear contribution to the deflection $v(x)$. In order to evaluate a numerical result, it is necessary to substitute the values of Young's modulus E and Poisson's ratio ν (5.1) and the geometry dimensions (5.4) in (5.5). Therefore, at $x = L$, the following value of deflection is calculated:

$$v(L) = -4.031 \cdot 10^{-3} \text{ m} \tag{5.6}$$

Another value of interest to be calculated in order to make a comparison with the other results is the maximum value of the shear stress at half length of the beam. For the case under investigation it results equal to:

$$max(\sigma_{xy}|_{x=L/2}) = -1.500 \cdot 10^2 \text{ kN/m}^2 \tag{5.7}$$

More precisely, $max(\sigma_{xy}|_{x=L/2})$ provides the maximum of its argument at a value of y within the cross-section height. In this case, the maximum of $\sigma_{xy}|_{x=L/2}$ is at y equal to 0. Then, Equation (5.7) is achieved by estimating $\tau(L/2)$, $\sigma_{x0}(L/2)$ and $\sigma_{x1}(L/2)$ from Equation (5.5) and, lastly, by substituting $\tau(L/2)$, $\sigma_{x0}(L/2)$ and $\sigma_{x1}(L/2)$ in Equation (4.12c).

Analytical solution for the displacement ODEs

Considering the system of the three ODEs (see Equation 4.24) and the boundary conditions (5.3), the problem under investigation (Figure 5.1) can be solved by means of the command DSolve:

$$\begin{aligned} v(x) &= \frac{24H^2Px + 15LPx^2 - 5Px^3 + 24H^2Px\nu}{20EH^3} \\ \theta(x) &= -\frac{3\left(2LPx - Px^2\right)}{4EH^3} \\ u(x) &= 0 \end{aligned} \tag{5.8}$$

After that, in order to evaluate a numerical result, it is necessary to consider the mechanical properties (5.1) and the geometry reported in (5.4). Therefore, with $x = L$, the deflection is calculated:

$$v(L) = -4.031 \cdot 10^{-3} \text{ m} \tag{5.9}$$

It can be noticed that the obtained result is the same as the one achieved for the six ODEs (see Equation (5.6)). In fact, the expressions of the deflection $v(x)$, arising from the six ODEs and the three ODEs, are equal.

Now, in order to calculate the maximum value of shear stress σ_{xy} at $x = L/2$, it is necessary to find the values of $v'(L/2)$, $\theta(L/2)$ and $\theta'(L/2)$, through (5.8), and then substitute them in Equation (4.23). Once $\tau(L/2)$, $\sigma_{x0}(L/2)$ and $\sigma_{x1}(L/2)$ are evaluated, the shear stress can be recovered by Equation (4.12c). Considering the geometry of the current case, Equation (4.12c) becomes:

$$\sigma_{xy} = \frac{(4y^4 - 4H^4)\,\tau(x)}{4H^4} \tag{5.10}$$

Therefore, substituting the values of $\tau(L/2)$ in (5.10) and considering $y = 0$, the following value of the shear stress at $x = L/2$ is obtained:

$$max(\sigma_{xy}|_{x=L/2}) = -1.500 \cdot 10^2 \text{ kN/m}^2 \tag{5.11}$$

5.2.2 Classical theory results

The classical beam theories are used in this section in order to evaluate the deflection at the free edge of the beam shown in Figure 5.1. In particular the principle of virtual work is considered, because it represents one of the possible integral forms to be used for studying a beam in Euler-Bernoulli hypotheses or Timoshenko hypotheses. Another value of interest is the maximum shear stress and it is computed at half length of the beam by means of the Jourawsky theory.

Euler-Bernoulli solution

Considering the Euler-Bernoulli hypotheses and the prismatic cantilever beam that is subject to a concentrated load P on the free edge, the principle of virtual work can be written as follows:

$$v(x) = \int_0^L \left[(L-x)\,\frac{P\,(L-x)}{EI}\right] dx \tag{5.12}$$

Where I represents the second moment of area, which results constant along the beam longitudinal axis for the current case (Figure 5.1). Considering the full expression of I and the cross-section base equal to 1 m, Equation (5.12) can be written as follows below, according to the expression of $t(x)$ (4.18b):

$$v(x) = \int_0^L \left[(L-x)\,\frac{12P\,(L-x)}{E(2H)^3}\right] dx \tag{5.13}$$

It can also be noticed that the first member of Equation (5.12) is the external work, whereas the second term is the internal work. After solving the integral (5.12), the deflection $v(x)$

is found:

$$v(x) = \frac{PL^3}{2EH^3} \tag{5.14}$$

Then considering the mechanical properties (5.1) and the geometry (5.4), it is possible to achieve the numerical result of the deflection at $x = L$.

$$v(L) = -4.000 \cdot 10^{-3} \text{ m} \tag{5.15}$$

Timoshenko solution

Considering the Timoshenko hypotheses and the prismatic cantilever beam that is subject to a concentrated load P on the free edge, the principle of virtual work can be written as follows:

$$v(x) = \int_0^L \left[(L-x) \frac{P(L-x)}{EI} \right] dx + \int_0^L \left[\frac{P}{(5/6)GA(x)} \right] dx \tag{5.16}$$

Where I represents the second moment of area, $A(x)$ is the cross-section area and G represents the shear modulus. Considering the full expression of I and $A(x)$ and assuming the cross-section base equal to 1 m, Equation (5.16) can be written as follows below, according to the expression of $t(x)$ (4.18b):

$$v(x) = \int_0^L \left[(L-x) \frac{12P(L-x)}{E(2H)^3} \right] dx + \int_0^L \left[\frac{P}{(5/6)G2H} \right] dx \tag{5.17}$$

It can also be noticed that the first member of Equation (5.16) is the external work, whereas the second term is the internal work. After solving the integral (5.16), the deflection $v(x)$ is found:

$$v(x) = \frac{PL^3}{2EH^3} + \frac{3PL}{5GH} \tag{5.18}$$

Then considering the mechanical properties (5.1) and the geometry (5.4), it is possible to achieve the numerical result of the deflection at $x = L$.

$$v(L) = -4.031 \cdot 10^{-3} \text{ m} \tag{5.19}$$

Jourawsky solution

The well-known Jourawsky formula is used to find an approximate solution of the shear stress distribution along the cross-section. Considering the prismatic beam, shown in

Figure 5.1, the Jourawsky formula is written as follows:

$$\sigma_{xy} = \frac{12P(1/2)(H-y)(H+y)}{(2H)^3} \tag{5.20}$$

Since the value to be evaluated is the maximum shear stress along the cross-section, in order to calculate $max(\sigma_{xy}|_{x=L/2})$, y is assumed equal to zero, then the mechanical property values (5.1) and the geometry (5.4) are substituted in (5.20). By doing this, the maximum shear stress at half length of the beam is obtained:

$$max(\sigma_{xy}|_{x=L/2}) = -1.500 \cdot 10^2 \text{ kN/m}^2 \tag{5.21}$$

5.2.3 FEM results

The finite element analysis is performed by using the software Abaqus. Focusing on the modelling and the main steps connected to it, first of all it is necessary to define the geometry of the beam. Therefore, choosing a "2D deformable planar space", the four points capable alone of describing the prismatic beam (see Figure 5.1), are inserted. Then, connecting them by two horizontal lines and two vertical lines, the beam is generated.

The second step concerns the definition of the mechanical properties, which must be assigned to the generated 2D body. Since the linear elasticity hypotheses are considered, the values of Young's modulus E and Poisson's ratio ν (see Equation 5.1) are sufficient to describe the mechanical behaviour of the beam. It is also important to define a section which contains information about the properties of the created part and depends on the type of region in question. For example, if the region is a deformable wire, shell, or 2D body, a section must be assigned to that region that provides information about the cross-section geometry. Likewise, a rigid region requires a section that describes its mass properties. In this analysis the chosen "Section Category" is "Homogeneous Solid" and defines the properties of the 2D created body.

Once the geometry and the mechanical properties are defined, the boundary conditions must be enforced. A fixed support is considered at the left edge of the beam, therefore the displacements in the directions of the beam axes are imposed equal to zero along the left border. Also, a concentrated load P is applied at the right edge and it is modelled as a "Surface Traction" load in order to avoid a high stress concentration in the applying point.

Lastly, an appropriate quadrangular mesh must be generated according to the dimension of the beam. In the case under investigation, since the beam height is equal to 1 m, the "Approximate global size" is chosen equal to 0.05 m on a total of twenty elements in the beam thickness. The rightness of this choice is mainly proven by an accurate convergence analysis, performed by using different values of the "Approximate global size" which are smaller and smaller.

The model is now ready to be analysed by creating a "job". After that, when the analysis is completed, it is possible to read the results. First of all, it is interesting to find

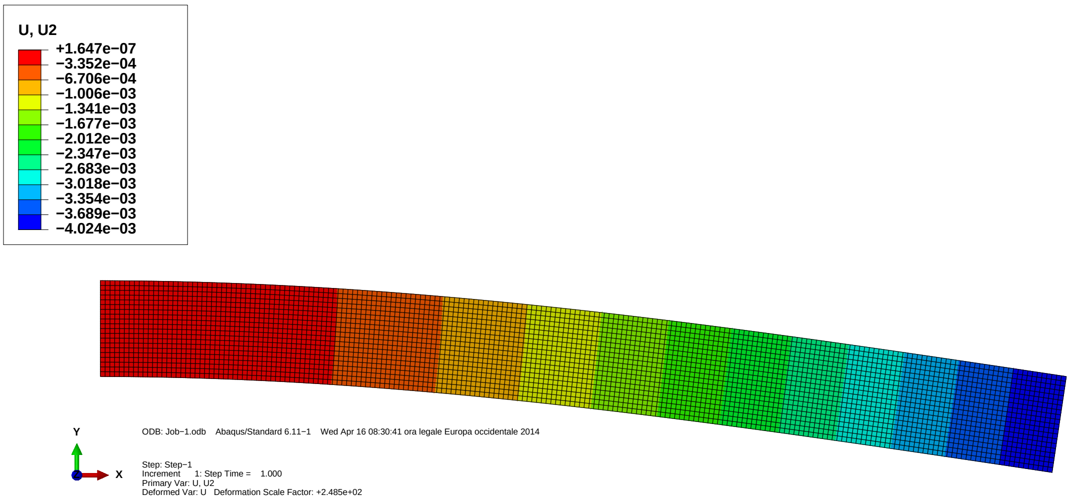

Figure 5.2: Results of "U2" obtained by using the software Abaqus for the cantilever prismatic beam with a concentrated load on the right edge

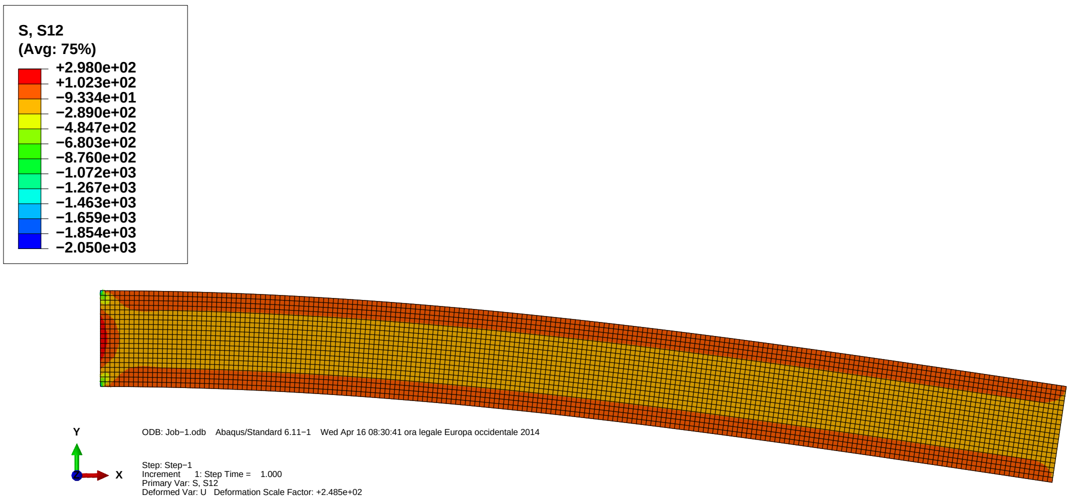

Figure 5.3: Results of "S12" obtained by using the software Abaqus for the cantilever prismatic beam with a concentrated load on the right edge

the deflection $v(x)$ on the right edge. Therefore, choosing "U" and "U2" from the model tree, it is possible to read the variation of the deflection along the beam longitudinal axis by the Figure 5.2.
By doing this, it is possible to read the deflection at the right end:

$$v(L) = -4.024 \cdot 10^{-3} \text{ m} \tag{5.22}$$

The same procedure is followed to evaluate the maximum shear stress at half length of the beam. Therefore, choosing "S" and "S12" from the model tree, Figure 5.3, which shows how the shear stress varies along the beam longitudinal axis, is obtained. In order to find the value of interest a "path" is created along the said cross-section. The resulting shear distribution is symmetric with respect to the beam axis and parabolic. The maximum is in correspondence of half cross-section and it results equal to:

$$max(\sigma_{xy}|_{x=L/2}) = -1.503 \cdot 10^{2} \text{ kN/m}^2 \tag{5.23}$$

5.2.4 Comparison of the results

Figure 5.4 plots how the deflection $v(x)$ varies along the beam axis, considering the solution obtained by the developed analytical model (AN), the finite element method (FE) and the two classical beam theories of Euler-Bernoulli (EB) and Timoshenko (T). The four curves are almost coincident, showing a high degree of matching among the adopted methods. Moreover, in Table 5.1 the Timoshenko solution is larger than the Euler-Bernoulli one, as expected because of the shear contribution in the former method. Since the Timoshenko kinematics is considered in the developed model, the analytical solution is equal to the Timoshenko one for this specific case.

Figure 5.5 compares the shear stress distributions at half length of the beam, respectively calculated with the Jourawsky formula (J), the analytical model (AN) and the finite element analysis (FE). Also for the stresses a matching among the considered solutions arises and the analytical solution is coincident with the Jourawsky solution (see Table 5.1).

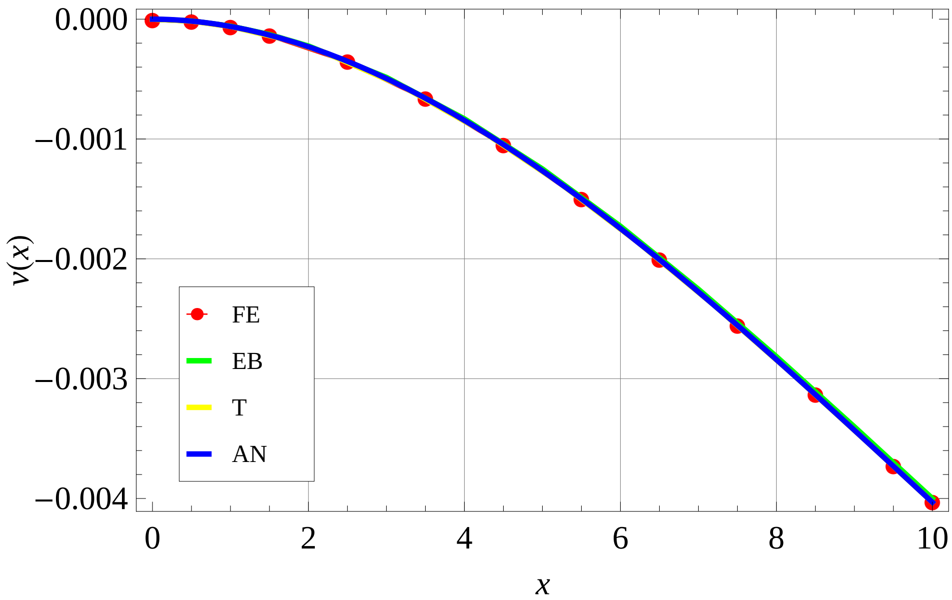

Figure 5.4: Deflection results for the prismatic beam. The abscissa x and the ordinate $v(x)$ represent the beam axis and the deflection. The adopted unit of measurement, for both axes, is m. The labels FE, EB, T and AN indicate the finite element, the Euler- Bernoulli, the Timoshenko and the analytical solution, respectively.

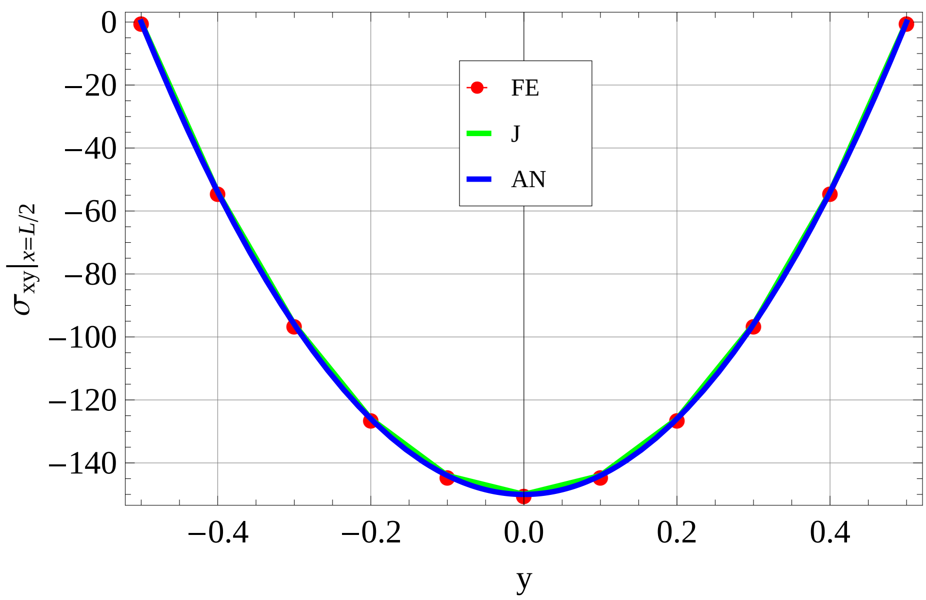

Figure 5.5: Shear stress results for the prismatic beam. The abscissa y indicates the axis along the beam thickness, using m as unit of measurement and the ordinate $\sigma_{xy}|_{x=L/2}$ indicates the shear stress at $x = L/2$, using $\mathrm{kN/m^2}$ as unit of measurement. The labels FE, J and AN represent the finite element, the Jourawsky and the analytical solution, respectively.

Table 5.1: List of the deflection results at $x = L$ and of the maximum shear stress results at $x = L/2$. e_v and e_σ are the percentage errors with respect to the finite element solution.

PRISMATIC BEAM

MODELS	$v(x)$[m]	$max(\sigma_{xy}\|_{x=L/2})$[kN/m^2]	e_v[%]	e_σ[%]
EULER-BERNOULLI	$-4.000 \cdot 10^{-3}$	–	$6.048 \cdot 10^{-1}$	–
TIMOSHENKO	$-4.031 \cdot 10^{-3}$	–	$1.705 \cdot 10^{-1}$	–
JOURAWSKY	–	$-1.500 \cdot 10^{2}$	–	$2.109 \cdot 10^{-1}$
ANALYTICAL	$-4.031 \cdot 10^{-3}$	$-1.500 \cdot 10^{2}$	$1.702 \cdot 10^{-1}$	$2.109 \cdot 10^{-1}$
FE (reference solution)	$-4.024 \cdot 10^{-3}$	$-1.503 \cdot 10^{2}$	0	0

5.3 Linearly tapered symmetric beam

The following geometry dimensions are assumed in order to evaluate the numerical solution of the problem shown in Figure 5.6:

$$
\begin{aligned}
H &= 0.25 \text{ m} \\
L &= 10 \text{ m} \\
A(L) &= 0.5 \text{ m}^2
\end{aligned}
\tag{5.24}
$$

Where the beam cross-section is assumed rectangular with a base equal to 1 m.

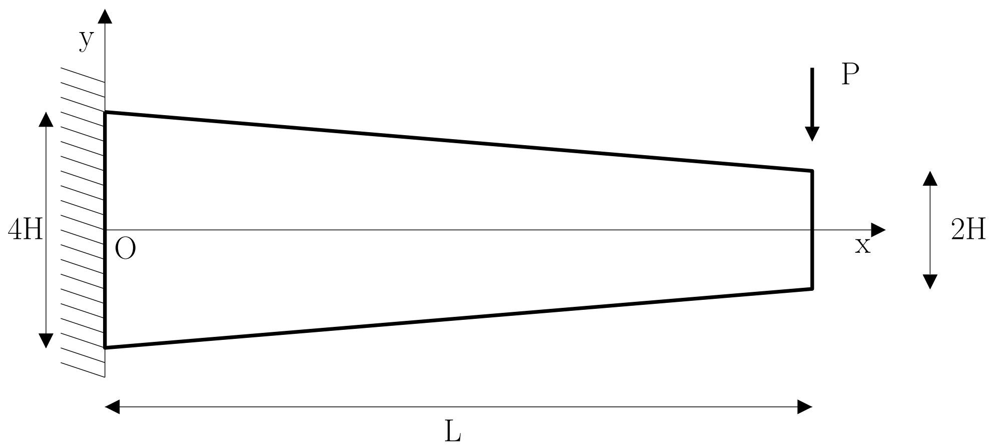

Figure 5.6: Cantilever linearly tapered symmetric beam

5.3.1 Mathematica results

The analysed beam presents a more complex geometry than the previous prismatic beam. Therefore, by using the command DSolve, it is not possible to obtain the analytical solution of the mixed ODEs and of the displacement ODEs. However, it is possible to proceed numerically with the command NDSolve.

Numerical solution for the mixed ODEs

Considering the system of the six ODEs (see Equation 4.27) and the boundary conditions (5.2) previously introduced, the problem shown in Figure 5.6 is numerically solved for the variables $\theta(x)$, $u(x)$, $v(x)$, $\sigma_{xo}(x)$, $\sigma_{x1}(x)$ and $\tau(x)$ by using the command NDsolve. The values of the mechanical properties and the geometry dimensions to be used are indicated in Equation (5.1) and (5.24), respectively. Focusing on the deflection $v(x)$, this can be estimated at the right edge of the beam:

$$v(L) = -6.577 \cdot 10^{-3} \text{ m} \tag{5.25}$$

Another value of interest to be computed, in order to make a comparison with the other results, is the maximum value of the shear stress at half length of the beam. Considering the geometry of the current case (Figure 5.6), the shear stress σ_{xy}, reported in Equation (4.12c), becomes:

$$\begin{aligned} \sigma_{xy} = \frac{1}{H^2 L(-2L+x)^2} \Big\{ L \Big[-H^2(-2L+x)^2 + L^2 y^2 \Big] \tau(x) + \\ - H^2(2L-x) \Big[Ly\sigma_{x0}(x) + H(2L-x)\sigma_{x1}(x) \Big] \Big\} \end{aligned} \tag{5.26}$$

It is important to notice that the expression of shear stress σ_{xy}, in (5.26), is function of x and y. As a consequence, it is necessary to solve $max(\sigma_{xy}|_{x=L/2})$ with respect to y. In this case, since the beam is symmetric with respect to the beam axis and according to the hypotheses on the displacement and stress field, the maximum of the shear stress is at $y = 0$. Therefore, substituting the values of $\tau(L/2)$, $\sigma_{x0}(L/2)$ and $\sigma_{x1}(L/2)$, numerically found by using the command NDSolve, in Equation (5.26), the following maximum value of the shear stress at $x = L/2$ is obtained:

$$max(\sigma_{xy}|_{x=L/2}) = -1.333 \cdot 10^2 \text{ kN/m}^2 \tag{5.27}$$

Numerical solution for the displacement ODEs

Considering the system of the three ODEs (see Equation 4.29) and the boundary conditions (5.3) previously introduced, the problem shown in Figure 5.6 is numerically solved for the variables $\theta(x)$, $u(x)$ and $v(x)$ and their derivatives, by using the command NDsolve. Therefore, at $x = L$, the deflection $v(x)$ results equal to:

$$v(L) = -6.581 \cdot 10^{-3} \text{ m} \tag{5.28}$$

Now, in order to calculate the maximum shear stress, at $x = L/2$, it is necessary to substitute the values of $v'(L/2)$, $\theta(L/2)$ and $\theta'(L/2)$, numerically obtained by the command NDSolve, in (4.28) and, this way, find the values of $\tau(L/2)$, $\sigma_{x0}(L/2)$ and $\sigma_{x1}(L/2)$. Once $\tau(L/2)$, $\sigma_{x0}(L/2)$ and $\sigma_{x1}(L/2)$ are known, the maximum value of shear stress at half length of the beam can be recovered through Equation (5.26) and considering y equal to 0, as previously discussed:

$$\sigma_{xy}|_{x=L/2} = -1.323 \cdot 10^{2} \text{ kN/m}^2 \tag{5.29}$$

5.3.2 Classical theory results

The classical beam theories are used in this section in order to evaluate the deflection at the free edge of the beam shown in Figure 5.6. In particular, the principle of virtual work is considered, because it represents one of the possible integral forms to be used for studying a beam in Euler-Bernoulli hypotheses or Timoshenko hypotheses. Another value of interest is the maximum shear stress and it is computed at half length of the beam by means of the Jourawsky theory.

Euler-Bernoulli solution

Considering the Euler-Bernoulli hypotheses and the prismatic cantilever beam that is subject to a concentrated load P on the free edge, the principle of virtual work can be written as follows:

$$v(x) = \int_0^L \left[(L-x) \, \frac{P\,(L-x)}{EI} \right] dx \tag{5.30}$$

Where I represents the second moment of area, which varies along the beam longitudinal axis for the current case (Figure 5.6). Considering the full expression of I and the cross-section base equal to 1 m, Equation (5.30) can be written as follows below according to the expression of $t(x)$ (4.25b):

$$v(x) = \int_0^L \left[(L-x) \frac{12P\,(L-x)}{E(-(2Hx)/(L)+4H)^3} \right] dx \tag{5.31}$$

It can also be noticed that the first member of Equation (5.30) is the external work, whereas the second term is the internal work. After solving the integral (5.30), the deflection $v(x)$ is found:

$$v(x) = \frac{3PL^3(-5+Log(256))}{16EH^3} \tag{5.32}$$

Then considering the mechanical properties (5.1) and the geometry (5.24), it is possible to achieve the numerical result of the deflection at $x = L$.

$$v(L) = -6.542 \cdot 10^{-3}\ \text{m} \tag{5.33}$$

Timoshenko solution

Considering the Timoshenko hypotheses and the prismatic cantilever beam that is subject to a concentrated load P on the free edge, the principle of virtual work can be written as follows:

$$v(x) = \int_0^L \left[(L-x) \frac{P\,(L-x)}{EI} \right] dx + \int_0^L \left[\frac{P}{(5/6)GA(x)} \right] dx \tag{5.34}$$

Where I represents the second moment of area, $A(x)$ is the cross-section area and G represents the shear modulus. Considering the full expression of I and $A(x)$ and assuming the cross-section base equal to 1 m, Equation (5.34) can be written as follows below, according to the expression of $t(x)$ (4.25b):

$$v(x) = \int_0^L \left[(L-x) \frac{12P\,(L-x)}{E(-(2Hx)/(L)+4H)^3} \right] dx + \int_0^L \left[\frac{P}{(5/6)G(-(2Hx)/(L)+4H)} \right] dx \tag{5.35}$$

It can also be noticed that the first member of Equation (5.34) is the external work, whereas the second term, is the internal work. After solving the integral (5.34), the deflection $v(x)$ is found:

$$v(x) = \frac{3PL^3(-5+Log(256))}{16EH^3} + \frac{3PLLog(2)}{5GH} \tag{5.36}$$

Then, considering the mechanical properties (5.1) and the geometry (5.24), it is possible to achieve the numerical result of the deflection at $x = L$.

$$v(L) = -6.585 \cdot 10^{-3} \text{ m} \tag{5.37}$$

Jourawsky solution

The well-known Jourawsky formula is used to find an approximate solution of the shear stress. Considering the tapered beam, shown in Figure 5.6, the Jourawsky formula is written as follows:

$$\sigma_{xy} = \frac{12P(1/2)((-(Hx)/(L)+2H)-y)((-(Hx)/(L)+2H)+y)}{(-(2Hx)/(L)+4H)^3} \tag{5.38}$$

Since the value to be evaluated is the maximum shear stress along the cross-section, in order to calculate $max(\sigma_{xy}|_{x=L/2})$, y is assumed equal to zero, then the mechanical property values (5.1) and the geometry (5.24) are substituted in Equation (5.38). By doing this, the maximum shear stress at half length of the beam is obtained:

$$max(\sigma_{xy}|_{x=L/2}) = -2.000 \cdot 10^2 \text{ kN/m}^2 \tag{5.39}$$

5.3.3 FEM results

The finite element analysis is performed by using the software Abaqus. Focusing on the modelling, the same procedure illustrated for the prismatic beam (for more details see Paragraph 5.2.3) is followed. First of all it is necessary to define the geometry of the beam, noticing that four points only are capable alone of describing the linearly tapered beam (see Figure 5.6). Then, connecting them by two oblique lines and two vertical lines, the beam is generated. After that, it is important to define the mechanical properties (see the two values introduced in (5.1)), and to enforce the boundary conditions, emphasizing that on the left end there is a fixed support and on the right end a concentrated load. Lastly, an appropriate quadrangular mesh must be generated according to the dimension of the beam. In the case under investigation, since the maximum beam height is equal to 1 m, the "Approximate global size" is chosen equal to 0.05 m. The rightness of this choice is mainly proven by an accurate convergence analysis, performed by using different values of the "Approximate global size" which are smaller and smaller.

The model is now ready to be analysed. The deflection on the right edge is the first value of interest. Therefore, choosing "U" and "U2" from the model tree, the variation of the deflection along the beam longitudinal axis is shown (Figure 5.7).

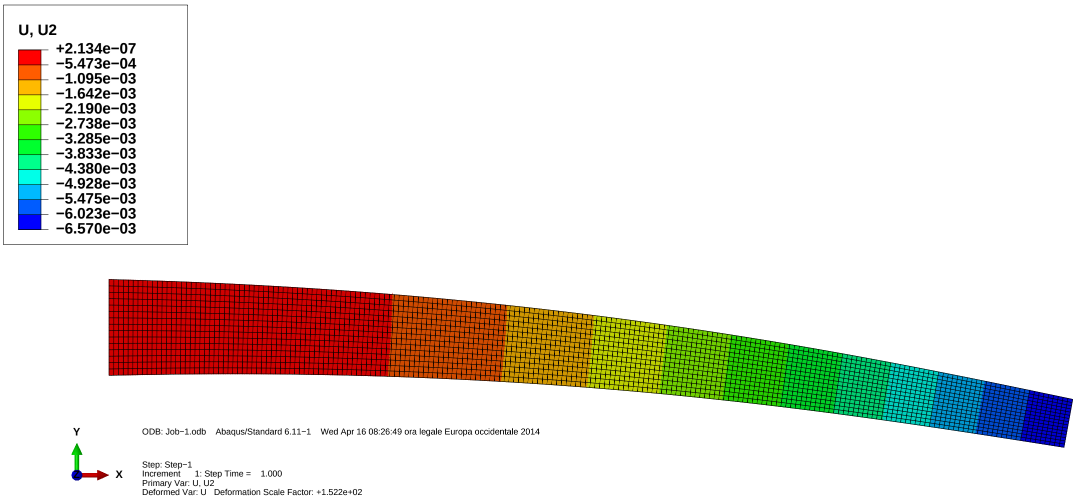

Figure 5.7: Results of "U2" obtained by using the software Abaqus for the cantilever linearly tapered symmetric beam with a concentrated load on the free edge

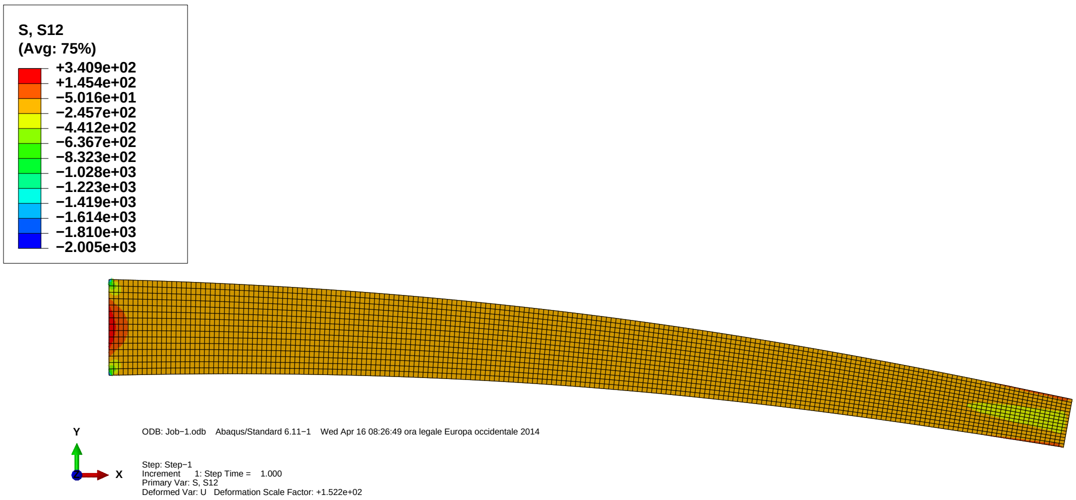

Figure 5.8: Results of "S12" obtained by using the software Abaqus for the cantilever linearly tapered symmetric beam with a concentrated load at the free edge

By doing this, it is possible to read the deflection at the right end:

$$v(L) = -6.570 \cdot 10^{-3} \text{ m} \tag{5.40}$$

The same procedure is followed to evaluate the maximum shear stress at half length of the beam. Therefore, choosing "S" and "S12" from the model tree, Figure 5.8 is obtained which shows how the shear stress varies along the beam longitudinal axis. In order to find the value of interest, a "path" is created along the said cross-section. The resulting shear distribution is symmetric with respect to the beam axis and parabolic. The maximum is in correspondence of half cross-section and it results equal to:

$$max(\sigma_{xy}|_{x=L/2}) = -1.334 \cdot 10^2 \text{ kN/m}^2 \tag{5.41}$$

5.3.4 Comparison of the results

Figure 5.9 plots how the deflection $v(x)$ varies along the beam axis, considering the solution obtained by the developed analytical model (AN), the finite element method (FE) and the two classical beam theories of Euler-Bernoulli (EB) and Timoshenko (T). The four curves are almost coincident, showing a high degree of matching among the adopted methods. Also, in Table 5.2 the analytical result is very similar to the Timoshenko solution, but not coincident. The main reason is that the developed model computes and naturally considers the correct shear factor (as previously discussed in Chapter 4). On the other hand, in the expression of the principle of virtual work, used to evaluate the deflection, the shear factor is always equal to 5/6 even if a tapered beam is investigated. This aspect represents a great advantage of the analytical model.

Figure 5.10 illustrates the shear stress profile at half length of the beam for each method. For the beam under investigation there is a clear mismatch between the Jourawsky solution (J) and the other two solutions (FE and AN). The Jourawsky theory is based on simple assumptions, certainly not suitable to calculate the shear stresses on tapered beams. When the beam is tapered, in fact, the stress values on the upper and lower cross-section borders are different from zero even if zero traction is considered on both of them (as Figure 5.10 shows for AN and FE solutions). The Jourawsky solution, instead, imposes that the shear stress be zero on the cross-section limits.

Figure 5.11 focuses on the analytical and the finite element solutions. It is possible to notice that the shear stress distribution, provided by the developed model, is almost constant and represents an average of the numerical distribution. Nevertheless, the mismatch between the two solutions is acceptable because the numerical solution is very similar to the analytical one.

Table 5.2: List of the deflection results at $x = L$ and of the maximum shear stress results at $x = L/2$. e_v and e_σ are the percentage errors with respect to the finite element solution.

LINEARLY TAPERED SYMMETRIC BEAM

MODELS	$v(x)$[m]	$max(\sigma_{xy}\|_{x=L/2})$[kN/m^2]	e_v[%]	e_σ[%]
EULER-BERNOULLI	$-6.542 \cdot 10^{-3}$	–	$4.295 \cdot 10^{-1}$	–
TIMOSHENKO	$-6.585 \cdot 10^{-3}$	–	$2.288 \cdot 10^{-1}$	–
JOURAWSKY	–	$-2.000 \cdot 10^{2}$	–	$4.993 \cdot 10^{1}$
ANALYTICAL	$-6.577 \cdot 10^{-3}$	$-1.333 \cdot 10^{2}$	$1.012 \cdot 10^{-1}$	$4.648 \cdot 10^{-2}$
FE (reference solution)	$-6.570 \cdot 10^{-3}$	$-1.334 \cdot 10^{2}$	0	0

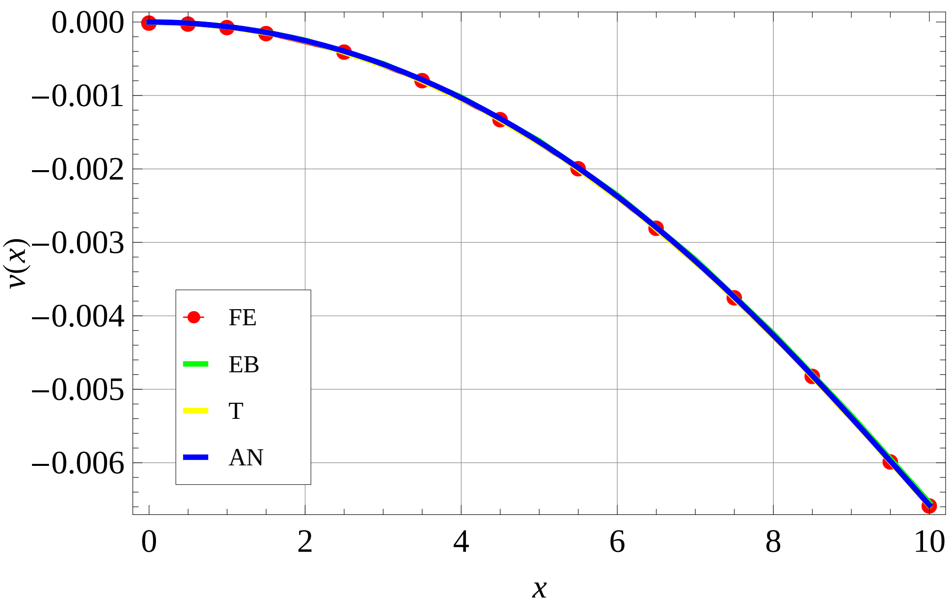

Figure 5.9: Deflection results for the linearly tapered symmetric beam. The abscissa x and the ordinate $v(x)$ represent the beam axis and the deflection. The adopted unit of measurement, for both axes, is m. The labels FE, EB, T and AN indicate the finite element, the Euler- Bernoulli, the Timoshenko and the analytical solution, respectively.

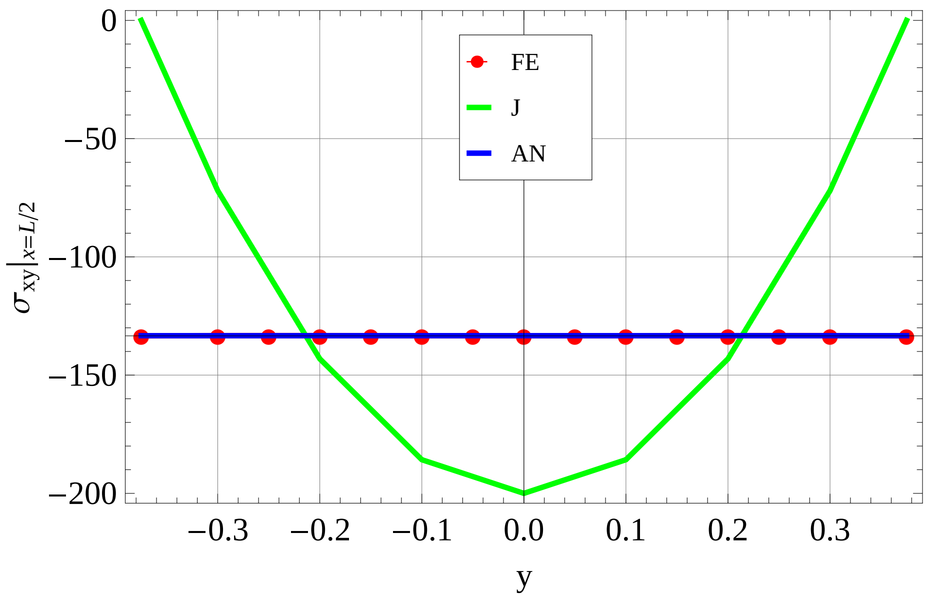

Figure 5.10: Shear stress results for the linearly tapered symmetric beam. The abscissa y indicates the axis along the beam thickness, using m as unit of measurement and the ordinate $\sigma_{xy}|_{x=L/2}$ indicates the shear stress at $x = L/2$, using $\mathrm{kN/m^2}$ as unit of measurement. The labels FE, J and AN represent the finite element, the Jourawsky and the analytical solution, respectively.

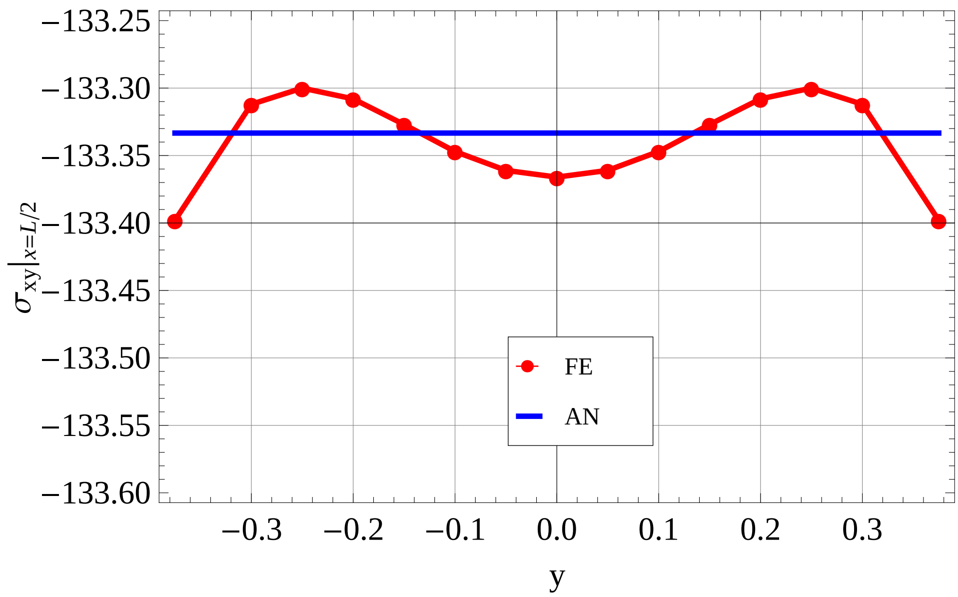

Figure 5.11: Shear stress results for the linearly tapered symmetric beam. The abscissa y indicates the axis along the beam thickness, using m as unit of measurement and the ordinate $\sigma_{xy}|_{x=L/2}$ indicates the shear stress at $x = L/2$, using $\mathrm{kN/m^2}$ as unit of measurement. The labels FE and AN represent the finite element and the analytical solution, respectively.

5.4 Linearly tapered non-symmetric beam

The following geometry dimensions are assumed in order to evaluate the numerical solution of the problem shown in Figure (Figure 5.12):

$$
\begin{aligned}
&H = 0.25 \text{ m} \\
&L = 10 \text{ m} \\
&A(L) = 0.5 \text{ m}^2
\end{aligned}
\tag{5.42}
$$

Where the beam cross-section is assumed rectangular with a base equal to 1 m.

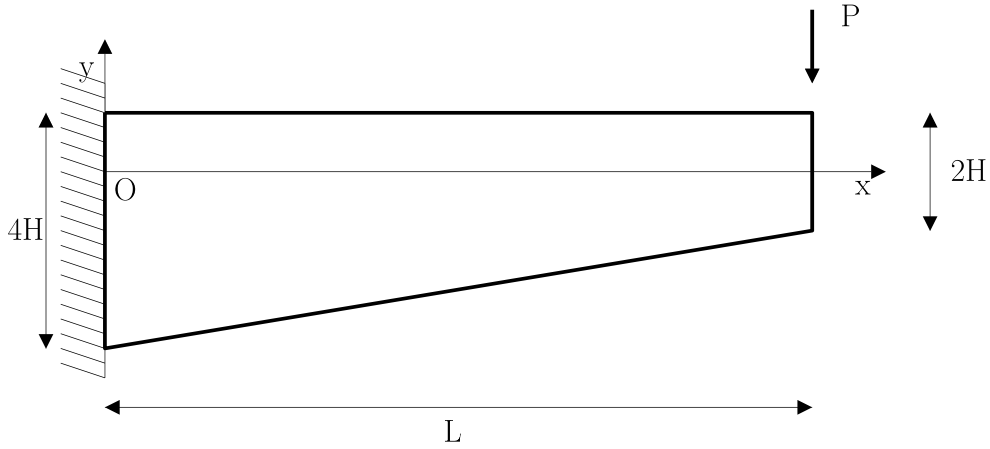

Figure 5.12: Cantilever linearly tapered non-symmetric beam

5.4.1 Mathematica results

The analysed beam presents a complex geometry with respect to the prismatic beam. Therefore, by using the command DSolve, it is not possible to obtain the analytical solution of the mixed ODEs and of the displacement ODEs. However, it is possible to proceed numerically with the command NDSolve.

Numerical solution for the mixed ODEs

Considering the system of the six ODEs (4.32) and the boundary conditions (5.2) previously introduced, the problem shown in Figure 5.12 is numerically solved for the variables $\theta(x)$, $u(x)$, $v(x)$, $\sigma_{xo}(x)$, $\sigma_{x1}(x)$ and $\tau(x)$ by using the command NDsolve. The values of the mechanical properties and the geometry dimensions to be used are indicated in equation

(5.1) and (5.42), respectively. Focusing on the deflection $v(x)$, this can be estimated at the right edge of the beam:

$$v(L) = -6.586 \cdot 10^{-3} \text{ m} \tag{5.43}$$

Another value of interest to be computed in order to make a comparison with the other results is the maximum value of the shear stress at half length of the beam. It is important to notice that the expression of shear stress σ_{xy} (see Equation 4.12c) is function of x and y. As a consequence, it is necessary to solve $max(\sigma_{xy}|_{x=L/2})$ with respect to y. By doing this, the maximum of the shear stress within the considered cross-section, is registered at the lower border. Therefore, substituting the values of $\tau(L/2)$, $\sigma_{x0}(L/2)$ and $\sigma_{x1}(L/2)$, numerically found by using the command NDSolve, and the expressions of $c(x)$ and $t(x)$ (see Equation 4.30a and 4.30b) in Equation (4.12c), the following maximum value of the shear stress at $x = L/2$ is obtained:

$$max(\sigma_{xy}|_{x=L/2}) = -2.667 \cdot 10^{2} \text{ kN/m}^2 \tag{5.44}$$

Numerical solution for the displacement ODEs

Considering the system of the three ODEs, whose full verbalization has been omitted in Chapter 4 due to the excessive length, and the boundary conditions (5.3) previously introduced, the problem shown in Figure 5.12 is numerically solved for the variables $\theta(x)$, $u(x)$ and $v(x)$ and their derivatives, by using the command NDsolve. Therefore, at $x = L$, the deflection $v(x)$ results equal to:

$$v(L) = -6.591 \cdot 10^{-3} \text{ m} \tag{5.45}$$

Now, in order to calculate the maximum shear stress, at $x = L/2$, it is necessary to substitute the values of $v'(L/2)$, $\theta(L/2)$ and $\theta'(L/2)$, numerically obtained by the command NDSolve, in the expression of $\tau(x)$, $\sigma_{x0}(x)$ and $\sigma_{x1}(x)$ obtained by using the static condensation method, but omitted in Chapter 4 due to their length. Once $\tau(L/2)$, $\sigma_{x0}(L/2)$ and $\sigma_{x1}(L/2)$ are known, the maximum value of shear stress at half length of the beam can be recovered through Equation (4.12c) and considering y equal to -0.5 m, as previously discussed:

$$max(\sigma_{xy}|_{x=L/2}) = -2.668 \cdot 10^{2} \text{ kN/m}^2 \tag{5.46}$$

5.4.2 Classical theory results

The classical beam theories are used in this section in order to evaluate the deflection at the free edge of the beam shown in Figure 5.12. In particular the principle of virtual work is considered, because it represents one of the possible integral forms to be used for studying a beam in Euler-Bernoulli hypotheses or Timoshenko hypotheses. Another value of interest is the maximum shear stress and it is computed at half length of the beam by means of the Jourawsky theory.

Euler-Bernoulli solution

Considering the Euler-Bernoulli hypotheses and the prismatic cantilever beam that is subject to a concentrated load P on the free edge, the principle of virtual work can be written as follows:

$$v(x) = \int_0^L \left[(L-x)\,\frac{P\,(L-x)}{EI} \right] dx \tag{5.47}$$

Where I represents the second moment of area which varies along the beam longitudinal axis for the current case (Figure 5.12). Considering the full expression of I and the cross-section base equal to 1 m, Equation (5.47) can be written as follows below, according to the expression of $t(x)$ (4.25b):

$$v(x) = \int_0^L \left[(L-x)\,\frac{12P\,(L-x)}{E(-(2Hx)/(L)+4H)^3} \right] dx \tag{5.48}$$

It can also be noticed that the first member of Equation (5.47) is the external work, whereas the second term is the internal work. After solving the integral (5.47), the deflection $v(x)$ is found:

$$v(x) = \frac{3PL^3(-5+Log(256))}{16EH^3} \tag{5.49}$$

Then, considering the mechanical properties (5.1) and the geometry (5.42), it is possible to achieve the numerical result of the deflection at $x = L$.

$$v(L) = -6.542 \cdot 10^{-3}\ \text{m} \tag{5.50}$$

Timoshenko solution

Considering the Timoshenko hypotheses and the prismatic cantilever beam that is subject to a concentrated load P on the free edge, the principle of virtual work can be written as follows:

$$v(x) = \int_0^L \left[(L-x)\, \frac{P\,(L-x)}{EI} \right] dx + \int_0^L \left[\frac{P}{(5/6)GA(x)} \right] dx \tag{5.51}$$

Where I represents the second moment of area, $A(x)$ is the cross-section area and G represents the shear modulus. Considering the full expression of I and $A(x)$ and assuming the cross-section base equal to 1 m, Equation (5.51) can be written as follows below, according to the expression of $t(x)$ (4.30b):

$$v(x) = \int_0^L \left[(L-x)\, \frac{12P\,(L-x)}{E(-(2Hx)/(L)+4H)^3} \right] dx + \int_0^L \left[\frac{P}{(5/6)G(-(2Hx)/(L)+4H)} \right] dx \tag{5.52}$$

It can also be noticed that the first member of Equation (5.51) is the external work, whereas the second term is the internal work. After solving the integral (5.51), the deflection $v(x)$ is found:

$$v(x) = \frac{3PL^3(-5+Log(256))}{16EH^3} + \frac{3PLLog(2)}{5GH} \tag{5.53}$$

Then, considering the mechanical properties (5.1) and the geometry (5.42), it is possible to achieve the numerical result of the deflection at $x = L$.

$$v(L) = -6.585 \cdot 10^{-3}\ \mathrm{m} \tag{5.54}$$

Jourawsky solution

The well-known Jourawsky formula is used to find an approximate solution of the shear stress. Considering the tapered beam, shown in Figure 5.12, the Jourawsky formula is written as follows:

$$\sigma_{xy} = \frac{12P(1/2)((-(Hx)/(L)+2H)-y)((-(Hx)/(L)+2H)+y)}{(-(2Hx)/(L)+4H)^3} \tag{5.55}$$

Since the value to be evaluate is the maximum shear stress within the cross-section height, y is assumed equal to 0, then the mechanical property values (5.1) and the geometry (5.42) are substituted in (5.55). By doing this, the maximum shear stress at half length of the beam is obtained:

$$max(\sigma_{xy}|_{x=L/2}) = -2.000 \cdot 10^2\ \mathrm{kN/m^2} \tag{5.56}$$

In this section it can be noticed that the same result, obtained for a linearly tapered symmetric beam, arises. This aspect represents a well-known limitation of Jourawsky theory. In fact, for the case under investigation, the maximum of the shear stress within the considered cross-section is at $y = -0.5$ m and not at $y = 0$. Therefore this theory is not able to approximate the shear stress distribution for a non-symmetric beam and, in other words, to distinguish the shear stress result between a symmetric beam and a non-symmetric one.

5.4.3 FEM results

The finite element analysis is performed by using the software Abaqus. Focusing on the modelling, the same procedure illustrated for the prismatic beam (for more details see Paragraph 5.2.3) is followed. First of all it is necessary to define the geometry of the beam, noticing that four points only are capable alone of describing the linearly tapered beam (see Figure 5.12). Then, connecting them by one horizontal line, one oblique line and two vertical lines, the beam is generated. After that, it is important to define the mechanical properties (see the two values introduced in (5.1)), and to enforce the boundary conditions, emphasizing that on the left end there is a fixed support and on the right end a concentrated load. Lastly, an appropriate quadrangular mesh must be generated according to the dimension of the beam. In the case under investigation, since the maximum beam height is equal to 1 m, the "Approximate global size" is chosen equal to 0.05 m. The rightness of this choice is mainly proven by an accurate convergence analysis, performed by using different values of the "Approximate global size" which are smaller and smaller.

The model is now ready to be analysed. The deflection on the right edge is the first value of interest. Therefore, choosing "U" and "U2" from the model tree, the variation of the deflection along the beam longitudinal axis is shown (Figure 5.13).

By doing this, it is possible to read the deflection at the right end:

$$v(L) = -6.578 \cdot 10^{-3} \text{ m} \tag{5.57}$$

The same procedure is followed to evaluate the maximum shear stress at half length of the beam. Therefore, choosing "S" and "S12" from the model tree, Figure 5.14 is obtained which shows how the shear stress varies along the beam longitudinal axis. In order to find the value of interest, a "path" is created along the said cross-section. The resulting shear distribution is non-symmetric with respect to the beam axis. The maximum is in

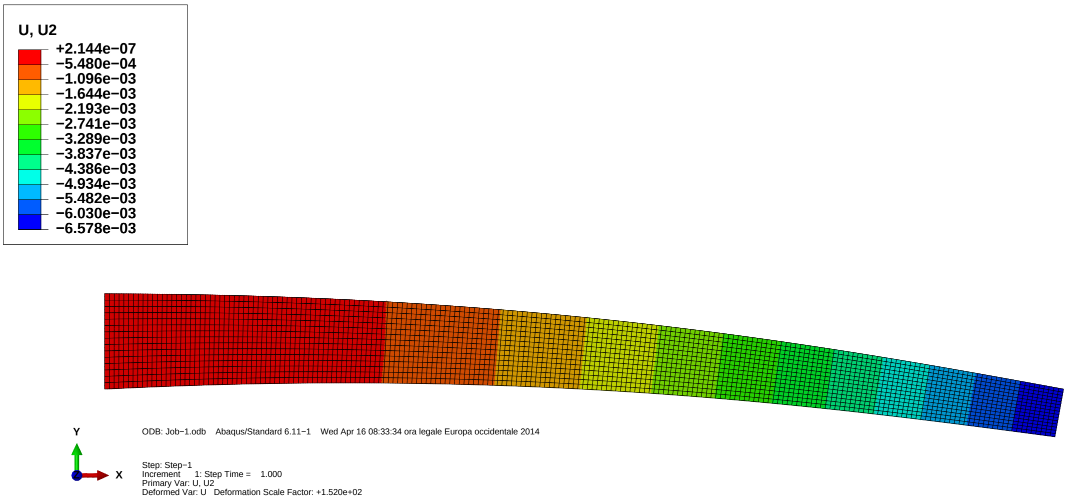

Figure 5.13: Results of "U2" obtained by using the software Abaqus for the cantilever linearly tapered non-symmetric beam with a concentrated load on the right edge

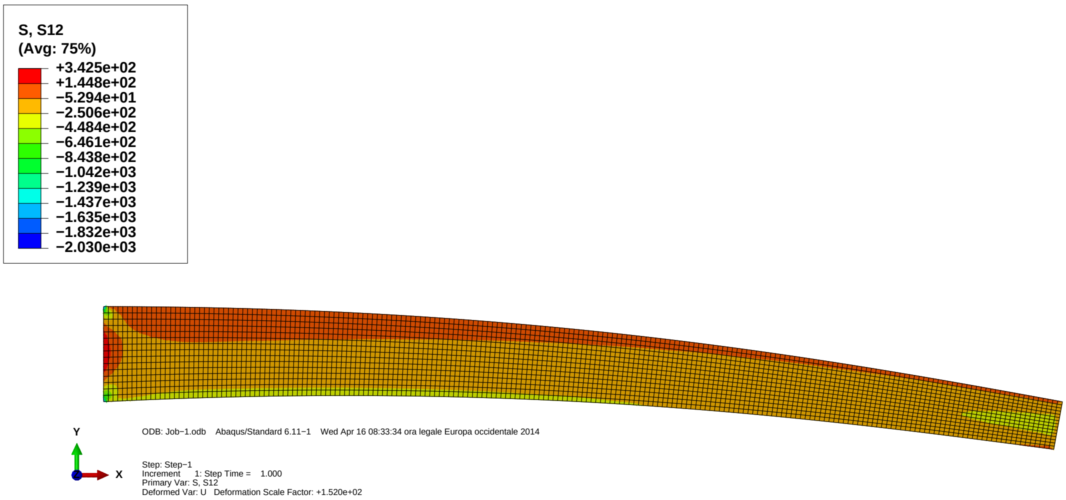

Figure 5.14: Results of "S12" obtained by using the software Abaqus for the cantilever linearly tapered non-symmetric beam with a concentrated load on the right edge

correspondence of the lower border and it results equal to:

$$max(\sigma_{xy}|_{x=L/2}) = -2.668 \cdot 10^2 \text{ kN/m}^2 \tag{5.58}$$

5.4.4 Comparison of the results

Figure 5.15 shows how the deflection $v(x)$ varies along the beam axis. Even though the four curves are almost coincident, the comparison among the deflection results in Table 5.2 and Table 5.3 clearly proves that the classical beam theories are unable to distinguish the case of a tapered symmetric beam from the case of a tapered non-symmetric beam.

Figure 5.16 illustrates the shear stress profile at half length of the beam. A high degree of matching between the analytical solution (AN) and finite element solution (FE) arises from the comparison. On the other hand, there is a mismatch between the Jourawsky solution (J) and the other two solutions (AN and FE). It is important to restate that the Jourawsky theory is not suitable to calculate the shear stresses of beams with a variable cross-section, and besides, non-symmetric with respect of their axis.

Table 5.3: List of the deflection results at $x = L$ and of the maximum shear stress results at $x = L/2$. e_v and e_σ are the percentage errors with respect to the finite element solution.

LINEARLY TAPERED NON-SYMMETRIC BEAM

MODELS	$v(x)$[m]	$max(\sigma_{xy}\|_{x=L/2})$[kN/m^2]	e_v[%]	e_σ[%]
EULER-BERNOULLI	$-6.542 \cdot 10^{-3}$	–	$5.512 \cdot 10^{-1}$	–
TIMOSHENKO	$-6.585 \cdot 10^{-3}$	–	$1.063 \cdot 10^{-1}$	–
JOURAWSKY	–	$-2.000 \cdot 10^2$	–	$2.503 \cdot 10^1$
ANALYTICAL	$-6.586 \cdot 10^{-3}$	$-2.667 \cdot 10^2$	$1.157 \cdot 10^{-1}$	$2.661 \cdot 10^{-2}$
FE (reference solution)	$-6.578 \cdot 10^{-3}$	$-2.668 \cdot 10^2$	0	0

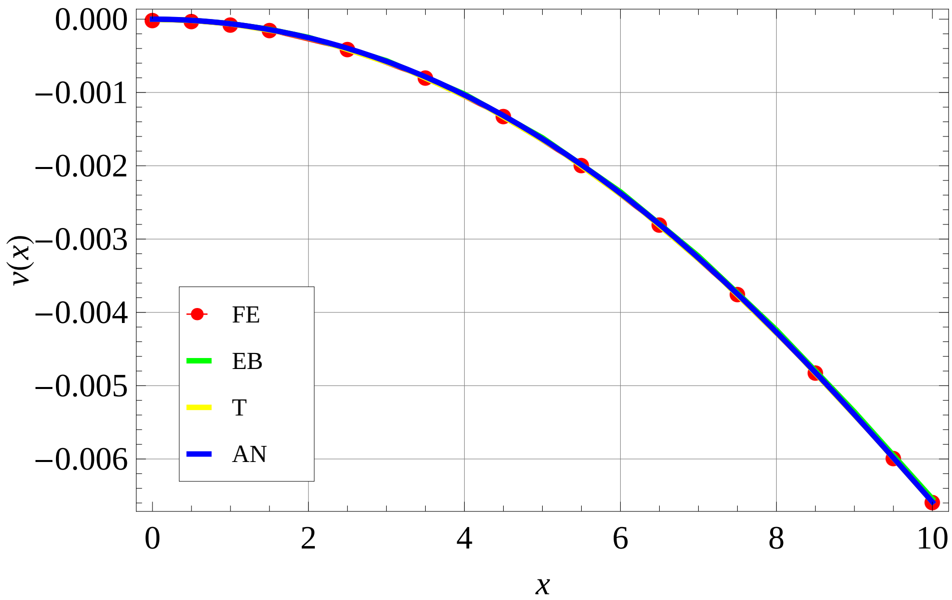

Figure 5.15: Deflection results for the linearly tapered non-symmetric beam. The abscissa x and the ordinate $v(x)$ represent the beam axis and the deflection. The adopted unit of measurement, for both axes, is m. The labels FE, EB, T and AN indicate the finite element, the Euler- Bernoulli, the Timoshenko and the analytical solution, respectively.

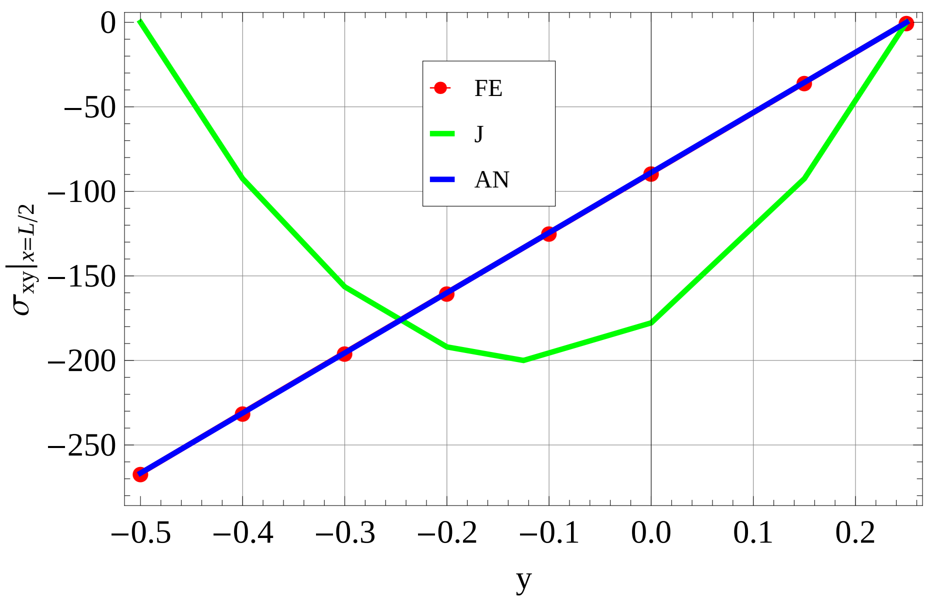

Figure 5.16: Shear stress results for the linearly tapered non-symmetric beam. The abscissa y indicates the axis along the beam thickness, using m as unit of measurement and the ordinate $\sigma_{xy}|_{x=L/2}$ indicates the shear stress at $x = L/2$, using $\mathrm{kN/m^2}$ as unit of measurement. The labels FE, J and AN represent the finite element, the Jourawsky and the analytical solution, respectively.

5.5 Curvilinearly tapered symmetric beam

The following geometry dimensions are assumed in order to evaluate the numerical solution of the problem shown in Figure 5.17:

$$H = 0.25 \text{ m}$$
$$L = 10 \text{ m} \tag{5.59}$$
$$A(L) = 0.1 \text{ m}^2$$

Where the beam cross-section is assumed rectangular with a base equal to 1 m.

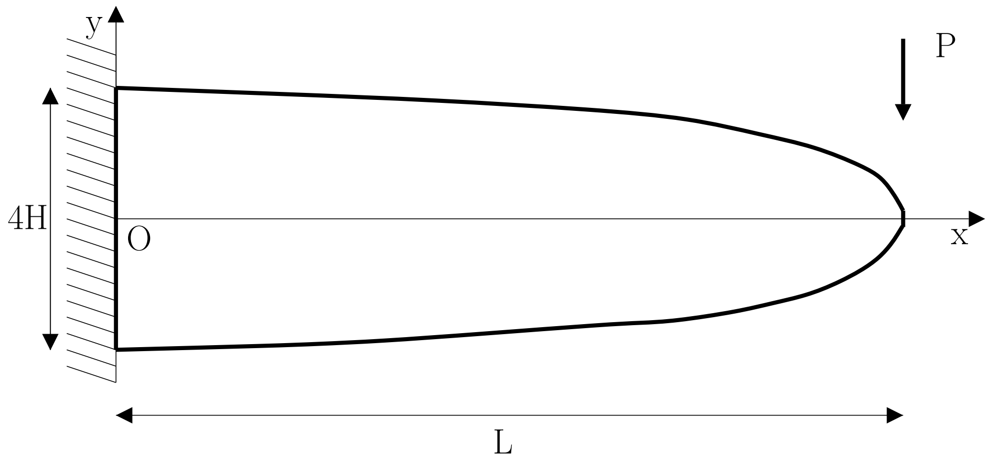

Figure 5.17: Cantilever curvilinearly tapered symmetric beam

5.5.1 Mathematica results

The analysed beam presents a very complex geometry with respect to the prismatic beam and the linearly tapered beams. Moreover, as shown in Paragraph 4.9, the system of the displacement ODEs is excessively long. As a consequence, the system of mixed ODEs only can numerically be solved by the command NDSolve.

Numerical solution for the mixed ODEs

Considering the system of the six ODEs (see Appendix A and Equation A.3) and the boundary conditions (5.2) previously introduced, the problem shown in Figure 5.17 is numerically solved for the variables $\theta(x)$, $u(x)$, $v(x)$, $\sigma_{xo}(x)$, $\sigma_{x1}(x)$ and $\tau(x)$ by using the command NDsolve. The values of the mechanical properties and the geometry dimensions to be used are indicated in Equation (5.1) and (5.59), respectively. Focusing on the deflection $v(x)$, this can be estimated at the right edge of the beam:

$$v(L) = -7.857 \cdot 10^{-3} \text{ m} \tag{5.60}$$

Another value of interest to be computed in order to make a comparison with the other results is the maximum value of the shear stress at half length of the beam. It is important to notice that the expression of shear stress σ_{xy} (see Equation 4.12c) is function of x and y. As a consequence, it is necessary to solve the maximum problem, $max(\sigma_{xy}|_{x=L/2})$, with respect to y. By doing this, the maximum value of the shear stress within the considered cross-section is registered at $y = 0$. Therefore, substituting the values of $\tau(L/2)$, $\sigma_{x0}(L/2)$ and $\sigma_{x1}(L/2)$, numerically found by using the command NDSolve, and the expressions of $c(x)$ and $t(x)$ (see Equation 4.33a and 4.33b) in Equation (4.12c), the following maximum value of the shear stress at $x = L/2$ is obtained:

$$max(\sigma_{xy}|_{x=L/2}) = -1.076 \cdot 10^{2} \text{ kN/m}^2 \tag{5.61}$$

5.5.2 Classical theory results

The classical beam theories are used in this section in order to evaluate the deflection at the free edge of the beam shown in Figure 5.17. In particular the principle of virtual work is considered, because it represents one of the possible integral forms to be used for studying a beam in Euler-Bernoulli hypotheses or Timoshenko hypotheses. Another value of interest is the maximum shear stress and it is computed at half length of the beam by means of the Jourawsky theory.

Euler-Bernoulli solution

Considering the Euler-Bernoulli hypotheses and the prismatic cantilever beam that is subject to a concentrated load P on the free edge, the principle of virtual work can be written as follows:

$$v(x) = \int_0^L \left[(L-x)\,\frac{P\,(L-x)}{EI} \right] dx \tag{5.62}$$

Where I represents the second moment of area which varies along the beam longitudinal axis for the current case (Figure 5.17). Considering the full expression of I and the cross-section base equal to 1 m, Equation (5.62) can be written as follows below, according to the expression of $t(x)$ (4.33b):

$$v(x) = \int_0^L \left[(L-x) \frac{12P\,(L-x)}{E\left(4\sqrt{H^2\,(1-(100x)/(101L))}\right)^3} \right] dx \tag{5.63}$$

It can also be noticed that the first member of Equation (5.62) is the external work, whereas the second term is the internal work. After solving the integral (5.62), the deflection $v(x)$ is found:

$$v(x) = \frac{101(1199+\sqrt{101})PL^3}{1000000EH^3} \tag{5.64}$$

Then, cosidering the mechanical properties (5.1) and the geometry (5.59), it is possible to achieve the numerical result of the deflection at $x = L$.

$$v(L) = -7.815 \cdot 10^{-3}\ \mathrm{m} \tag{5.65}$$

Timoshenko solution

Considering the Timoshenko hypotheses and the prismatic cantilever beam that is subject to a concentrated load P on the free edge, the principle of virtual work can be written as follows:

$$v(x) = \int_0^L \left[(L-x) \frac{P\,(L-x)}{EI} \right] dx + \int_0^L \left[\frac{P}{(5/6)GA(x)} \right] dx \tag{5.66}$$

Where I represents the second moment of area, $A(x)$ is the cross-section area and G represents the shear modulus. Considering the full expression of I and $A(x)$ and assuming the cross-section base equal to 1 m, Equation (5.66) can be written as follows below, according to the expression of $t(x)$ (4.33b):

$$\begin{aligned} v(x) = {} & \int_0^L \left[(L-x) \frac{12P\,(L-x)}{E\left(4\sqrt{H^2\,(1-(100x)/(101L))}\right)^3} \right] dx + \\ & + \int_0^L \left[\frac{P}{(5/6)G\left(4\sqrt{H^2\,(1-(100x)/(101L))}\right)} \right] dx \end{aligned} \tag{5.67}$$

It can also be noticed that the first member of Equation (5.66) is the external work, whereas the second term is the internal work. After solving the integral (5.66), the deflection $v(x)$

is found:

$$v(x) = \frac{101(1199+\sqrt{101})PL^3}{1000000EH^3} + \frac{3PL(-101+\sqrt{101})}{500GH} \tag{5.68}$$

Then, considering the mechanical properties (5.1) and the geometry (5.59), it is possible to achieve the numerical result of the deflection at $x = L$.

$$v(L) = -7.872 \cdot 10^{-3}\ \mathrm{m} \tag{5.69}$$

Jourawsky solution

The well-known Jourawsky formula is used to find an approximate solution of the shear stress. Considering the tapered beam, shown in Figure 5.17, the Jourawsky formula is written as follows:

$$\sigma_{xy} = \frac{12P\left[\left(2\sqrt{H^2\left(1-(100x)/(101L)\right)}\right)-y\right]\left[\left(2\sqrt{H^2\left(1-(100x)/(101L)\right)}\right)+y\right]}{2\left(4\sqrt{H^2\left(1-(100x)/(101L)\right)}\right)^3} \tag{5.70}$$

Since the value to be evaluate is the maximum shear stress within the cross-section height, y is assumed equal to 0, then the mechanical property values (5.1) and the geometry (5.59) are substituted in (5.70). By doing this, the maximum shear stress at half length of the beam is obtained:

$$max(\sigma_{xy}|_{x=L/2}) = -2.111 \cdot 10^2\ \mathrm{kN/m^2} \tag{5.71}$$

5.5.3 FEM results

The finite element analysis is performed by using the software Abaqus. Focusing on the modelling, the same procedure illustrated for the prismatic beam (see Paragraph 5.2.3) is followed. First of all it is necessary to define the geometry of the beam noticing that two vertical lines and one spline are necessary to describe the curvilinearly tapered beam shown in Figure 5.17. More in details, the spline is generated through fifteen points, considering a beam length equal to 10.1 m. Then, by means the command "Auto-Trim", the spline is cutted at $x = 10$ m and it is now possible to connect the upper and lower borders with two vertical lines. The second step of the modelling concerns the definitions of the mechanical properties (see the two values introduced in (5.1)), and the enforcement of the boundary conditions, emphasizing that on the left end there is a fixed support and on the right end a concentrated load. Lastly, an appropriate quadrangular mesh must be generated according to the dimension of the beam. In the case under investigation, since the maximum beam height is equal to 1 m, the "Approximate global size" is chosen equal to 0.05 m. The rightness of this choice is mainly proven by an accurate convergence analysis, performed by using different values of the "Approximate global size" which are smaller and smaller.

The model is now ready to be analysed. The deflection on the right edge is the first

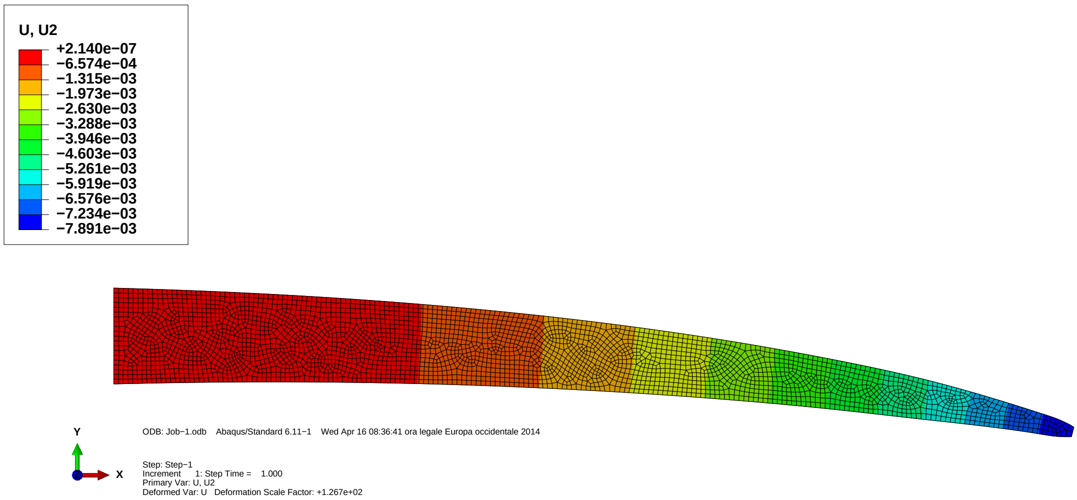

Figure 5.18: Results of "U2" obtained by using the software Abaqus for the cantilever curvilinearly tapered symmetric beam with a concentrated load on the right edge

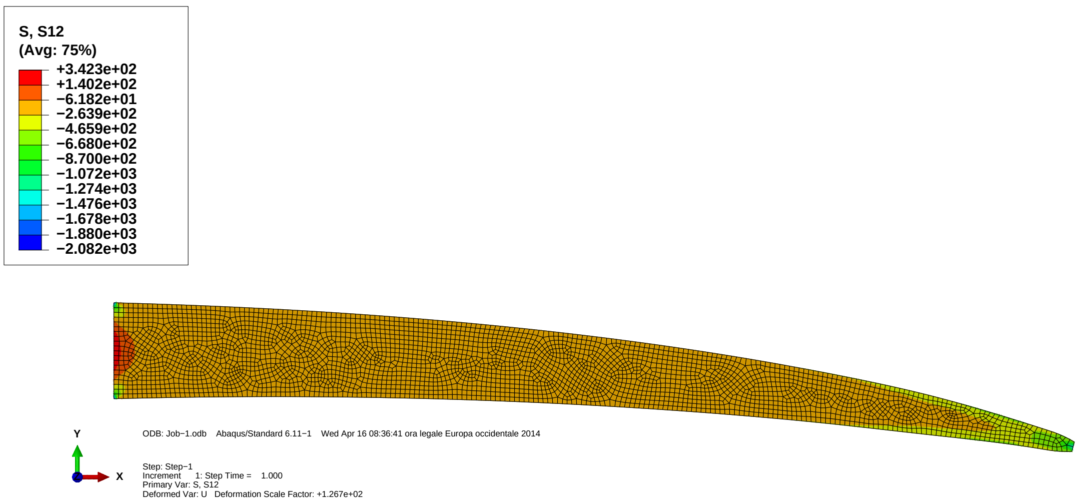

Figure 5.19: Results of "S12" obtained by using the software Abaqus for the cantilever curvilinearly tapered symmetric beam with a concentrated load on the right edge

value of interest. Therefore, choosing "U" and "U2" from the model tree, the variation of the deflection along the beam longitudinal axis is shown (Figure 5.18). By doing this, it is possible to read the deflection at the right end:

$$v(L) = -7.891 \cdot 10^{-3} \text{ m} \tag{5.72}$$

The same procedure is followed to evaluate the maximum shear stress at half length of the beam. Therefore, choosing "S" and "S12" from the model tree, Figure 5.19 is obtained which shows how the shear stress varies along the beam longitudinal axis. In order to find the value of interest, a "path" is created along the said cross-section. The resulting shear distribution is symmetric with respect to the beam axis. The maximum is in correspondence of half cross-section and it results equal to:

$$max(\sigma_{xy}|_{x=L/2}) = -1.085 \cdot 10^2 \text{ kN/m}^2 \tag{5.73}$$

5.5.4 Comparison of the results

As shown in Figure 5.20, the four curves are almost coincident and the deflection results, at the right end of the beam, are very similar (see Table 5.4). Therefore, the considered methods in the matter of the deflection match. On the other hand, as expected, an evident mismatch arises between the Jourawsky solution and the shear stress distributions provided by the developed model and the finite element analysis (see Figure 5.21).

Table 5.4: List of the deflection results at $x = L$ and of the maximum shear stress results at $x = L/2$. e_v and e_σ are the percentage errors with respect to the finite element solution.

CURVILINEARLY TAPERED SYMMETRIC BEAM

MODELS	$v(x)$[m]	$max(\sigma_{xy}\|_{x=L/2})$[kN/m^2]	e_v[%]	e_σ[%]
EULER-BERNOULLI	$-7.815 \cdot 10^{-3}$	–	$9.631 \cdot 10^{-1}$	–
TIMOSHENKO	$-7.872 \cdot 10^{-3}$	–	$2.407 \cdot 10^{-1}$	–
JOURAWSKY	–	$-2.111 \cdot 10^{2}$	–	$9.440 \cdot 10^{1}$
ANALYTICAL	$-7.857 \cdot 10^{-3}$	$-1.076 \cdot 10^{2}$	$4.309 \cdot 10^{-1}$	$8.605 \cdot 10^{-1}$
FE (reference solution)	$-7.891 \cdot 10^{-3}$	$-1.085 \cdot 10^{2}$	0	0

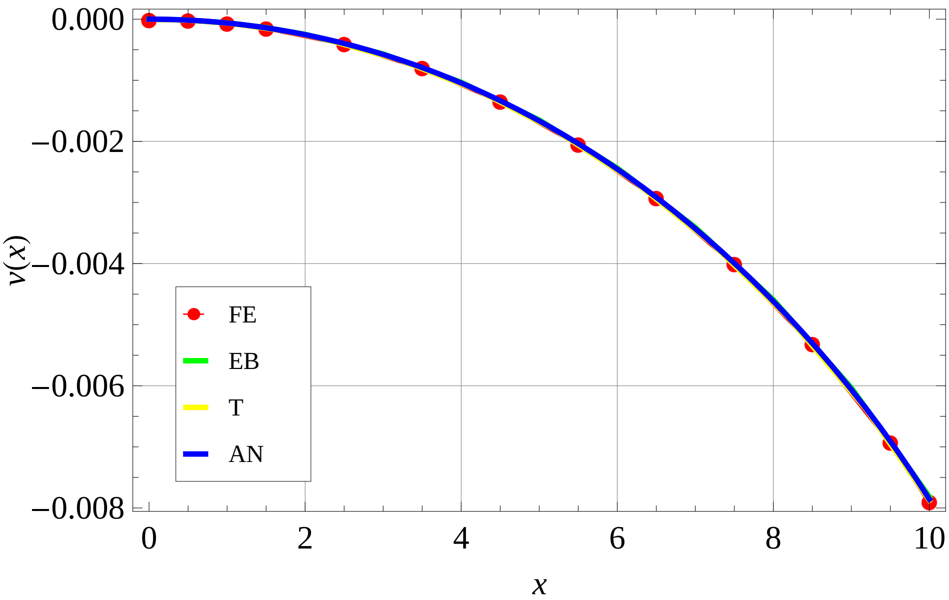

Figure 5.20: Deflection results for the curvilinearly tapered non-symmetric beam. The abscissa x and the ordinate $v(x)$ represent the beam axis and the deflection. The adopted unit of measurement, for both axes, is m. The labels FE, EB, T and AN indicate the finite element, the Euler- Bernoulli, the Timoshenko and the analytical solution, respectively.

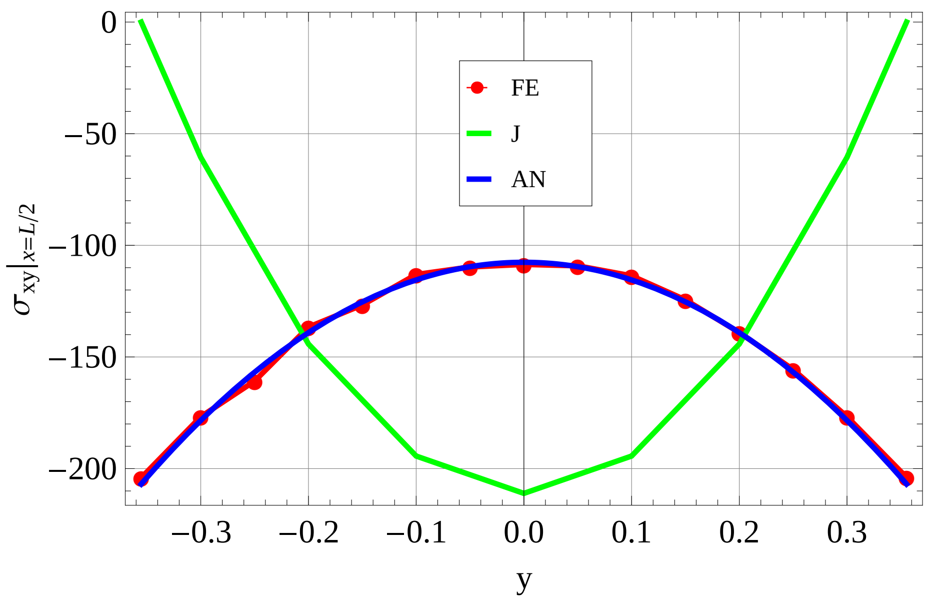

Figure 5.21: Shear stress results for the curvilinearly tapered non-symmetric beam. The abscissa y indicates the axis along the beam thickness, using m as unit of measurement and the ordinate $\sigma_{xy}|_{x=L/2}$ indicates the shear stress at $x = L/2$, using $\mathrm{kN/m^2}$ as unit of measurement. The labels FE, J and AN represent the finite element, the Jourawsky and the analytical solution, respectively.

5.6 Curvilinearly tapered non-symmetric beam

The following geometry dimensions are assumed in order to evaluate the numerical solution of the problem shown in Figure 5.22:

$$\begin{aligned} H &= 0.25 \text{ m} \\ L &= 10 \text{ m} \\ A(L) &= 0.5 \text{ m}^2 \end{aligned} \tag{5.74}$$

Where the beam cross-section is assumed rectangular with a base equal to 1 m.

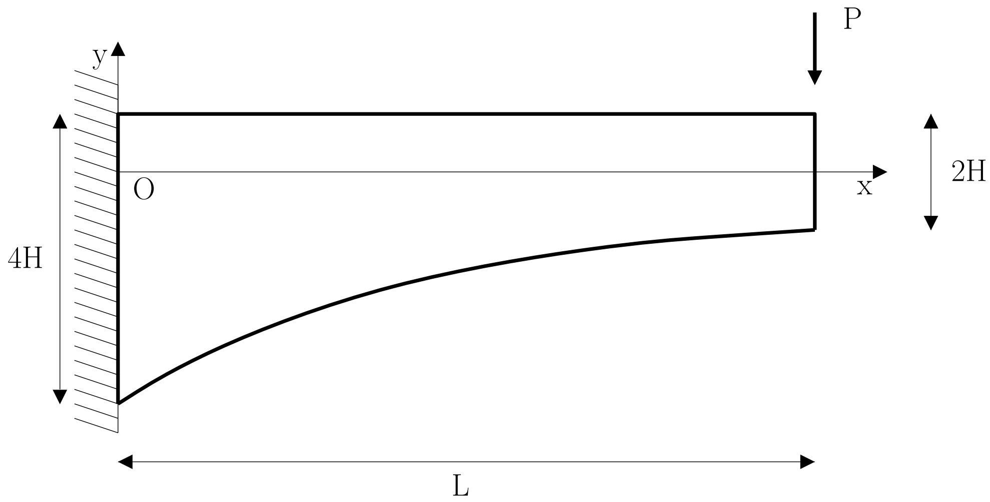

Figure 5.22: Cantilever curvilinear tapered beam

5.6.1 Mathematica results

The analysed beam presents a complex geometry with respect to the prismatic beam. Therefore, by using the command DSolve, it is not possible to obtain the analytical solution of the mixed ODEs and of the displacement ODEs. However, it is possible to proceed numerically with the command NDSolve.

Numerical solution for the mixed ODEs

Considering the system of the six ODEs (see appendix A and equation A.2) and the boundary conditions (5.2) previously introduced, the problem shown in Figure 5.22 is numerically solved for the variables $\theta(x)$, $u(x)$, $v(x)$, $\sigma_{xo}(x)$, $\sigma_{x1}(x)$ and $\tau(x)$ by using the command

NDsolve. The values of the mechanical properties and the geometry dimensions to be used are indicated in equation (5.1) and (5.74), respectively. Focusing on the deflection $v(x)$, this can be estimated at the right edge of the beam:

$$v(L) = -9.488 \cdot 10^{-3} \text{ m} \tag{5.75}$$

Another value of interest to be computed in order to make a comparison with the other results is the maximum value of the shear stress at half length of the beam. It is important to notice that the expression of shear stress σ_{xy} (see equation 4.12c) is function of x and y. As a consequence, it is necessary to solve the maximum problem $max(\sigma_{xy}|_{x=L/2})$ with respect to y. By doing this, the maximum value of the shear stress within the considered cross-section is registered at the lower border. Therefore, substituting the values of $\tau(L/2)$, $\sigma_{x0}(L/2)$ and $\sigma_{x1}(L/2)$, numerically found by using the command NDSolve, and the expressions of $c(x)$ and $t(x)$ (see Equation 4.34a and 4.34b) in equation (4.12c), the following maximum value of the shear stress at $x = L/2$ is obtained:

$$max(\sigma_{xy}|_{x=L/2}) = -3.840 \cdot 10^2 \text{ kN/m}^2 \tag{5.76}$$

Numerical solution for the displacement ODEs

Considering the system of the three ODEs, whose full verbalization has been omitted in Chapter 4 due to the excessive length, and the boundary conditions (5.3) previously introduced, the problem shown in Figure 5.22 is numerically solved for the variables $\theta(x)$, $u(x)$ and $v(x)$ and their derivatives, by using the command NDsolve. Therefore, at $x = L$, the deflection $v(x)$ results equal to:

$$v(L) = -9.497 \cdot 10^{-3} \text{ m} \tag{5.77}$$

Now, in order to calculate the maximum shear stress, at $x = L/2$, it is necessary to substitute the values of $v'(L/2)$, $\theta(L/2)$ and $\theta'(L/2)$, numerically obtained by the command NDSolve, in the expression of $\tau(x)$, $\sigma_{x0}(x)$ and $\sigma_{x1}(x)$ obtained by using the static condensation method, but omitted in Chapter 4 due to their length. Once $\tau(L/2)$, $\sigma_{x0}(L/2)$ and $\sigma_{x1}(L/2)$ are known, the maximum value of shear stress at half length of the beam can be recovered through Equation (4.12c) and considering y equal to -0.375 m, as previously discussed:

$$\sigma_{xy}|_{x=L/2} = -3.838 \cdot 10^2 \text{ kN/m}^2 \tag{5.78}$$

5.6.2 Classical theory results

The classical beam theories are used in this section in order to evaluate the deflection at the free edge of the beam shown in Figure 5.22. In particular the principle of virtual work is considered, because it represents one of the possible integral forms to be used for studying a beam in Euler-Bernoulli hypotheses or Timoshenko hypotheses. Another value of interest is the maximum shear stress and it is computed at half length of the beam by means of the Jourawsky theory.

Euler-Bernoulli solution

Considering the Euler-Bernoulli hypotheses and the prismatic cantilever beam that is subject to a concentrated load on the free edge P, the principle of virtual work can be written as follows:

$$v(x) = \int_0^L \left[(L-x)\, \frac{P\,(L-x)}{EI} \right] dx \tag{5.79}$$

Where I represents the second moment of area which varies along the beam longitudinal axis for the current case (Figure 5.22). Considering the full expression of I and the cross-section base equal to 1 m, the equation (5.79) can be written as follows below, according to the expression of $t(x)$ (4.34b):

$$v(x) = \int_0^L \left[(L-x)\, \frac{12P\,(L-x)}{E\,(H + 2Hx^2/L^2 - 4Hx/L + 3H)^3} \right] dx \tag{5.80}$$

It can also be noticed that the first member of the equation (5.79) is the external work, whereas the second term is the internal work. After solving the integral (5.79), the deflection $v(x)$ is found:

$$v(x) = \frac{3\pi P L^3}{64 E H^3} \tag{5.81}$$

Then, considering the mechanical properties (5.1) and the geometry (5.74), it is possible to achieve the numerical result of the deflection at $x = L$.

$$v(L) = -9.425 \cdot 10^{-3} \text{ m} \tag{5.82}$$

Timoshenko solution

Considering the Timoshenko hypotheses and the prismatic cantilever beam that is subject to a concentrated load on the free edge P, the principle of virtual work can be written as follows:

$$v(x) = \int_0^L \left[(L-x) \frac{P\,(L-x)}{EI} \right] dx + \int_0^L \left[\frac{P}{(5/6)GA(x)} \right] dx \tag{5.83}$$

Where I represents the second moment of area, $A(x)$ is the cross-section area and G represents the shear modulus. Considering the full expression of I and $A(x)$ and assuming the cross-section base equal to 1 m, the equation (5.83) can be written as follows below, according to the expression of $t(x)$ (4.34b):

$$\begin{aligned} v(x) = & \int_0^L \left[(L-x) \frac{12P\,(L-x)}{E\,(H+2Hx^2/L^2-4Hx/L+3H)^3} \right] dx + \\ & + \int_0^L \left[\frac{P}{(5/6)G\,(H+2Hx^2/L^2-4Hx/L+3H)} \right] dx \end{aligned} \tag{5.84}$$

It can also be noticed that the first member of the equation (5.83) is the external work, whereas the second term is the internal work. After solving the integral (5.83), the deflection $v(x)$ is found:

$$v(x) = \frac{3\pi PL^3}{64EH^3} + \frac{3PL\pi}{20GH} \tag{5.85}$$

Then, considering the mechanical properties (5.1) and the geometry (5.74), it is possible to achieve the numerical result of the deflection at $x = L$.

$$v(L) = -9.474 \cdot 10^{-3} \text{ m} \tag{5.86}$$

Jourawsky solution

The well-known Jourawsky formula is used to find an approximate solution of the shear stress. Considering the tapered beam, shown in Figure 5.22, the Jourawsky formula is written as follows:

$$\sigma_{xy} = \frac{12P\left[(H+2Hx^2/L^2-4Hx/L+3H)/2-y\right]\left[(H+2Hx^2/L^2-4Hx/L+3H)/2+y\right]}{2\,(H+2Hx^2/L^2-4Hx/L+3H)^3} \tag{5.87}$$

Since the value to be evaluate is the maximum shear stress along the cross-section, y is assumed equal to 0, then the mechanical property values (5.1) and the geometry (5.74) are substituted in (5.87). By doing this, the maximum shear stress at half lenght of the beam is obtained:

$$max(\sigma_{xy}|_{x=L/2}) = -2.400 \cdot 10^2 \text{ kN/m}^2 \tag{5.88}$$

In this section it can clearly be noticed a well-known limitation of Jourawsky theory. In fact, for the case under investigation, the maximum of the shear stress along the considered cross-section is at the lower border and not at half cross-section. Therefore, as expected, this theory is not able to approximate the shear stress distribution for a non-symmetric beam.

5.6.3 FEM results

The finite element analysis is performed by using the software Abaqus. Focusing on the modelling, the same procedure illustrated for the prismatic beam (see Paragraph 5.2.3) is followed. First of all it is necessary to define the geometry of the beam noticing that two vertical lines, one horizontal line and one spline are necessary to describe the curvilinearly tapered beam shown in Figure 5.22. The second step of the modelling concerns the definitions of the mechanical properties (see the two values introduced in (5.1)), and the enforcement of the boundary conditions, emphasizing that on the left end there is a fixed support and on the right end a concentrated load. Lastly, an appropriate quadrangular mesh must be generated according to the dimension of the beam. In the case under investigation, since the maximum beam height is equal to 1 m, the "Approximate global size" is chosen equal to 0.05 m. The rightness of this choice is mainly proven by an accurate convergence analysis, performed by using different values of the "Approximate global size" which are smaller and smaller.

The model is now ready to be analysed. The deflection on the right edge is the first value of interest. Therefore, choosing "U" and "U2" from the model tree, the variation of the deflection along the beam longitudinal axis is shown (Figure 5.23).

By doing this, it is possible to read the deflection at the right end:

$$v(L) = -9.298 \cdot 10^{-3} \text{ m} \tag{5.89}$$

The same procedure is followed to evaluate the maximum shear stress at half length of the beam. Therefore, choosing "S" and "S12" from the model tree, Figure 5.24 is obtained which shows how the shear stress varies along the beam longitudinal axis. In order to find the value of interest, a "path" is created along the said cross-section. The resulting shear distribution is non-symmetric with respect to the beam axis. The maximum is in

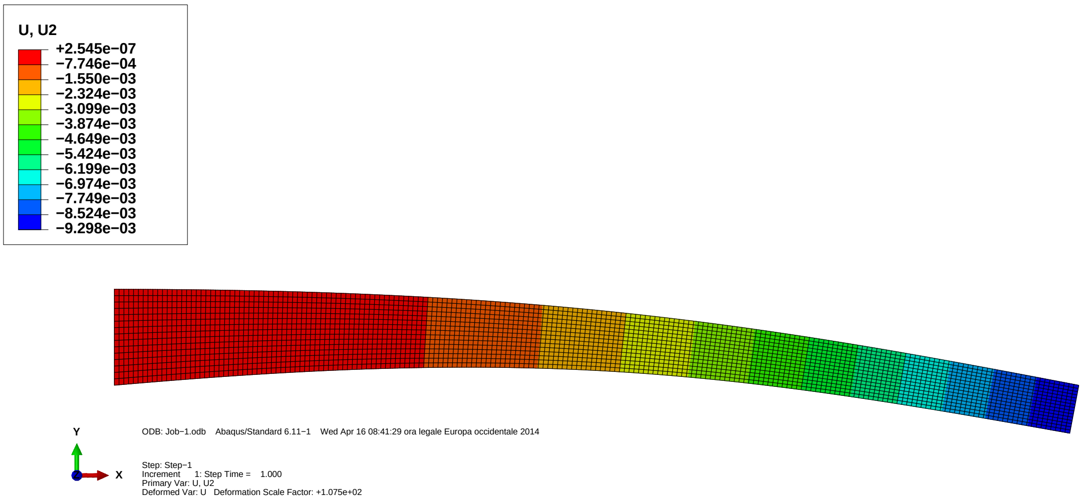

Figure 5.23: Results of "U2" obtained by using the software Abaqus "U2" for the cantilever curvilinearly tapered non-symmetric beam with a concentrated load on the right edge

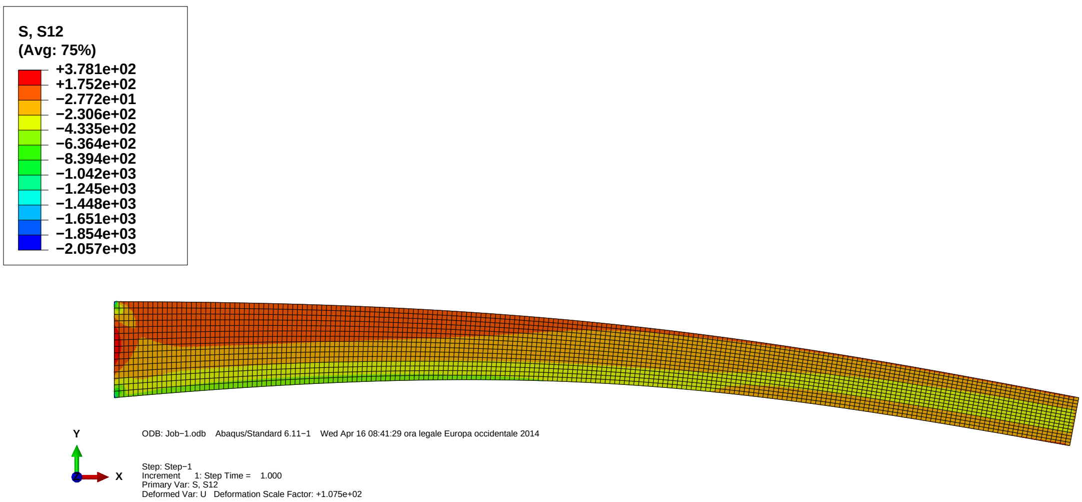

Figure 5.24: Results of "S12" obtained by using the software Abaqus for the cantilever curvilinearly tapered non-symmetric beam with a concentrated load on the right edge

correspondence of the lower border and it results equal to:

$$max(\sigma_{xy}|_{x=L/2}) = -3.850 \cdot 10^2 \text{ kN/m}^2 \tag{5.90}$$

5.6.4 Comparison of the results

As shown in Figure 5.25, the four curves are almost coincident. Moreover, in Table 5.5, it is possible to notice that the deflection results, at the right end of the beam, are very similar, especially the Timoshenko solution and the analytical result.

Figure 5.26 plots the shear stress profiles at half length of the beam. The shear stress results provided by the analytical model and the finite element analysis match almost perfectly. On the other hand, a mismatch arises between the latter and the Jourawsky solution, as previously shown for the other cases.

Table 5.5: List of the deflection results at $x = L$ and of the maximum shear stress results at $x = L/2$. e_v and e_σ are the percentage errors with respect to the finite element solution.

CURVILINEARLY TAPERED NON-SYMMETRIC BEAM

MODELS	$v(x)$[m]	$max(\sigma_{xy}\|_{x=L/2})$[kN/m^2]	e_v[%]	e_σ[%]
EULER-BERNOULLI	$-9.425 \cdot 10^{-3}$	–	$1.359 \cdot 10^{0}$	–
TIMOSHENKO	$-9.474 \cdot 10^{-3}$	–	$1.886 \cdot 10^{0}$	–
JOURAWSKY	–	$-2.400 \cdot 10^{2}$	–	$3.766 \cdot 10^{1}$
ANALYTICAL	$-9.488 \cdot 10^{-3}$	$-3.840 \cdot 10^{2}$	$2.038 \cdot 10^{0}$	$2.556 \cdot 10^{-1}$
FE (reference solution)	$-9.298 \cdot 10^{-3}$	$-3.850 \cdot 10^{2}$	0	0

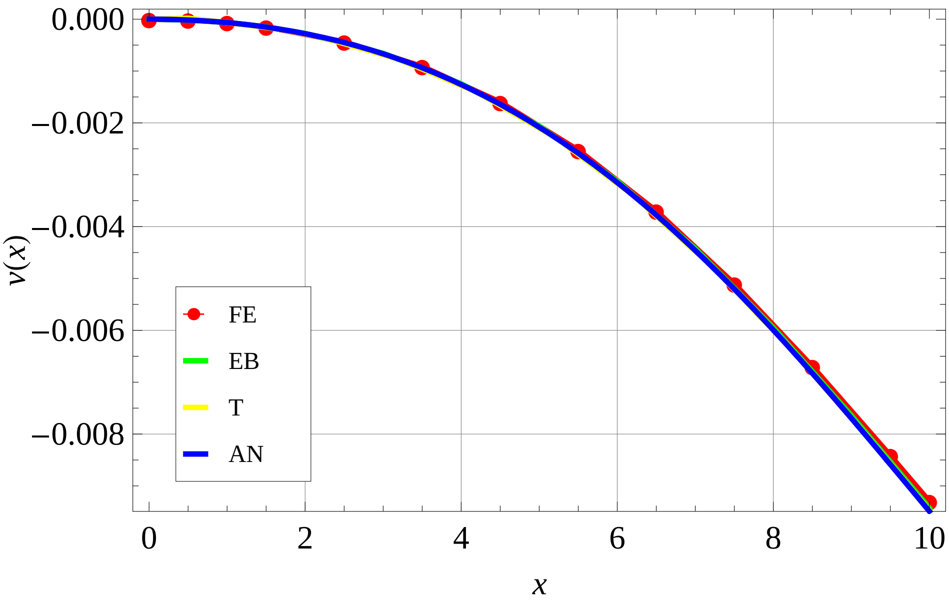

Figure 5.25: Deflection results for the curvilinearly tapered non-symmetric beam. The abscissa x and the ordinate $v(x)$ represent the beam axis and the deflection. The adopted unit of measurement, for both axes, is m. The labels FE, EB, T and AN indicate the finite element, the Euler- Bernoulli, the Timoshenko and the analytical solution, respectively.

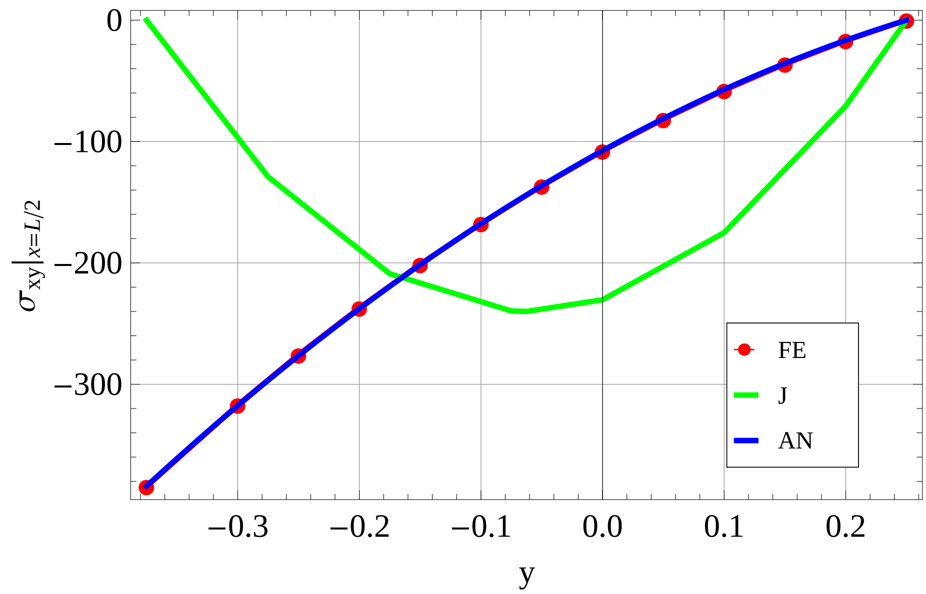

Figure 5.26: Shear stress results for the curvilinearly tapered non-symmetric beam. The abscissa y indicates the axis along the beam thickness, using m as unit of measurement and the ordinate $\sigma_{xy}|_{x=L/2}$ indicates the shear stress at $x = L/2$, using $\mathrm{kN/m^2}$ as unit of measurement. The labels FE, J and AN represent the finite element, the Jourawsky and the analytical solution, respectively.

5.7 Conclusions on results

The developed analytical model provides results both in terms of deflections and stresses. They are also very similar to the ones obtained with the finite element analysis.

As previously shown for each beam, even though the curves of the deflection are almost coincident, the adopted classical beam models present two limitations with respect to the model under investigation. The former is that they are unable to distinguish the case of a symmetric beam from the case of a non-symmetric one. The latter is that the solution evaluated by means of the Timoshenko theory does not consider the exact value of the shear factor for the case of tapered beams. The developed model, instead, naturally takes the correct value of shear factor into account (see Chapeter 4).

The validity of this work is made more explicit by the comparison of the shear stress results. As expected, the Jourawsky theory is not suitable to evaluate the shear stress for tapered beams. The main reason is that, in order to guarantee the equilibrium on the upper and lower limits of the body, the shear stress must be different from zero on them. Moreover, when the beam is non-symmetric with respect to the longitudinal axis, the shear stress profile is non-symmetric too.

A further important observation about the prismatic beam is that the solution of the mixed ODEs coincides with the solution of the displacement ODEs. On the other hand, for the other analysed beams, there is a difference between the two solutions, albeit negligible. As it is possible to notice in Equation (5.2) and (5.3), the boundary condition definition is based on the simplified shear theory of Jourawsky. Nevertheless, the boundary conditions, used in the developed model, have an acceptable accuracy, even if it is important to notice that they are not exactly true for the study of a tapered beam.

In Figure 5.27 and 5.28, the errors with respect to the finite element solution are plotted. Figure 5.27 shows that all errors, related to the developed model, are less than 2.5%, a percentage certainly acceptable in engineering practise. Furthermore, even though the analytical model provides the worst result for the curvilinearly tapered non-symmetric beam, the solution is not too different from the Timoshenko solution. The validity of the model is made more explicit in Figure 5.28, where it is evident a high degree of matching between the analytical results and the finite element solutions and a mismatch between them and the Jourawsky results.

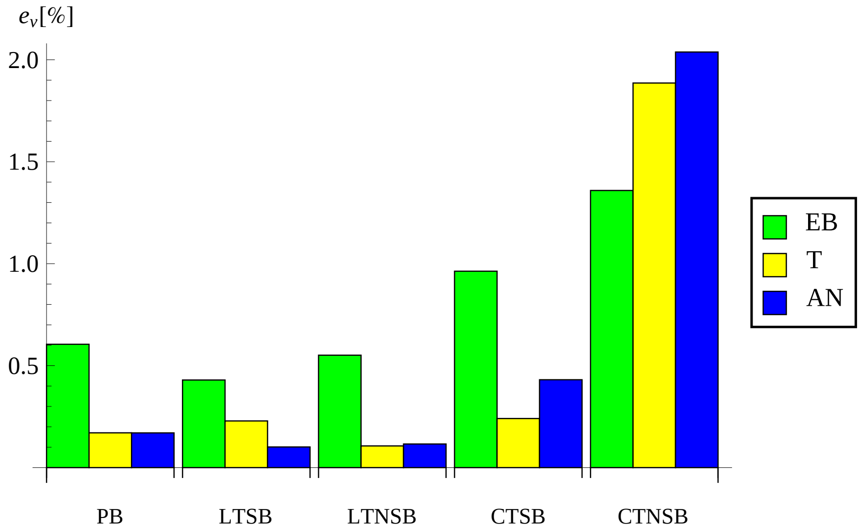

Figure 5.27: Percentage error of the deflection results evaluated with respect to the FE solution. The labels, FE, EB, T and AN, indicate the finite element, the Euler-Bernoulli, the Timoshenko and the analytical solutions. The labels, PB, LTSB, LTNSB, CTSB and CTNSB, indicate prismatic beam, linearly tapered symmetric beam, linearly tapered non-symmetric beam, curvilinearly tapered symmetric beam and curvilinearly tapered non-symmetric beam, respectively.

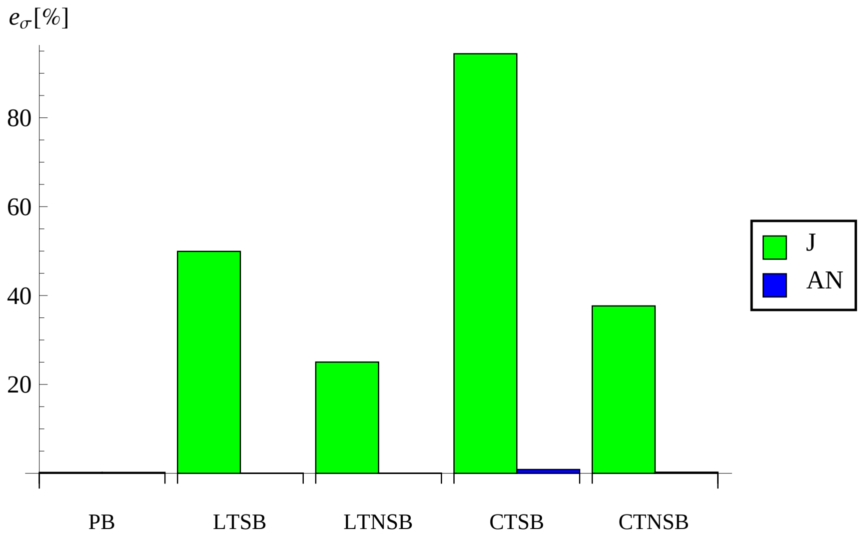

Figure 5.28: Percentage error of the shear stress results evaluated with respect to the FE solution. The labels, FE, J and AN, indicate the finite element, the Jourawsky and the analytical solutions. The labels, PB, LTSB, LTNSB, CTSB and CTNSB, indicate prismatic beam, linearly tapered symmetric beam, linearly tapered non-symmetric beam, curvilinearly tapered symmetric beam and curvilinearly tapered non-symmetric beam, respectively.

Chapter 6

Conclusions and further developments

The studies conducted in this thesis were particularly successful because they allowed the modelling of beams with relatively complex geometries through simple kinematic assumptions, guaranteeing highly accurate results nonetheless.

The beam has been modelled as a 2D body made of a linear elastic isotropic material. This is equivalent to imposing the plane stress state hypotheses to a 3D body or to considering that the beam width is negligible.

The Total Potential Energy principle and the Hellinger-Reissner principle have been introduced in order to formulate this elastic problem. In the first one, the displacement field only is considered as variable of the problem. In the second one, also the stress field is assumed as fundamental variable. The main advantage of using the Hellinger-Reissner formulation is the possibility to accurately describe the stress profiles, even if a simple kinematics and simple assumptions on the stresses are considered. In this work, the hypotheses on the displacement and stress fields have been properly chosen in a way that they would meet the criteria of the dimensional reduction method.

Starting from the Hellinger-Reissner functional, a system of mixed differential equations, in both stress and displacement variables, has been analytically derived for a generic non-prismatic planar beam by using the software Mathematica. Then, by properly introducing five examples of prismatic and non-prismatic beams, the system of differential equations in displacement variables only has been recovered for each of them.

The simplest analysed case is a prismatic beam. It has been studied with the Total Potential Energy and the Hellinger-Reissner approaches in order to emphasize that a mixed method provides a better accuracy to the model. In the differential equations obtained by Hellinger-Reissner formulation, the shear factor has naturally appeared. On the other hand, the Total Potential Energy formulation has provided a solution devoid of this factor.

This aspect is very important for the study of tapered beams, because it means that the calculation of the shear factor is naturally considered in the developed model.

The other analysed cases concern linearly and curvilinearly tapered beams, in both symmetric and a non-symmetric configurations. The comparison of the differential equations obtained for each case has shown that the more complex the geometry of the beam, the more sophisticated the equations to study its behaviour need to be. Then, important additional terms have naturally appeared in the differential equations of non-symmetric beams, proving that the developed model takes the coupling between the axial and bending behaviours into account.

After that, imposing suitable boundary conditions, the solution of the differential equations has been calculated with reasonable computational time and by means of computers usually available in engineering practise. The validity of the developed model has been clearly noticed by comparing its results to the results obtained with the finite element analysis and with the classical beam theories. The model has provided results, both in terms of deflections and stresses, very similar to the finite element solution with a relative difference less than 2%.

It may be concluded that The developed model is capable of giving a accurate stress profiles even if a simple kinematics and simple assumptions on the stress field have been considered. The developed model can be used as base for further studies such as on non-homogeneous tapered beams, 3D tapered beams and beams characterized by more diverse constitutive laws.

Appendix A

Mathematica equations

A.1 Hellinger-Reissner integral form used in Paragraph 4.3

$$
\begin{aligned}
-\int_0^L &(\frac{2}{3}t(x)\delta\tau(x)\theta(x) + \frac{2}{3}t(x)\delta\theta(x)\tau(x) + \frac{16t(x)\delta\tau(x)\tau(x)}{15E} + \frac{16\nu t(x)\delta\tau(x)\tau(x)}{15E} + \\
&+ \frac{t(x)\delta\sigma_{\mathrm{x0}}(x)\sigma_{\mathrm{x0}}(x)}{E} + \frac{t(x)\delta\sigma_{\mathrm{x1}}(x)\sigma_{\mathrm{x1}}(x)}{3E} - \frac{4t(x)\tau(x)\delta\sigma_{\mathrm{x0}}(c)c'(c)}{3E} + \\
&- \frac{4\nu t(x)\tau(x)\delta\sigma_{\mathrm{x0}}(x)c'(x)}{3E} - \frac{4t(x)\delta\tau(x)\sigma_{\mathrm{x0}}(x)c'(x)}{3E} - \frac{4\nu t(x)\delta\tau(x)\sigma_{\mathrm{x0}}(x)c'(x)}{3E} + \\
&+ \frac{2t(x)\delta\sigma_{\mathrm{x0}}(x)\sigma_{\mathrm{x0}}(x)c'(x)^2}{E} + \frac{2t(x)\delta\sigma_{\mathrm{x1}}(x)\sigma_{\mathrm{x1}}(x)c'(x)^2}{3E} + \frac{t(x)\delta\sigma_{\mathrm{x0}}(x)\sigma_{\mathrm{x0}}(x)c'(x)^4}{E} + \\
&+ \frac{t(x)\delta\sigma_{\mathrm{x1}}(x)\sigma_{\mathrm{x1}}(x)c'(x)^4}{3E} - \frac{2}{3}\mathrm{v}(x)\delta\tau(x)t'(x) - \frac{2}{3}\delta\mathrm{v}(x)\tau(x)t'(x) + \mathrm{u}(x)\delta\sigma_{\mathrm{x0}}(x)t'(x) + \\
&- \frac{1}{6}t(x)\theta(x)\delta\sigma_{\mathrm{x1}}(x)t'(x) - \frac{2t(x)\tau(x)\delta\sigma_{\mathrm{x1}}(x)t'(x)}{3E} - \frac{2\nu t(x)\tau(x)\delta\sigma_{\mathrm{x1}}(x)t'(x)}{3E} + \\
&+ \delta\mathrm{u}(x)\sigma_{\mathrm{x0}}(x)t'(x) - \frac{1}{6}t(x)\delta\theta(x)\sigma_{\mathrm{x1}}(x)t'(x) - \frac{2t(x)\delta\tau(x)\sigma_{\mathrm{x1}}(x)t'(x)}{3E} + \\
&- \frac{2\nu t(x)\delta\tau(x)\sigma_{\mathrm{x1}}(x)t'(x)}{3E} + \mathrm{v}(x)\delta\sigma_{\mathrm{x0}}(x)c'(x)t'(x) + \delta\mathrm{v}(x)\sigma_{\mathrm{x0}}(x)c'(x)t'(x) + \\
&+ \frac{4t(x)\delta\sigma_{\mathrm{x1}}(x)\sigma_{\mathrm{x0}}(x)c'(x)t'(x)}{3E} + \frac{4t(x)\delta\sigma_{\mathrm{x0}}(x)\sigma_{\mathrm{x1}}(x)c'(x)t'(x)}{3E} + \\
&+ \frac{4t(x)\delta\sigma_{\mathrm{x1}}(x)\sigma_{\mathrm{x0}}(x)c'(x)^3t'(x)}{3E} + \frac{4t(x)\delta\sigma_{\mathrm{x0}}(x)\sigma_{\mathrm{x1}}(x)c'(x)^3t'(x)}{3E} + \\
&+ \frac{1}{2}\mathrm{v}(x)\delta\sigma_{\mathrm{x1}}(x)t'(x)^2 + \frac{t(x)\delta\sigma_{\mathrm{x0}}(x)\sigma_{\mathrm{x0}}(x)t'(x)^2}{6E} - \frac{\nu t(x)\delta\sigma_{\mathrm{x0}}(x)\sigma_{\mathrm{x0}}(x)t'(x)^2}{3E} + \\
&+ \frac{1}{2}\delta\mathrm{v}(x)\sigma_{\mathrm{x1}}(x)t'(x)^2 + \frac{t(x)\delta\sigma_{\mathrm{x1}}(x)\sigma_{\mathrm{x1}}(x)t'(x)^2}{2E} + \frac{\nu t(x)\delta\sigma_{\mathrm{x1}}(x)\sigma_{\mathrm{x1}}(x)t'(x)^2}{3E} +
\end{aligned}
$$

$$
\begin{aligned}
&+\frac{5t(x)\delta\sigma_{\mathrm{x}0}(x)\sigma_{\mathrm{x}0}(x)c'(x)^2t'(x)^2}{6E}+\frac{7t(x)\delta\sigma_{\mathrm{x}1}(x)\sigma_{\mathrm{x}1}(x)c'(x)^2t'(x)^2}{6E}+\\
&+\frac{t(x)\delta\sigma_{\mathrm{x}1}(x)\sigma_{\mathrm{x}0}(x)c'(x)t'(x)^3}{3E}+\frac{t(x)\delta\sigma_{\mathrm{x}0}(x)\sigma_{\mathrm{x}1}(x)c'(x)t'(x)^3}{3E}+\\
&+\frac{t(x)\delta\sigma_{\mathrm{x}0}(x)\sigma_{\mathrm{x}0}(x)t'(x)^4}{16E}+\frac{t(x)\delta\sigma_{\mathrm{x}1}(x)\sigma_{\mathrm{x}1}(x)t'(x)^4}{48E}-\frac{2}{3}t(x)\mathrm{v}(x)\delta\tau'(x)+\\
&-\frac{2}{3}t(x)\delta\mathrm{v}(x)\tau'(x)+t(x)\mathrm{u}(x)\left(\delta\sigma_{\mathrm{x}0}\right)'(x)+t(x)\mathrm{v}(x)c'(x)\left(\delta\sigma_{\mathrm{x}0}\right)'(x)+\\
&+\frac{1}{6}t(x)^2\theta(x)\left(\delta\sigma_{\mathrm{x}1}\right)'(x)+\frac{1}{2}t(x)\mathrm{v}(x)t'(x)\left(\delta\sigma_{\mathrm{x}1}\right)'(x)+t(x)\delta\mathrm{u}(x)\left(\sigma_{\mathrm{x}0}\right)'(x)+\\
&+t(x)\delta\mathrm{v}(x)c'(x)\left(\sigma_{\mathrm{x}0}\right)'(x)+\frac{1}{6}t(x)^2\delta\theta(x)\left(\sigma_{\mathrm{x}1}\right)'(x)+\frac{1}{2}t(x)\delta\mathrm{v}(x)t'(x)\left(\sigma_{\mathrm{x}1}\right)'(x)+\\
&+t(x)\mathrm{v}(x)\delta\sigma_{\mathrm{x}0}(x)c''(x)+t(x)\delta\mathrm{v}(x)\sigma_{\mathrm{x}0}(x)c''(x)+\frac{1}{2}t(x)\mathrm{v}(x)\delta\sigma_{\mathrm{x}1}(x)t''(x)+\\
&+\frac{1}{2}t(x)\delta\mathrm{v}(x)\sigma_{\mathrm{x}1}(x)t''(x)\big)\,dx
\end{aligned}
\tag{A.1}
$$

A.2 Six ODEs for the curvilinearly tapered symmetric beam used in Paragraph 4.9

$$\frac{40}{E}\sqrt{H^2\left(\frac{1}{100}-\frac{x}{101L}\right)}\left(5E\theta(x)+8(1+\nu)\tau(x)-5\left(-\frac{200H^2(1+\nu)\sigma_{\mathrm{x1}}(x)}{\sqrt{101}L\sqrt{\frac{H^2(101L-100x)}{L}}}-E\mathrm{v}'(x)\right)\right)=0$$

$$\frac{40}{E}\sqrt{H^2\left(\frac{1}{100}-\frac{x}{101L}\right)}\left(\left(48+\frac{480000H^4}{10201L^2\left(-\frac{101L}{100}+x\right)^2}+\frac{400H^2(8-16\nu)}{101L\left(\frac{101L}{100}-x\right)}\right)\sigma_{\mathrm{x0}}(x)-48E\mathrm{u}'(x)\right)=0$$

$$\frac{40}{E}\sqrt{H^2\left(\frac{1}{100}-\frac{x}{101L}\right)}\left(-\left(16+\frac{160000H^4}{10201L^2\left(-\frac{101L}{100}+x\right)^2}+\frac{320000H^2(3+2\nu)}{101L(101L-100x)}\right)\sigma_{\mathrm{x1}}(x)+\right.$$
$$\left.-\frac{32H^2\left(150E\theta(x)+200(1+\nu)\tau(x)+E\left(150\mathrm{v}'(x)+(-101L+100x)\theta'(x)\right)\right)}{\sqrt{101}L\sqrt{\frac{H^2(101L-100x)}{L}}}\right)=0$$

$$\frac{H\left(-50\sigma_{\mathrm{x0}}(x)+(101L-100x)\left(\sigma_{\mathrm{x0}}\right)'(x)\right)}{L\sqrt{\frac{H^2(101L-100x)}{L}}}=0$$

$$\frac{101L\sqrt{\frac{H^2(101L-100x)}{L}}\tau(x)+\sqrt{101}H^2\left(50\sigma_{\mathrm{x1}}(x)+(101L-100x)\left(\sigma_{\mathrm{x1}}\right)'(x)\right)}{L}=0$$

$$\frac{2400H^2\left(\sigma_{\mathrm{x1}}\right)'(x)}{101L}=\frac{16H^2\left(50\tau(x)+(-101L+100x)\tau'(x)\right)}{\sqrt{101}L\sqrt{\frac{H^2(101L-100x)}{L}}} \tag{A.2}$$

A.3 Six ODEs for the curvilinearly tapered non-symmetric beam used in Paragraph 4.10

$$\frac{H}{EL}\left(2L^2-2Lx+x^2\right)\left(5EL^2\theta(x)+8L^2(1+\nu)\tau(x)+5\left(-4H(L-x)(1+\nu)\sigma_{\mathrm{x0}}(x)+\right.\right.$$
$$\left.\left.+4H(L-x)(1+\nu)\sigma_{\mathrm{x1}}(x)+EL^2\mathrm{v}'(x)\right)\right)=0$$

$$\frac{1}{EL}H\left(2L^2-2Lx+x^2\right)\left(8HL^6(L-x)(1+\nu)\tau(x)-\left(3L^8+256H^4(L-x)^4+\right.\right.$$
$$\left.-16H^2L^4(L-x)^2(-2+\nu)\right)\sigma_{\mathrm{x0}}(x)+256H^4L^4\sigma_{\mathrm{x1}}(x)+32H^2L^6\sigma_{\mathrm{x1}}(x)-1024H^4L^3x\sigma_{\mathrm{x1}}(x)+$$
$$-64H^2L^5x\sigma_{\mathrm{x1}}(x)+1536H^4L^2x^2\sigma_{\mathrm{x1}}(x)+32H^2L^4x^2\sigma_{\mathrm{x1}}(x)-1024H^4Lx^3\sigma_{\mathrm{x1}}(x)+256H^4x^4\sigma_{\mathrm{x1}}(x)+$$
$$\left.+3EL^8\mathrm{u}'(x)+6EHL^7\mathrm{v}'(x)-6EHL^6x\mathrm{v}'(x)\right)=0$$

$$\frac{1}{EL^{10}}32H\left(2L^2-2Lx+x^2\right)\left(-\left(L^8+256H^4(L-x)^4+16H^2L^4(L-x)^2(2+\nu)\right)\sigma_{\mathrm{x1}}(x)+\right.$$
$$+H\left(6EL^6(-L+x)\theta(x)-8L^6(L-x)(1+\nu)\tau(x)+256H^3L^4\sigma_{\mathrm{x0}}(x)+32HL^6\sigma_{\mathrm{x0}}(x)+\right.$$
$$-1024H^3L^3x\sigma_{\mathrm{x0}}(x)-64HL^5x\sigma_{\mathrm{x0}}(x)+1536H^3L^2x^2\sigma_{\mathrm{x0}}(x)+32HL^4x^2\sigma_{\mathrm{x0}}(x)+$$
$$-1024H^3Lx^3\sigma_{\mathrm{x0}}(x)+256H^3x^4\sigma_{\mathrm{x0}}(x)-6EL^7\mathrm{v}'(x)+6EL^6x\mathrm{v}'(x)+2EL^8\theta'(x)+$$
$$\left.\left.-2EL^7x\theta'(x)+EL^6x^2\theta'(x)\right)\right)=0$$

$$\frac{H\left(-2(L-x)\sigma_{\mathrm{x0}}(x)+\left(2L^2-2Lx+x^2\right)\left(\sigma_{\mathrm{x0}}\right)'(x)\right)}{L}=0$$

$$\frac{H\left(2L^2-2Lx+x^2\right)\left(2L^2\tau(x)+H\left(2(L-x)\sigma_{\mathrm{x1}}(x)+\left(2L^2-2Lx+x^2\right)\left(\sigma_{\mathrm{x1}}\right)'(x)\right)\right)}{L}=0$$

$$\frac{8H\left(-2(L-x)\tau(x)+\left(2L^2-2Lx+x^2\right)\tau'(x)\right)}{L^2}=$$
$$=\frac{24H^2}{L^4}\left(\left(-4L^2+6Lx-3x^2\right)\sigma_{\mathrm{x0}}(x)+\left(4L^2-6Lx+3x^2\right)\sigma_{\mathrm{x1}}(x)+\right.$$
$$\left.+\left(2L^3-4L^2x+3Lx^2-x^3\right)\left(\left(\sigma_{\mathrm{x0}}\right)'(x)-\left(\sigma_{\mathrm{x1}}\right)'(x)\right)\right) \tag{A.3}$$

Bibliography

Abdel-Jaber, M., A. Al-Qaisia, M. Abdel-Jaber, and R. Beale (2008). Nonlinear natural frequencies of an elastically restrained tapered beam. *Journal of Sound and Vibration 313*(3-5), 772 – 783.

Abell, M. and J. Braselton (2008). *Mathematica by Example*. Mathematica by Example Series. Elsevier Science.

Arnold, D. and R. Falk (1988). A new mixed formulation for elasticity. *Numerische Mathematik 53*(1-2), 13–30.

Arturo Tena Colunga, Member, A. (1996). Stiffness formulation for nonprismatic beam elements. *Journal of Structural Engineering 122*(12), 1484–1489.

Auricchio, F., G. Balduzzi, and C. Lovadina (2010). A new modeling approach for planar beams: finite-element solutions based on mixed variational derivations. *Journal of Mechanics of Materials and Structures 5*(5), 771–794.

Banerjee, J. R. and F. W. Williams (1985). Exact Bernoulli-Euler dynamic stiffness matrix for a range of tapered beams. *International Journal for Numerical Methods in Engineering 21*(12), 2289–2302.

Banerjee, J. R. and F. W. Williams (1986). Exact Bernoulli-Euler static stiffness matrix for a range of tapered beam-columns. *International Journal for Numerical Methods in Engineering 23*(9), 1615–1628.

Bathe, K. (1982). *Finite Element Procedures in Engineering Analysis*. Prentice-Hall civil engineering and engineering mechanics series. Prentice-Hall.

Bauchau, O. and J. Craig (2009). Euler-Bernoulli beam theory. In O. Bauchau and J. Craig (Eds.), *Structural Analysis*, Volume 163 of *Solid Mechanics and Its Applications*, pp. 173–221. Springer Netherlands.

Berdichevskii, V. (1979). Variational-asymptotic method of constructing a theory of shells PMM vol. 43, no.4, 1979, pp. 664-687. *Journal of Applied Mathematics and Mechanics 43*, 711–736.

Boley, B. A. (1963). On the Accuracy of the Bernoulli-Euler Theory for Beams of Variable Section. *Journal of Applied Mechanics 30*, 373.

Courant, R. et al. (1943). Variational methods for the solution of problems of equilibrium and vibrations. *Bull. Amer. Math. Soc 49*(1), 1–23.

Hazrat, R. (2010). *Mathematica®: A Problem-Centered Approach*. Springer Undergraduate Mathematics Series. Springer.

Hodges, D., A. Rajagopal, J. Ho, and W. Yu (2011). Stress and strain recovery for the in-plane deformation of an isotropic tapered strip-beam. *Journal of Mechanics of Materials and Structures 5*(6), 963–975.

Hodges, D. H., J. C. Ho, and W. Yu (2008). The effect of taper on section constants for in-plane deformation of an isotropic strip. *Journal of Mechanics of Materials and Structures 3*(3), 425–440.

Kantorovich, L. and V. Krylov (1964). *Approximate methods of higher analysis*. Interscience.

Kardestuncer, H., D. Norrie, and F. Brezzi (1987). *Finite element handbook*. McGraw-Hill reference books of interest: Handbooks. McGraw-Hill.

Li, G.-Q. and J.-J. Li (2002). A tapered Timoshenko-Euler beam element for analysis of steel portal frames. *Journal of Constructional Steel Research 58*(12), 1531 – 1544.

Paz, M. and W. Leigh (2004). *Structural Dynamics: Theory and Computation ; [updated with SAP2000]*. Structural Dynamics: Theory and Computation. Springer US.

RAO, S. (2011). *The Finite Element Method in Engineering*. Elsevier Science.

Reddy, J. (2002). *Energy Principles and Variational Methods in Applied Mechanics*. Wiley.

Reddy, J. (2006). *An Introduction to the Finite Element Method*. McGraw-Hill Series in Mechanical Engineering. McGraw-Hill Education.

Rosa, M. D., M. Lippiello, M. Maurizi, and H. Martin (2010). Free vibration of elastically restrained cantilever tapered beams with concentrated viscous damping and mass. *Mechanics Research Communications 37*(2), 261 – 264.

Timoshenko, S. (1976). *Strength of Materials: Elementary theory and problems*. Strength of Materials. R. E. Krieger Pub. Co.

Timoshenko, S. and J. Goodier (1951). *Theory of Elasticity, by S. Timoshenko and J. N. Goodier,... 2nd Edition*. McGraw-Hill book Company.

Timoshenko, S. and D. Young (1965). *Theory of Structures [by] S.P. Timoshenko [and] D.H. Young*. McGraw-Hill.

Vogelius, M. and I. Babuška (1981a). On a dimensional reduction method. I. The optimal selection of basis functions. *Math. Comp. 37*(155), 31–46.

Vogelius, M. and I. Babuška (1981b). On a dimensional reduction method. II. Some approximation-theoretic results. *Math. Comp. 37*(155), 47–68.

Vogelius, M. and I. Babuška (1981c). On a dimensional reduction method. III. A posteriori error estimation and an adaptive approach. *Math. Comp. 37*(156), 361–384.

Weaver, W. and P. Johnston (1986). *Finite Elements for Structural Analysis*. Prentice-Hall civil engineering and engineering mechanics series. Prentice-Hall.

Wellin, P. (2013). *Programming with Mathematica®: An Introduction*. Cambridge University Press.